This is to certify that the
dissertation entitled

DYNAMICS OF EMBEDDED FLUOROPHORES IN MODEL BILAYER LIPID MEMBRANES

presented by

AARON JAY GREINER

has been accepted towards fulfillment
of the requirements for the

Ph.D. degree in Chemical Engineering

Robert Mark Worden
Major Professor's Signature

12/15/2009
Date

DYNAMICS OF EMBEDDED FLUOROPHORES IN MODEL BILAYER LIPID MEMBRANES

By

AARON JAY GREINER

A DISSERTATION

Submitted to
Michigan State University
in partial fulfillment of the requirements
for the degree of

DOCTOR OF PHILOSOPHY

Chemical Engineering

2009

ABSTRACT

DYNAMICS OF EMBEDDED FLUOROPHORES IN MODEL BILAYER LIPID MEMBRANES

By

AARON JAY GREINER

Membrane fluidity refers to the rate of translational, rotational, and trans-leaflet lipid diffusion in bilayer lipid membranes (BLMs). It is an important physical property of the BLM that can affect the rate at which molecules diffuse across the membrane, the signaling and communication between cells, and the activity and function of membrane proteins. Membrane fluidity often depends on the interactions between constituent lipids in the BLM or between lipids and other membrane-bound molecules or macromolecules.

This dissertation focuses on four studies that involved the use of optical techniques to measure the dynamics of fluorescently-tagged lipids in synthetic model BLM systems that mimic the behavior of cell membranes. The primary tools used for characterization were fluorescence recovery after pattern photobleaching (FRAPP), which measures translational diffusion in two-dimensional supported bilayer lipid membranes (sBLMs), and time-correlated single photon counting (TCSPC), which measures rotational diffusion in three-dimensional spherical liposomes in solution. Our results showed that the diffusion of lipid fluorophores in model BLMs can significantly increase or decrease upon the addition of molecules or macromolecules to the bilayer. For example, both sonicated and extruded 1,2-dioleoyl-sn-glycero-3-phosphocholine (DOPC) liposomes were less fluid upon incorporation of cholesterol, likely to the result of

cholesterol molecules interacting with the hydrophobic acyl chains of the bilayer and causing the membrane to become more rigid. Addition of the lipid 1,2-dioleoyl-*sn*-glycero-3-[phospho-*rac*-(1-glycerol)] (DOPG) to DOPC sBLMs again resulted in a decrease in membrane fluidity. In this case, however, the reduced fluidity likely resulted from hydrogen bonding between constituent lipid head groups in the membrane. When single acyl chain lysophospholipids were added to DOPC sBLMs, the membrane fluidity increased. This is likely due to a reduction in van der Waals interactions between hydrophobic acyl chains. However, the fluidity decreased when a fraction of the lysophospholipids was converted to fatty acids by enzymatic activity of NEST (NTE esterase domain), the catalytic domain of neuropathy target esterase (NTE). The observed decrease in fluidity is attributed to the enhanced packing of fatty acids, relative to lysophospholipids, in the hydrophobic region of the bilayer. A maximum NEST protein concentration in fluid sBLMs formed from proteoliposome reconstitution was estimated and it was demonstrated qualitatively that microsomal membrane proteins at sufficiently high concentrations can decrease the fluidity of sBLMs reconstituted from microsomes.

The results of these studies give a fundamental understanding of some of the important interactions that influence the fluidity of model BLM interfaces. The results may be useful in the design of BLM-based biosensor devices, the performance of which may depend upon BLM properties such as fluidity. They may also provide insight into the interactions that affect fluidity in cell membranes.

To my mom, dad, family, and all of the teachers and professors who have been outstanding mentors throughout my academic career.

ACKNOWLEDGEMENTS

I would like to thank my committee members, Dr. R. Mark Worden, Dr. Robert Y. Ofoli, Dr. Ilsoon Lee, and Dr. Gary J. Blanchard for being excellent mentors and for teaching me to focus on novel, important, and fundamental research throughout my doctoral work at MSU. I would also like to thank Dr. Rudy J. Richardson for donating the NEST protein plasmid and helping in the interpretation of data obtained with NEST, Dr. Nichole Hein and Lee Alexander for their help purifying NEST, and Dr. Monique Lapinski, Angelines Castro-Forero, Dr. Sachin Jadhav, Heather Pillman, Dr. Brian Hassler, Dr. Neeraj Kohli, and Dr. Sachin Vaidya for their thoughtful scientific discussions and collaborative efforts in research.

TABLE OF CONTENTS

LIST OF TABLES

LIST OF FIGURES

NOMENCLATURE

t	time
τ	fluorescence lifetime
τ_{OR}	reorientation time
D	average diffusion rate
D_i	diffusion rate with respect to axis i
A_i	ith pre-exponential factor
D_w	wobbling diffusion coefficient
$I_{\|\|}(t)$	time-dependent light emission intensity polarized parallel to incident beam
$I_{\perp}(t)$	time-dependent light emission intensity polarized perpendicular to incident beam
$r(t)$	time-dependent anisotropy function
$r(\infty)$	infinite-time anisotropy
$r(0)$	initial, zero-time anisotropy
η	solvent viscosity
y	number of data points in each data set in ANOVA
θ_0	semi-angle of the fluorophore confining cone volume
k_B	Boltzmann's constant
k	total data sets compared in ANOVA
$f(t)$	time-dependent post bleach fluorescence
D_L	average translational diffusion coefficient
a	Ronchi ruling stripe periodicity
m	mobile fraction

q	parameter used in ANOVA analysis, found from table of critical values for F distributions
v	studentized degrees of freedom
α	value corresponding to the confidence level in ANOVA analysis
V	spherical volume
T	temperature
Tu	Tukey parameter
p	statistical p-value
n	number of model parameters

LIST OF ACRONYMS

ANOVA	analysis of variance
BLM	bilayer lipid membrane
DFP	diisopropylphosphorofluoridate
DLS	dynamic light scattering
DOPC	1-palmitoyl-2-hydroxy-*sn*-glycero-3-phosphocholine
DOPG	1,2-dioleoyl-*sn*-glycero-3-[Phospho-*rac*-(1-glycerol)]
ER	endoplasmic reticulum
FFA	free fatty acid
FRAPP	fluorescence recovery after pattern photobleaching
IC_{50}	half-maximal inhibitory concentration
p-lysoPC	1-palmitoyl-2-hydroxy-*sn*-glycero-3-phosphocholine
MD	molecular dynamics
MSE	mean square for error
NBD-PC	1-oleoyl-2-[12-[(7-nitro-2-1,3-benzoxadiazol-4-yl)amino]dodecanoyl]-*sn*-glycero-3-phosphocholine nitro-benzo derivative
NBE-PE	1,2-dioleoyl-*sn* glycero-3-phosphoethanolamine-N-7-nitro-2-1,3-benzoxadiazol-4-yl
NEST	neuropathy target esterase catalytic domain
NTE	neuropathy target esterase
PC	phosphatidylcholine
PG	phosphatidylglycerol
PMSF	phenylmethylsulfonyl fluoride

RC	photosynthetic reaction center
SAM	self-assembled monolayer
SD	standard deviation
SDS-PAGE	sodium dodecyl sulfate polyacrylamide gel electrophoresis
sBLM	supported bilayer lipid membrane
tBLM	tethered bilayer lipid membrane
TCSPC	time-correlated single photon counting
TEM	transmission electron microscopy
TF	tissue factor

1. INTRODUCTION

1.1. Overview and Significance of the Problem

This dissertation outlines four fundamental investigations that involved the measurement of the diffusion of fluorescently tagged lipid molecules embedded in model bilayer lipid membranes (BLMs) of different compositions. Model BLMs mimic biological cell membranes and allow fundamental membrane properties to be measured in a well-defined, reproducible system. Model BLMs were formed with molecules such as lipids, cholesterol, and fatty acids, and macromolecules such as membrane-associated proteins. Lipid fluorophore diffusion in model BLMs was measured optically by monitoring fluorescence emission upon excitation with a laser beam.

The overall goal of the studies was to obtain a fundamental understanding of the effect of incorporated molecules and macromolecules on the rotational and/or translational diffusion of lipid fluorophores in model BLMs. The measurement of such fluorophore diffusion is useful in assessing membrane fluidity,[1] which plays important roles in cell signaling, cell adhesion, and membrane protein functionality.[2,3] In response to environmental stresses such as temperature, salt concentration, and presence of solvents, cells adapt by increasing or decreasing membrane fluidity in an effort to minimize cellular damage or prevent cell death.[2] The results of this work may be used to design bilayer interfaces for BLM-based biosensor and bioelectronic devices and may provide insight into the important interactions that influence fluidity in cell membranes.

Liposomes are stable, spherically shaped model bilayers that enclose aqueous cores. They are precursors to the formation of model supported bilayer lipid membranes (sBLMs) when they adsorb to a hydrophilic interface, fuse together, and rupture. Such sBLMs are two-dimensional and have a thin film (~1 Å) of water that separates the hydrophilic head of the lower leaflet of the bilayer from the substrate.[4] Liposomes can also be used in the formation of model tethered bilayer lipid membranes (tBLMs) in which the bilayer is physically elevated above the surface, typically by several nanometers. The formation of sBLMs and tBLMs is often monitored with techniques such as surface plasmon resonance, electrochemical impedance spectroscopy, atomic force microscopy, and quartz crystal microgravimetry.[5-8]

Sonication and extrusion are two common methods of liposome preparation. Since the mechanism of forming liposomes by sonication (acoustic energy) is vastly different than extrusion (pressure drop across a polycarbonate membrane), there is some degree of uncertainty as to whether the diffusion transport properties in model membranes prepared by the two techniques can be directly compared. In the first study of this dissertation, we examined whether the rotational and translational diffusion coefficients of lipid fluorophores in model membranes prepared by sonication and extrusion can be directly compared. We also assessed the effect of the two preparation techniques on the mean size and size distribution of liposomes.

The second study was conducted to gain a fundamental understanding of the effect of lipid head group intermolecular interactions on membrane fluidity. We measured rotational and translational diffusion coefficients of fluorophores in phosphatidylglycerol (PG) model BLMs in which the head groups have a tendency to

form relatively strong hydrogen bonds, and in phosphatidylcholine (PC) model BLMs in which head groups interact primarily via relatively weak van der Waals and screened electrostatic forces.[9-11]

In the third study, we incorporated NEST (NTE esterase domain), the catalytic domain of the membrane protein neuropathy target esterase (NTE), into model BLMs to study the effect of free fatty acids (FFA) from enzyme-induced lysophospholipid hydrolysis on membrane dynamics. This study was motivated by the hypothesis that NTE may have a physiological role of regulating the physicochemical properties of membranes, including their fluidity.

Unlike tBLM interfaces, sBLMs are often unsuitable for studies involving membrane proteins because interactions between the underlying surface and such proteins have the potential to cause conformational changes that inhibit activity.[12,13] However, it has been shown that certain trans-membrane proteins retain proper functionality in fluid sBLMs even when the protein itself is immobile.[14,15] Results of the fourth study show that, at sufficiently large lipid to protein ratios, fluid sBLMs can be formed following the adsorption and rupture of yeast cell membrane fragments called microsomes and synthetic membrane-associated protein-containing liposomes termed proteoliposomes. We assessed the fluidity of sBLMs produced by reconstituting microsomes with relatively high and low concentrations of membrane protein on silica, and also determined a range of concentrations of NEST (used here as a model membrane-associated protein) that can be used in proteoliposomes to form sBLMs.

These studies are important for several reasons. The first study demonstrated that, while the physical characteristics of liposomes depend on the method of preparation, the

dynamics of fluorophores in BLMs constituted from such systems are independent of the method of liposome formation. This finding is significant because it establishes that results from studies that utilize the two liposome preparation methods can be directly compared. In the second, third, and fourth studies, lipids, fatty acids, and macromolecules were shown to measurably influence model BLM fluidity. This research provides a deeper understanding of how constituent molecules influence model BLM fluidity and may provide insight into the molecules that affect fluidity of cell membranes. Given that the functionality of certain membrane proteins has been shown to depend on membrane fluidity,[16-20] the performance of BLM-based devices that incorporate membrane proteins may rely on the ability to manipulate membrane fluidity. Understanding the molecules that influence model membrane fluidity, the mechanisms that underlie these effects, and how the activity of membrane proteins changes with increasing or decreasing fluidity will allow for better design of bilayer interfaces for BLM-based devices. The results of our work with sBLMs and liposomes may be used to design BLM-based biosensors and bioelectronic devices

1.2. Background

1.2.1. Structure and Function of Biological Membranes

The membrane is one of the most important components of living cells. It separates the cell cytoplasm from its surroundings, and is generally depicted as a fluid heterogeneous BLM comprising mainly phospholipids, cholesterol, carbohydrates, and proteins. One of the primary functions of BLMs is to maintain a homeostatic state within

a cell by acting as a semi-permeable barrier preventing entry of toxic molecules, most polar molecules, ions, and macromolecules, while allowing the passage of non-polar and small polar molecules such as water.[21] Another primary function of the BLM is to provide an environment for membrane proteins to function.[22] Unlike prokaryotic cells, many processes that occur in eukaryotic cells involve organelles that incorporate BLMs.[21] These processes include aerobic respiration in mitochondria, protein synthesis in the Golgi apparatus, and protein transport and folding in the endoplasmic reticulum.[21]

The basic building blocks of most BLMs are phospholipids, which are amphipathic molecules composed of one glycerol moiety bonded to a phosphate-based hydrophilic head group and one or two hydrophobic fatty acid tails attached to the glycerol base via ester bonds (Figure 1.1). BLM stability arises primarily from van der Waals and hydrophobic interactions between the acyl chains of the lipid.[21] A wide range of cationic, anionic, and zwitterionic molecules constitute the hydrophilic head group of phospholipids. Fatty acid chains of different lengths and degrees of saturation make up the hydrophobic portion of lipids. The various combinations of hydrophilic head groups and hydrophobic tail groups allow for a multitude of lipids, each with unique physical properties such as phase transition temperature, solubility, and diffusivity in a membrane structure.[22,23]

1.2.2. Model Membranes: Liposomes, Supported Bilayer Membranes, and Tethered Bilayer Membranes

Mimicking of *in vivo* characteristics of biological membranes with artificial model membranes *in vitro* has led to a more comprehensive understanding of, for

example, membrane protein functionality, lipid-lipid interactions in membranes, and physical properties of membranes. Three common examples of model membranes are liposomes (lipid vesicles), sBLMs, and tBLMs. Liposomes are spherically shaped bilayer structures that form spontaneously when phospholipids such as phosphatidylcholine (PC) are added to water. Liposomes can be unilamellar or multilamellar, with sizes typically ranging from tens of nanometers to several microns depending, on the preparation technique. Liposomes are commonly used in drug delivery due to their unique ability to store hydrophilic species in the aqueous core and hydrophobic compounds in the acyl chain region of the BLM.[24]

McConnell and coworkers were the first to develop artificial, two-dimensional sBLMs on silica surfaces using molecular self-assembly via liposome fusion.[25] sBLMs have also been formed on quartz and mica surfaces in the same manner.[25,26] There are three fundamental mechanisms by which sBLMs are formed from liposomes.[27] In the first, vesicles adsorb to a surface and rupture immediately as a result of highly favorable lipid-surface interactions, forming individual bilayer patches that associate over time to form a uniform sBLM. This is usually the case when liposomes comprising a positively charged lipid such as 1,2-dioleoyl-3-trimethylammonium-propane (DOTAP) and a zwitterionic lipid such as 1,2-dioleoyl-sn-glycero-3-phosphocholine (DOPC) associate with a negatively charged quartz or silica surface via strong electrostatic interactions. In the second, vesicles adsorb to the surface and do not undergo fusion and subsequent rupture until a critical surface coverage is reached. This occurs with the DOTAP/DOPC system at a moderate salt concentration. The salt screens lipid/surface electrostatic attraction. The third way involves the adsorption of a supported lipid monolayer on a

surface by Langmuir-Blodgett deposition, followed by formation of the upper leaflet by the fusion of liposomes.[28]

tBLMs are two-dimensional model membranes that are physically elevated above the underlying substrate by tethering molecules or a polymer cushion.[29] tBLM systems are generally used for studies involving membrane proteins.[30-34] The elevation above the underlying substrate allows room for proper protein or channel conformation and prevents undesirable interactions between the protein and the substrate. Construction of tBLMs typically involves first the formation of a self-assembled monolayer (SAM) that acts as the lower bilayer leaflet followed by the adsorption of liposomes that rupture to form the upper bilayer leaflet. Many biosensor and bioelectronic devices that incorporate membrane proteins and ion channels in model membranes utilize tBLM systems. In addition, tBLMs can be formed on conductive substrates such as gold, making it possible to characterize the interface electrochemically.

1.3. Outline of this Dissertation

1.3.1. Comparison of Liposomes Formed by Sonication and Extrusion: Rotational and Translational Diffusion of an Embedded Fluorophore

Chapter 3 of this dissertation describes collaborative work with Dr. Gary J. Blanchard and Dr. Monique M. Lapinski of the Department of Chemistry and Angelines Castro-Forero of the Department of Chemical Engineering and Materials Science.[35] Each of the collaborators made equal contributions to the work.

Liposomes used as model BLMs are typically prepared by sonication or extrusion. The basic mechanism for breaking down large multilamellar vesicles to relatively small unilamellar vesicles varies greatly with each process. Sonication involves exposure of the sample to acoustic energy, while extrusion involves the use of mechanical energy to force the lipids through a porous polycarbonate membrane via pressure driven flow. Since these processes differ greatly, it is conceivable that the physical and molecular scale properties of liposomes prepared by the two techniques would be different, making it difficult to directly compare model BLM systems reconstituted from sonication and extrusion. The goal of this study was to explore potential differences by using fluorescence recovery after pattern photobleaching (FRAPP) to measure translational diffusion coefficients of fluorophores in sBLMs, time-correlated single photon counting (TCSPC) to measure fluorescence lifetimes and rotational diffusion coefficients of fluorophores in liposomes, and dynamic light scattering (DLS) and transmission electron microscopy (TEM) to assess physical characteristics such as mean liposome sizes and size distributions.

1.3.2. Effect of Hydrogen Bonding on Rotational and Translational Dynamics of a Head Group-bound Fluorophore in Bilayer Membranes

Over the past ten to fifteen years, molecular dynamics (MD) simulations have provided much insight into the molecular level lipid-lipid and lipid-protein interactions in BLMs, with the most commonly modeled lipids being zwitterionic PC and phosphatidylethanolamine.[10] Results of MD simulations have recently been published that involve anionic lipids such as phosphatidylserine and PG.[11] PG lipids have a glycerol

moiety in the head group, which radial distribution functions from simulations have shown interact strongly with phosphate oxygen atoms and carbonyl groups of neighboring lipids in the BLM structure via hydrogen bonding.[10] MD simulations also predict that water molecules form "water bridges" between phosphate oxygen atoms of adjacent phospholipids via hydrogen bonding. For zwitterionic PC membranes, radial distribution functions show interaction between the positively charged nitrogen of the choline head group and the negatively charged phosphate of neighboring lipids in addition to the aforementioned "water bridges." The interactions between head groups of PG lipids in a membrane structure involve mainly hydrogen bonds, while screened electrostatic interactions are more prevalent between head groups of PC lipids.

We hypothesized that the rotational and translational diffusion of head-group-tethered fluorophores in BLMs would be affected by intermolecular lipid head group interactions. Chapter 4 of this dissertation describes this work, which used FRAPP and TCSPC measurements to gain insight into the rotational and translational diffusion of fluorophores in liposomes and sBLMs, respectively, consisting of the two structurally different lipids, PC and PG.[36] This work was done in collaboration with Dr. Gary J. Blanchard and Heather A. Pillman of the Department of Chemistry, with equal contributions from collaborators.

1.3.3. Influence of Lysophospholipid Hydrolysis by the Catalytic Domain of Neuropathy Target Esterase on Bilayer Lipid Membrane Fluidity

Neuropathy target esterase (NTE) is an important medically relevant membrane protein found in human neurons and other cell types. NTE inhibition by organophosphate

compounds has been shown to be directly linked to the onset of a type of paralysis known as organophosphorous induced delayed neuropathy (OPIDN) as well as motor neuron disease.[37,38] Recent studies suggest that NEST selectively hydrolyzes a specific class of lipid molecules called lysophospholipids.[39] The hydrolysis of one lysophospholipid yields one fatty acid molecule and one hydrophilic glycerophosphocholine head group. Although the physiological role of NTE is poorly understood, published reports indicate that the cellular function of NTE may involve the control of cytotoxic accumulation of lysophopspholipids.[40,41] This work involved use of an assay for measuring free fatty acid (FFA) concentrations, in conjunction with FRAPP, DLS, and TEM to study the effect of NEST-induced lysophospholipid hydrolysis on the dynamics of fluorophores in model sBLMs. By extension of our work done with NEST and model membranes, we postulate that NTE may play a role in influencing the fluidity of cell membranes by means of lysophospholipid hydrolysis. This work is described in Chapter 5 of this dissertation and involved collaboration with Professor Rudy J. Richardson of the School of Public Health, Department of Neurology at the University of Michigan.

1.3.4. Effect of Membrane Protein Concentration on the Translational Dynamics of an Embedded Fluorophore in Supported Bilayer Membranes Constituted from Proteoliposomes

tBLM interfaces are generally considered suitable platforms for the characterization of the functionality of membrane proteins. sBLM interfaces have also been used to study the activity and functionality of trans-membrane proteins.[15] However,

the effect of membrane protein concentration on the rupture of proteoliposomes to form fluid sBLMs is not well-understood.

In this study, we used FRAPP to determine whether fluid sBLMs with incorporated proteins can be formed on silica substrates over a range of lipid to protein ratios. We formed interfaces on silica using yeast microsomal membrane fragments as well as proteoliposomes comprising synthetic DOPC lipids and NEST, which was used here as a model membrane-associated protein. We qualitatively assessed the effect of membrane proteins on sBLM reconstitution with microsomal membrane fragments and quantitatively determined a range of protein concentrations that would lead to sBLM formation with DOPC and NEST proteoliposomes. This work is described in Chapter 6 of this dissertation and involved collaboration with Dr. Sachin R. Jadhav of the Department of Chemical Engineering and Materials Science, with equal contributions from each collaborator. We acknowledge Dr. R. Michael Garavito of the Department of Biochemistry and Molecular Biology for supplying the microsome samples.

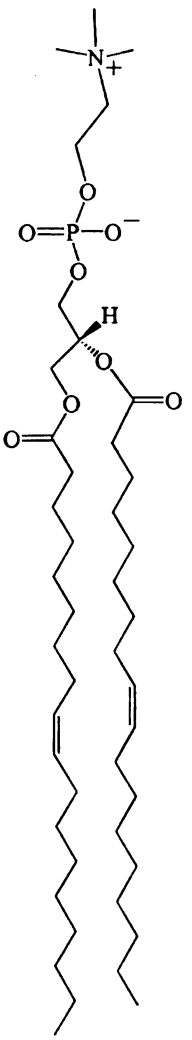

Figure 1.1. Molecular structure of a common lipid in mammalian cell membranes, 1,2-dioleoyl-*sn*-glycero-3-phosphocholine (DOPC). The phosphate and choline groups comprise the hydrophilic head group and the dioleoyl acyl chains constitute the hydrophobic tail group.

2. EXPERIMENTAL METHODS

2.1. Overview

The two fluorescence techniques used to monitor the dynamics of lipid fluorophores in this dissertation are FRAPP, to measure translational diffusion in two-dimensional sBLMs, and TCSPC, to measure rotational diffusion in spherical liposomes. Detailed explanations as well as diagrams of the experimental setups for each technique are included in this chapter.

2.2. Fluorescence Recovery After Pattern Photobleaching

FRAPP is generally used to measure mobile fractions and lateral diffusion coefficients of fluorescently tagged lipids in sBLMs on glass, quartz, silica, and mica surfaces. This is done by selectively photobleaching sections of the sample and recording the fluorescence recovery due to the diffusion of fluorophores from the non-photobleached fringes. Since it is difficult to determine the translational diffusion of fluorophores embedded within liposomes, it is common to reconstitute liposomes in the form of sBLMs on substrates such as those mentioned above. The transformation of liposomes to sBLMs is accomplished through a series of steps that begin with vesicle adsorption, transition into vesicle-surface and vesicle-vesicle interactions, and end with vesicle fusion and/or rupture and subsequent bilayer formation.[26,27,42,43] Translational diffusion coefficients and mobile fractions of fluorophores in sBLMs can be extracted from the FRAPP data using a model developed by Starr and Thompson.[44]

The experimental setup (Figures 2.1 and 2.2) consisted of a double syringe pump used to simultaneously infuse and withdraw solutions from a custom-made 1 mL flow cell, an inverted microscope with a 32x objective lens, an argon ion laser, a side-on photomultiplier tube (PMT), a photon counter, and a fast preamplifier. The 488 nm line of the laser was directed through a 5x beam expander connected to a pair of optical flats used to toggle between a low intensity (20 μW) monitoring beam for continuous fluorescence detection and a high intensity (500 mW) beam for photobleaching fluorophores. A Ronchi ruling of 25 μm periodicity was placed in the back image plane of the microscope to create a fringe pattern on the sample. An aperture was placed in front of the PMT to restrict the observation area, to prevent unbleached fluorophores from diffusing from outside the bleached area to the observation zone during measurements of the fluorescence recovery. The photobleached area was approximately 200 μm in diameter, while the observed area was 75 μm, as shown in Figure 2.3.

To conduct these measurements, a selected region of the sBLM was exposed to an intense laser beam, causing an irreversible photodegradation or bleaching of fluorophores in the illuminated regions of the fringe pattern. After photobleaching, fluorescence recovery in the monitored region occurred at a rate determined by the translational diffusion of unbleached fluorophores behind the dark fringes at the time of photobleaching. Thus, the fluorescence recovery data enables estimation of the translational diffusion coefficient of the fluorophores.[25]

2.3. Time Correlated Single Photon Counting

Fluorescence lifetime and time-resolved orientational anisotropy data of fluorophores in liposomes can be measured with TCSPC, which is useful for detecting low intensity light signals with picosecond time resolution.[45] In our work, fluorescence lifetime data were used to assess differences in the local environment of fluorophores, while anisotropy data were used to estimate the confined volume in which a fluorophore rotates as well as the rate of rotation within that volume, using a hindered rotor model developed by Lipari and Kinosita[46,47] or the free rate of rotation of the fluorophore as a Type I (prolate) or Type II (oblate) rotor using a free rotor model by Chuang and Eisenthal.[48] Detailed discussions of the hindered rotor and free rotor models are given in Chapters 3 and 4, respectively.

The TCSPC experimental apparatus (Figure 2.4) has been described elsewhere.[49,50] The essential features include a 7 W mode-locked Nd:YAG CW laser that produces 1064 nm pulses for 100 ps at a frequency of 76 MHz. Usually, the second or third harmonic of this light is used to excite a cavity dumped dye laser, which typically has outputs of ~ 50 mW with ~ 5 ps pulses at a ~ 4 MHz repetition rate. The beam is then split into a reference beam and a sample beam, which can be frequency-doubled depending on the excitation wavelength of the fluorophore in the sample. The sample beam then travels through a set of neutral density filters into a vertical polarizer before contacting the sample solution. Emitted light is collected at 90° from the incident excitation beam, and a Glan-Taylor (G-T) prism is used to polarize the emitted light 54.7° with respect to the excitation polarization for fluorescence lifetime measurements, and either parallel (0°) or perpendicular (90°) to the excitation polarization for anisotropy

measurements. The transient fluorescence signals are directed through a monochromator and subsequently detected with a microchannel plate photomultiplier tube (MCP PMT). The electronics used to temporally resolve the fluorescence transients includes a constant fraction discriminator (CFD) to determine the maximum signal, and a time-to-amplitude converter (TAC) biased amplifier.

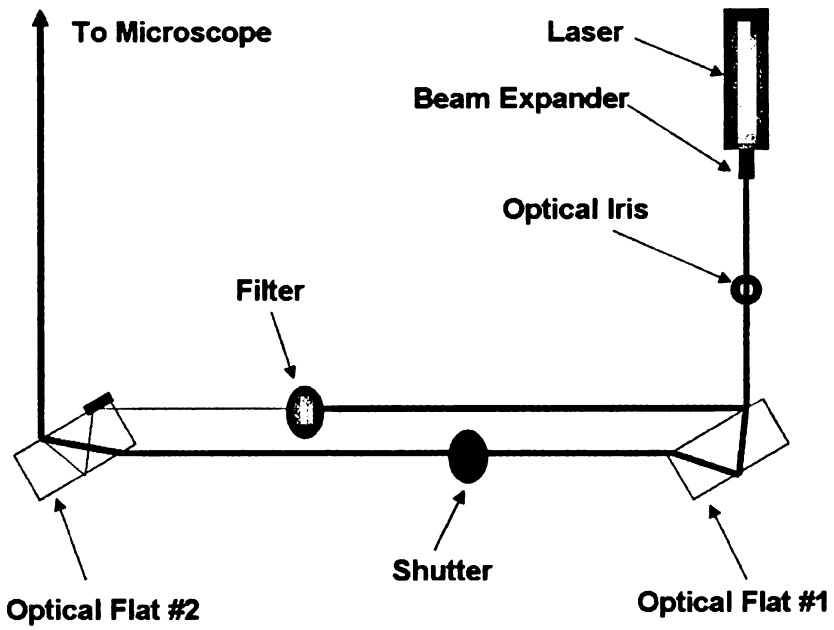

Figure 2.1. Schematic diagram of the FRAPP experimental setup. The laser beam is split into a low intensity monitoring beam (through a filter) and a high intensity photobleaching beam at optical flat #1. The beams are recombined at optical flat #2 prior to impingement on the sample.

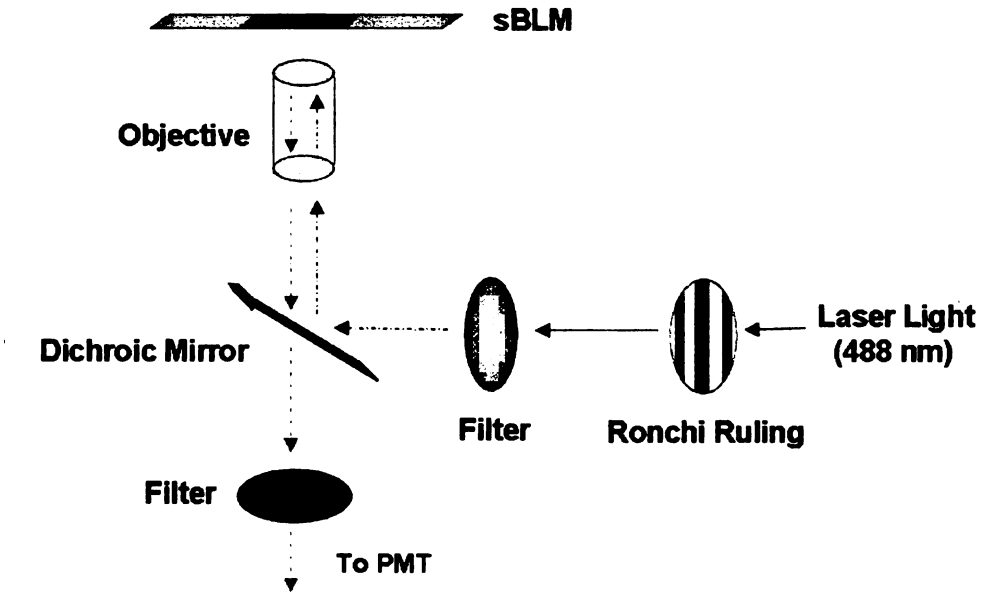

Figure 2.2. Schematic diagram of the FRAPP experimental setup before and after the laser beam reaches the sample. The dichroic mirror reflects the excitation laser light, while allowing fluorescent light emitted from the interface to pass through to the detector. Key: sBLM: supported bilayer lipid membrane; PMT: photomultiplier tube.

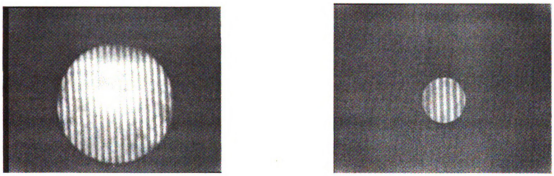

(A) (B)

Figure 2.3. A) Fringe pattern in the illuminated area (diameter = 200 μm) obtained using a 100 lines per inch (25 μm periodicity) Ronchi ruling. B) Observation area (diameter = 75 μm), restricted by placing an aperture in the camera/photomultiplier tube image plane.

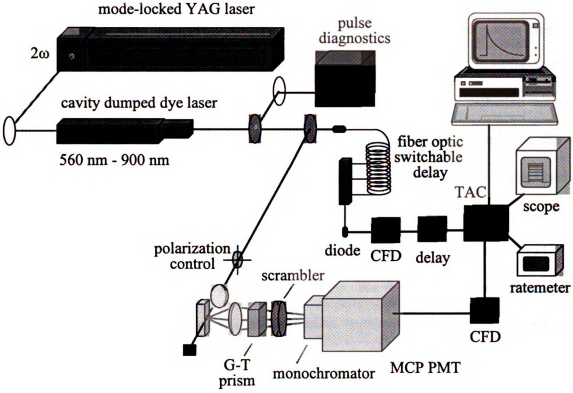

Figure 2.4. Schematic diagram of the TCSPC experimental setup. Key: G-T: Glan-Taylor prism; MCP-PMT: microchannel-plate photomultiplier tube; CFD: constant fraction discriminator; TAC: time to amplitude converter.

3. COMPARISON OF LIPOSOMES FORMED BY SONICATION AND EXTRUSION: ROTATIONAL AND TRANSLATIONAL DIFFUSION OF AN EMBEDDED FLUOROPHORE

3.1. Abstract

We report on the mean diameter and size distribution of liposomes formed by extrusion and sonication, two widely used methods for liposome preparation. We determined the morphology of liposomes by TEM and the mean diameter and size distribution by DLS. We also address the issue of whether the diffusion transport properties of model bilayers prepared by the two techniques differ at the molecular and mesoscopic levels. We used the phospholipid DOPC, with and without cholesterol, to form liposomes, incorporating 18:1-12:0 NBD-PC as a lipid fluorophore to probe dynamics. The rotational and translational diffusion of 18:1-12:0 NBD-PC was characterized by TCSPC and FRAPP, respectively. We found that, despite the apparent differences in mean diameter and size distribution, both methods of preparation produced liposomes that exhibited the same molecular and mesoscopic scale environment.

3.2. Introduction

BLMs are important components of all cellular systems, and a much research has been conducted to understand how to use model membranes as a means of comprehending biological systems. One effective way to create model BLMs in solution is to form liposome structures by the self-assembly of phospholipids in an aqueous environment. An additional way is to induce the rupture of liposomes onto a planar

surface to form sBLMs. Liposomes can be created by a number of methods[51-54] with their size ranging from tens of nanometers to microns depending on the technique used to create them. Two of the most common techniques used to prepare liposomes are extrusion[55-60] and bath sonication,[61] with each method yielding different mean diameters and size distributions.

The extrusion method is used to produce monodisperse, unilamellar liposomes of a predetermined size.[55-60,62] Typically, a lipid suspension is forced through a polycarbonate membrane with a well-defined pore size to produce vesicles with a characteristic diameter near the pore size of the membrane used to prepare them. One significant advantage of extrusion is that the resulting mean liposome diameter and size distribution are fairly reproducible from batch-to-batch.

Sonication is also used widely to prepare of liposome samples. With this method, lipid solutions are agitated using acoustic energy from either a bath or a probe tip sonicator. The induced pressure breaks up large multilamellar liposomes into relatively small liposomes that may be either unilamellar or multilamellar in composition.[61] The time of sonication ultimately determines the liposome size, with the smallest radius being in the range of 10.25 ± 0.55 nm.[63] An advantage of sonication over extrusion is that it is less time-consuming; however, the resulting liposome batch-to-batch mean diameter and size distribution are not as reproducible as those prepared by extrusion.

Because the basic mechanism of breaking down large liposomes to relatively small liposomes differs greatly with sonication and extrusion, it is conceivable that the properties of liposomes prepared by the two techniques would be different. This is an important issue because it bears on whether or not experimental data acquired for model

BLMs formed by the two different techniques can be compared directly. The goal of this study was to evaluate the mean diameter, size distribution, and rotational and translational dynamics of small unilamellar liposomes prepared by bath sonication and by extrusion, to determine if the method of preparation has any influence on these selected bilayer properties. We explored the potential differences by using FRAPP to measure translational diffusion coefficients and mobile fractions in sBLMs, TCSPC to measure fluorescence lifetimes and rotational diffusion coefficients in liposomes, and dynamic light scattering (DLS) and transmission electron microscopy (TEM) to assess mean liposome diameters and size distributions.

3.3. Materials and Methods

3.3.1. Vesicle Preparation by Extrusion

Phospholipids DOPC, 18:1-12:0 NBD-PC, and cholesterol were purchased from Avanti Polar Lipids Inc. (Alabaster, AL) and used as received. Figure 3.1 shows the molecular structures of the lipids used in this study. DOPC was chosen as the primary lipid in our studies because of its low transition temperature (-20°C),[64] ensuring that the resulting lipid bilayers would be fluid at room temperature (23 ± 2°C). The fluorophore 18:1–12:0 NBD-PC, which will be referred to as NBD-PC throughout the remainder of this dissertation, was chosen to ensure structural similarity to the phospholipid to which it is tethered (DOPC, 18:1). In addition, there is a significant body of knowledge on the properties of this fluorophore,[65-67] making it an attractive choice for probing BLM structures. For each sample, 1 mM lipid solutions containing DOPC/NBD-PC (98:2,

mol/mol) or DOPC/cholesterol/NBD-PC (68:30:2, mol/mol/mol) were prepared. The chloroform solvent was evaporated from the lipid mixture and the dry lipid film was hydrated using HEPES® buffer (Sigma-Aldrich, St. Louis, MO) containing NaCl (Fisher Scientific, Fair Lawn, NJ). The buffer (10 mM HEPES®, 150 mM NaCl, pH 7.4) was prepared using purified water from a Milli-Q Plus water purification system (Millipore, Bedford, MA). The mixtures were processed five times through a freeze-thaw-vortex cycle to ensure complete mixing of the sample constituents. Each cycle consisted of immersion in liquid nitrogen for 5 min, followed by immersion in a 60°C water bath for 5 min and vortexing for 2 min. After the freeze-thaw-vortex cycle, the solutions were extruded through two 400 nm pore diameter polycarbonate membrane filters using a mini-extruder (Avanti Polar Lipids Inc., Alabaster, AL). The pre-extruded vesicle suspension was then extruded eleven times through two polycarbonate membranes (Avanti Polar Lipids Inc., Alabaster, AL) with a nominal pore diameter of 100 nm. All extrusions were performed at room temperature (23 ± 2°C).

3.3.2. Vesicle Preparation by Sonication

Lipid mixtures with the same compositions as those used for the extrusion experiments were used to form liposomes by sonication. The chloroform-solvated lipid mixtures were dried under nitrogen and placed under vacuum at -45°C for 3 h. The dried lipid mixtures were then hydrated in buffer (10 mM HEPES®, 150 mM NaCl, pH 7.4), and sonicated for 20 min using a bath ultrasonic cleaner (Branson 1510, Branson Ultrasonic Corporation, Danbury, CT). Fresh liposome solutions were prepared prior to each experiment.

3.3.3. Transmission Electron Microscopy Imaging

A 10 μL aliquot of each sample was fixed on a Formvar® nickel-coated grid using a solution containing 2% uranyl acetate stain in water. Images were acquired using a transmission electron microscope (TEM, JEOL 100CX) operated at an accelerating voltage of 100 kV.

3.3.4. Dynamic Light Scattering

DLS was performed with a Protein Solutions DynaPro-MS/X system (Wyatt Technology Corporation, Santa Barbara, CA) on DOPC/NBD-PC liposome solutions, with and without cholesterol, to determine mean liposome diameters and size distributions. Liposome solutions were diluted by a factor of ten with buffer and placed in a polyethylene cuvette for measurement. A total of three measurements were made for each lipid composition.

3.3.5. Excitation and Emission Spectra

Steady state excitation and emission spectra (Figure 3.2) were acquired for vesicle samples, for the purpose of characterizing the NBD fluorophore band positions. We used an emission spectrometer (Spex Fluorolog 3, Edison, NJ) for all measurements, set to a spectral bandpass of 3 nm for both excitation and emission monochromators.

3.3.6. Time-Correlated Single Photon Counting

Fluorescence lifetimes and reorientation times of fluorophores in liposomes were measured with TCSPC. This information was used to assess the rotational diffusion coefficients and the local environment of fluorophores. The experimental TCSPC setup is described in Section 2.3 of this dissertation. For each lipid system considered in this work, three separate liposome solutions were interrogated with TCSPC.

3.3.7. Deposition of Supported Lipid Bilayers

Fused silica microscope slides (75 mm x 25 mm x 1 mm) were purchased from Technical Glass Products, Inc. (Painesville, OH). They were cleaned by bath sonication (Branson 1510, Branson Ultrasonic Corporation, Danbury, CT) in detergent solution for 20 min, rinsed with DI water, baked at 160°C for 4 h and plasma treated (Harrick Plasma, Ithaca, NY) with oxygen under vacuum (200 mTorr) for 10 min immediately before bilayer deposition. sBLMs were deposited by vesicle fusion in a custom made flow cell.[68] The flow cell was initially washed with buffer, followed by a 1 h incubation with the liposome solution and a final buffer wash to remove any unadsorbed liposomes. All experiments were performed at room temperature (23 ± 2°C).

3.3.8. Fluorescence Recovery After Pattern Photobleaching

FRAPP was used to determine translational diffusion coefficients and mobile fractions in sBLMs. The experimental FRAPP setup is described in Section 2.2 of this dissertation. For each lipid system considered in this work, three separate sBLM

interfaces were formed on silica slides and each interface was interrogated with FRAPP at five different locations of the bilayer.

3.3.9. Statistical Analysis

Data fitting was accomplished using OriginPro 7.5 (OriginLab Corporation, Northampton MA) which uses the Levenberg-Marquardt algorithm for non-linear least squares fitting. An F-test of comparison was conducted to determine whether an exponential model using n parameters provided a statistically significant improvement in the goodness of the fit of fluorescence lifetime and fluorescence anisotropy data than an exponential model using n-1 parameters. Rotational diffusion coefficients (D_W), translational diffusion coefficients (D_L), and particle diameters are reported as means ± standard deviation (SD). Multiple comparison ANOVA with a post-hoc Tukey test ($p < 0.05$) was used to determine if differences among the means were statistically significant.

3.4 Results and Discussion

The purpose of this work was to compare two methods of liposome preparation, extrusion and bath sonication, to determine if the method of preparation affects the size and dynamical properties of the resulting liposomes and sBLMs constituted from the liposomes.

We were primarily concerned with three issues in this work: the physical attributes (mean diameter and size distribution) of liposomes formed by the two methods, and the rotational and translational dynamics of fluorophores in liposomes and sBLMs,

respectively. We also studied how the incorporation of cholesterol in liposomes affected each of these issues. We expected that there would be a marked change in the organization of BLMs with the addition of this component. Each of the issues described above are considered individually.

3.4.1. Liposome Mean Diameter and Size Distribution

We used TEM and DLS to evaluate the mean diameter and size distribution of liposomes formed by extrusion and sonication. TEM images (Figure 3.3) show a single shell surrounding each liposome, suggesting that liposomes formed by the two methods are both unilamellar in structure. However, the images provide little utility in evaluating absolute sizes because of potentially large distortions induced by vacuum. Also, the high-energy electron beam used in imaging could, in principle, damage liposome structures. Such distortions may appear in the form of non-spherical structures. While appealing from a visual perspective, TEM images do not lend themselves readily to the evaluation of the size distribution of the liposomes. To address these issues, we also characterized the liposomes by DLS, a technique that measures the hydrodynamic diameter of particles suspended in solution. Because DLS collects scattering information on an ensemble of particles, it is a relatively simple matter to obtain information on the particle size distribution.[69-72]

The mean diameters of vesicles formed by extrusion were 112 ± 6 nm with (Figure 3.4) and without (Figure 3.5) cholesterol. Thus, it appears that the presence of cholesterol has no apparent influence on the size of liposomes formed by extrusion. This is not surprising, since we expected that the extruded vesicles would be close to 100 nm

in diameter, with or without cholesterol, based on the size of the pores in the polycarbonate membranes used to prepare them.[55,56] On the other hand, liposomes formed by sonication had diameters of 64 ± 3 nm with cholesterol (Figure 3.6) and 28 ± 2 nm without cholesterol (Figure 3.7), showing a significant influence of cholesterol on size. The mean liposomes sizes of the four aforementioned systems are summarized in Table 3.1.

The size of sonicated liposomes, although smaller than those made by extrusion in this study, can be controlled by the duration of sonication.[61] We also note that liposomes formed by sonication had a bimodal size distribution, with and without cholesterol, while liposomes formed by extrusion only had a distinct bimodal size distribution when they contained cholesterol. It is not clear if there is a compositional difference between cholesterol-containing vesicles in the two distribution zones.

3.4.2. Fluorescence Lifetimes and Rotational Diffusion in Liposomes

We measured the fluorescence lifetime and induced orientational anisotropy of tethered NBD fluorophores using TCSPC. The data provided by lifetime and anisotropy measurements are different but complementary. For all of the liposome systems studied here (sonicated and extruded, with and without cholesterol), we observed a fluorescence population decay (Table 3.2) that can be fitted to a two-component exponential model using F-statistic analysis. This behavior has been reported for NBD tethered to phospholipids in a variety of environments.[65,73-76] The fluorescence lifetime of NBD is sensitive to the polarity of its immediate environment, where the shorter lifetime corresponds to the NBD fluorophore existing in a more polar environment.[77] For NBD

fluorophores tethered to the acyl chain of a phospholipid, it has been established that the fluorophore can "loop back" to position itself in close proximity to the polar head group region of the bilayer in which it resides.[65-67,78] The longer lifetime in this model corresponds to the NBD fluorophore residing closer to the nonpolar region of the lipid bilayer. Based on our observation of two fluorescence lifetimes, it is possible that the fluorophore exists in two discrete populations during the timescale of the measurement. However, the fact that we observe two lifetime values that differ by more than 4.5 ns while the proposed environments for NBD are only separated by a few angstroms is consistent with the fluorophore existing in a dielectric gradient that changes substantially over the length scale of the fluorophore itself.[77,79] We therefore believe that there is effectively only one environment, hence one fluorescence lifetime, that the fluorophore experiences, and the fact that we measure two fluorescence lifetimes experimentally is a result of the fluorophore moving in a dielectric gradient.

For all of the liposome systems we studied, the two fluorescence lifetimes are essentially the same with $\tau_1 \approx 2$ ns and $\tau_1 \approx 6$ ns (Table 3.2). We note that the relative contributions of the two lifetime components depend to some degree on liposome composition for the sonicated liposomes (~ 0.05 in the absence of cholesterol versus 0.3 with cholesterol, as opposed to ~ 0.3 for both extruded liposomes). This likely led to the large differences in the ratio of pre-exponential factors [$A_1/(A_1+A_2)$ and $A_2/(A_1+A_2)$] obtained for the sonicated liposomes, particularly in the absence of cholesterol. However, owing to the structural complexity of these liposomes and the comparatively limited information contained in the lifetime data, it would be speculative to suggest that either

the structure of the liposome or the positional distribution of the NBD fluorophores accounts for the observed differences in prefactors.

The fundamental principle in TCSPC measurements is that fluorophores with absorption dipoles oriented parallel to the incident polarization are preferentially excited, creating anisotropy in the system. For the anisotropy decay measurements reported here, the chemical information contained in these experiments is in the form of the decay functionality of *r(t)*:

$$r(t) = \frac{I_{\parallel}(t) - I_{\perp}(t)}{I_{\parallel}(t) + 2I_{\perp}(t)} \tag{3.1}$$

where $I_{||}(t)$ and $I_{\perp}(t)$ are the emission intensities polarized parallel and perpendicular to the vertically polarized incident excitation pulse, respectively.

Hypothetically, if a fluorophore is placed in solution, it will assume all possible orientations with equal probability, hence the infinite-time anisotropy will decay to zero. However, if the same fluorophore is incorporated into a BLM, it will likely not be able to assume all orientations with equal probability due to its confinement, and as a result, $r(\infty)$ will decay to a non-zero value. A fluorophore that is associated in a BLM typically does not have the structural freedom to fully re-randomize its orientation within its environment following excitation, giving rise to an infinite-time anisotropy. The zero-time parameter *r(0)* is determined by the angle between the excited and emitted transition dipole moments of the fluorophore, and $r(\infty)$ serves as a gauge for the orientational confinement that the fluorophore experiences.[47]

In our experiments, the NBD fluorophore was tethered to the tail group of a membrane bilayer constituent, and the anisotropy decay for this system was treated in the context of a hindered rotor model.[46,80-82] The tethered NBD fluorophore does not have the structural freedom to orientationally re-randomize fully within its hydrophobic environment in the BLM following excitation, which gives rise to an infinite time anisotropy, $r(\infty)$. For such systems, the function $r(t)$ is governed by

$$r(t) = r(\infty) + ((r(0) - r(\infty)) \exp(-t / \tau_{OR}) \tag{3.2}$$

where $r(\infty)$ is the infinite-time anisotropy and $r(0)$ is the zero-time anisotropy. The parameter τ_{OR} is the reorientation time. This is related to the orientational relaxation time of the fluorophore within its confining volume, and is approximated by[47, 82]

$$\tau_{OR} = \frac{7{\theta_0}^2}{24 D_w} \tag{3.3}$$

where D_w is the "wobbling" diffusion coefficient and θ_0 is the semi-angle of the confining cone volume of the fluorophore, which is related to the zero- and infinite-time anisotropies by[47]

$$\sqrt{\frac{r(\infty)}{r(0)}} = 0.5\cos\theta_0 \,(1 + \cos\theta_0) \tag{3.4}$$

The values of θ_0 for the extruded and sonicated vesicles, both with and without cholesterol, are given in Table 3.3.

For each of the systems tested, the cone angles are the same within experimental uncertainty, regardless of the method of liposomes preparation. We note that, for the systems containing cholesterol, the recovered cone angles are measurably smaller (ca. 60° vs. ca. 40°) for both the extruded and sonicated liposomes in comparison to the systems containing only the phospholipid and the fluorophore. This finding is consistent with literature reports indicating that the addition of cholesterol to a bilayer serves to make the bilayer less fluid.[83-87] Our data point to not only a slightly longer τ_{OR} for the cholesterol-containing system, but also a more restricted volume (θ_0). From these data we find $D_W \sim 100$ MHz for the phospholipid bilayer with no cholesterol, and $D_W \sim 45$ MHz with the addition of cholesterol. It is interesting to note that there is an apparent difference in τ_{OR} for the cholesterol-containing liposomes. This difference in reorientation time, while suggestive of a different environment formed by the two methods, cannot be taken simply at face value. The cone angles recovered for these two liposomes are the same within experimental uncertainty, and when the fundamental quantity D_W is extracted from the θ_0 and τ_{OR} data, we find that there is no statistically discernible difference for the liposomes formed by extrusion versus those by sonication.

It is important to emphasize that, in all of the anisotropy data, we do not find any measurable differences between the molecular environments of the liposomes formed by extrusion and sonication. While there is a slight difference in the fast component of the NBD fluorescence lifetime for sonicated versus extruded liposomes containing

cholesterol, this finding is not reflected in the anisotropy decay dynamics, which are arguably a more sensitive probe of the local environment of the fluorophore. With this information, we turn to the translational diffusion behavior of the tethered fluorophore in sBLMs formed from each type of liposome.

3.4.3. Translational Diffusion in Supported Bilayer Membranes

Measurement of the fluorescence recovery in sBLMs provided information on the diffusion coefficient and mobile fraction of fluorescent lipids within the membrane. Equation (3.5) was fit to the photobleaching recovery data,[44]

$$f(t) = f(0) + \frac{m}{2}[1 - f(0)]\left\{1 - \left(\frac{8}{\pi^2}\right)\exp\left(-\frac{4\pi^2 D_L t}{a^2}\right) + \frac{1}{9}\exp\left(-\frac{36\pi^2 D_L t}{a^2}\right)\right\} \quad (3.5)$$

where $f(t)$ is the post-bleach fluorescence ($t > 0$) normalized with respect to the constant prebleach fluorescence ($t < 0$), with t=0 being the time of the bleach pulse, D_L is the average translational diffusion coefficient of the fluorophores within the bleached area, and m is the mobile fraction. The parameter a is the stripe periodicity of the Ronchi ruling in the sample plane. Equation (3.5) assumes a single diffusing species (fluorophores in the fluid sBLM) and one immobile species (fluorophores residing in unruptured vesicles attached to the surface).

Equation (3.5) was fitted to the FRAPP data for each of the systems, and the best-fit values of D_L and m were extracted (Table 3.4). These FRAPP data provided two important pieces of information. The first is that, for a given liposome composition, the

fitted values of D_L and m were the same for liposomes made by extrusion and sonication. Thus, differences in size between liposomes prepared by extrusion and sonication did not seem to affect the translational diffusion of the resulting sBLMs. The second important finding is that, as expected, the presence of cholesterol in the bilayer served to make the fluorophore less fluid. This result was fully consistent with the anisotropy decay data presented earlier, as well as previous findings that the addition of cholesterol to a phospholipid bilayer decreases the translational diffusion of the lipids.[44,88] Figure 3.5 shows a representative fluorescence recovery curve obtained for a sBLM of DOPC containing NBD-PC as a fluorescent probe.

3.5. Conclusions

The goal of this study was to compare the physical size and dynamic properties of liposomes prepared by sonication to those prepared by extrusion. Liposomes formed by the two schemes were characterized in solution and in sBLMs formed via liposome fusion on a fused silica substrate. The effect of cholesterol on the properties of the liposomes and sBLMs was also evaluated. Our findings demonstrate that, while the mean diameter and size distributions of the liposomes do indeed depend on the manner by which they are prepared, the molecular and mesoscopic organization of the BLMs, as sensed through the dynamics of a tethered fluorophore, do not depend on the manner of liposome formation. The molecular scale organization of the bilayers is determined by interactions between the constituent species, which themselves do not depend on the manner in which the bilayer is formed.

3.6. Recommendations for Future Work

We have shown that the mean diameter and size distribution of liposomes depend on the technique used to prepare them. Although bimodal size distributions were observed in both sonicated and extruded DOPC/cholesterol liposomes, the lipid/cholesterol composition associated with each peak in the distribution in unknown. It would be interesting to investigate the effect of liposome preparation methods on the compositions of the populations in each size grouping of the bimodal distribution.

This study would involve the preparation of extruded and sonicated liposomes using several lipid:cholesterol mole ratios. DLS would then be used to characterize the bimodal distributions. The two populations would then be separated using a technique such as centrifugation and doing a compositional analysis of each population would be performed using techniques such as high performance liquid chromatography and mass spectroscopy.

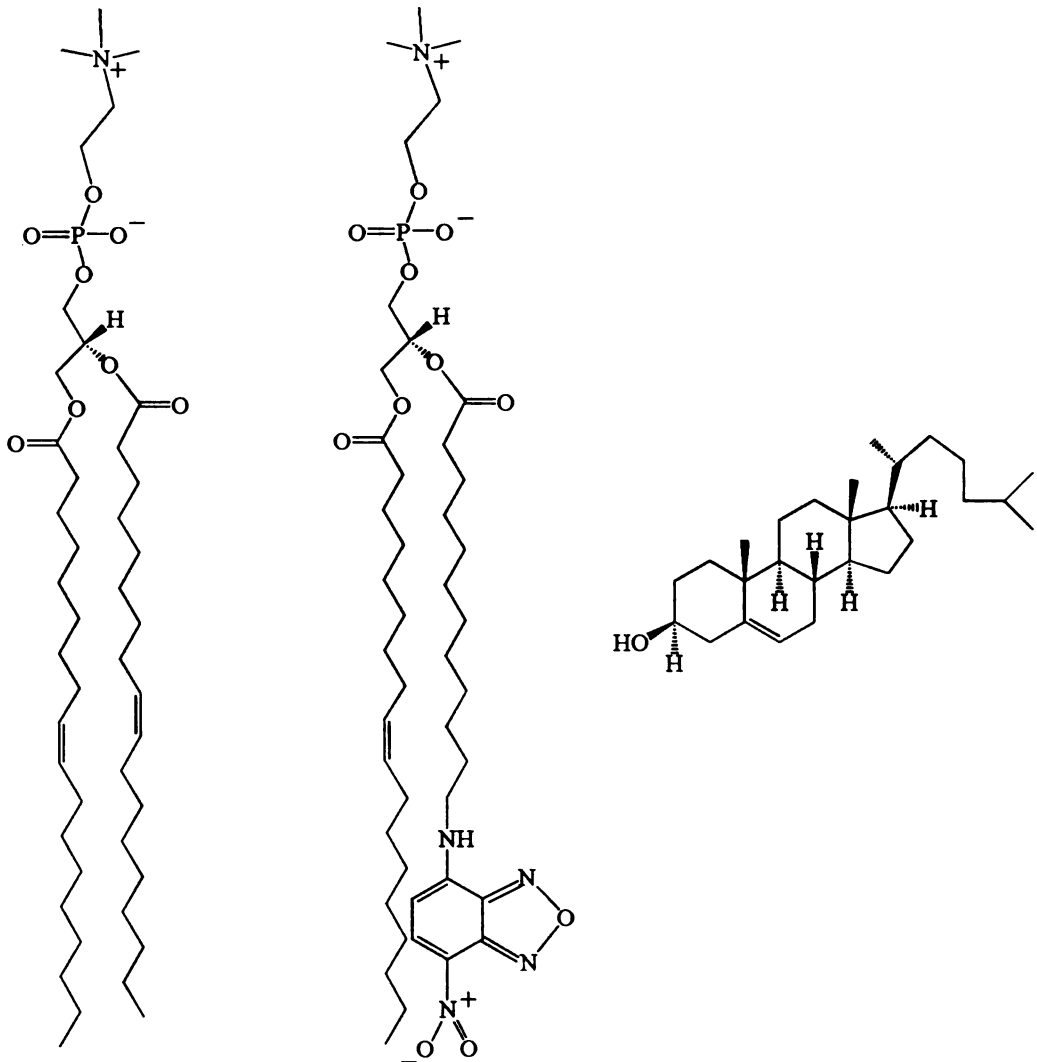

(a) (b) (c)

Figure 3.1. Molecular structures of lipids used in this study: (a) 1,2-dioleoyl-*sn*-glycero-3-phosphocholine (DOPC), (b) 1-oleoyl-2-[12-[(7-nitro-2-1,3-benzoxadiazol-4-yl)amino]dodecanoyl]-*sn*-glycero-3-phosphocholine (18:1-12:0 NBD-PC), (c) cholesterol.

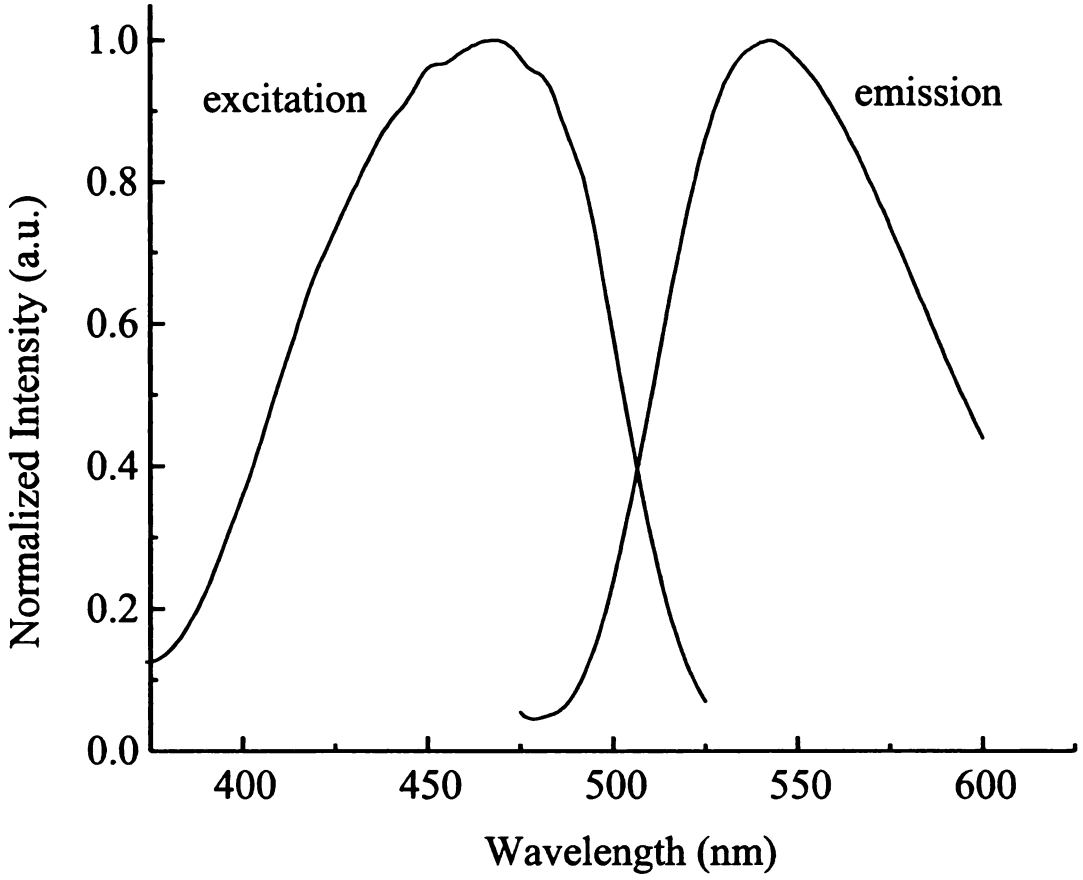

Figure 3.2. Representative excitation and emission spectra of extruded liposomes containing 98 mol% DOPC and 2 mol% NBD-PC. Both spectra have been normalized for clarity of presentation.

(a)

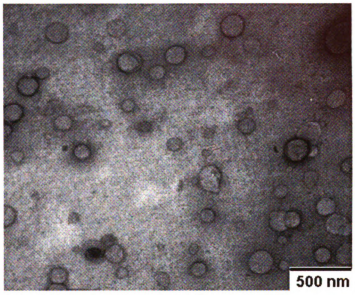

(b)

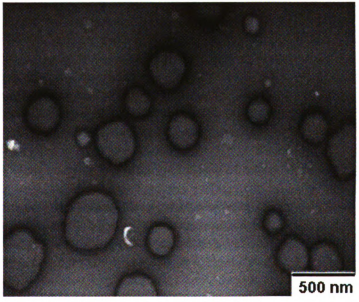

Figure 3.3. TEM images of liposomes comprising 98 mol% DOPC and 2 mol% NBD-PC produced by (a) extrusion and (b) sonication.

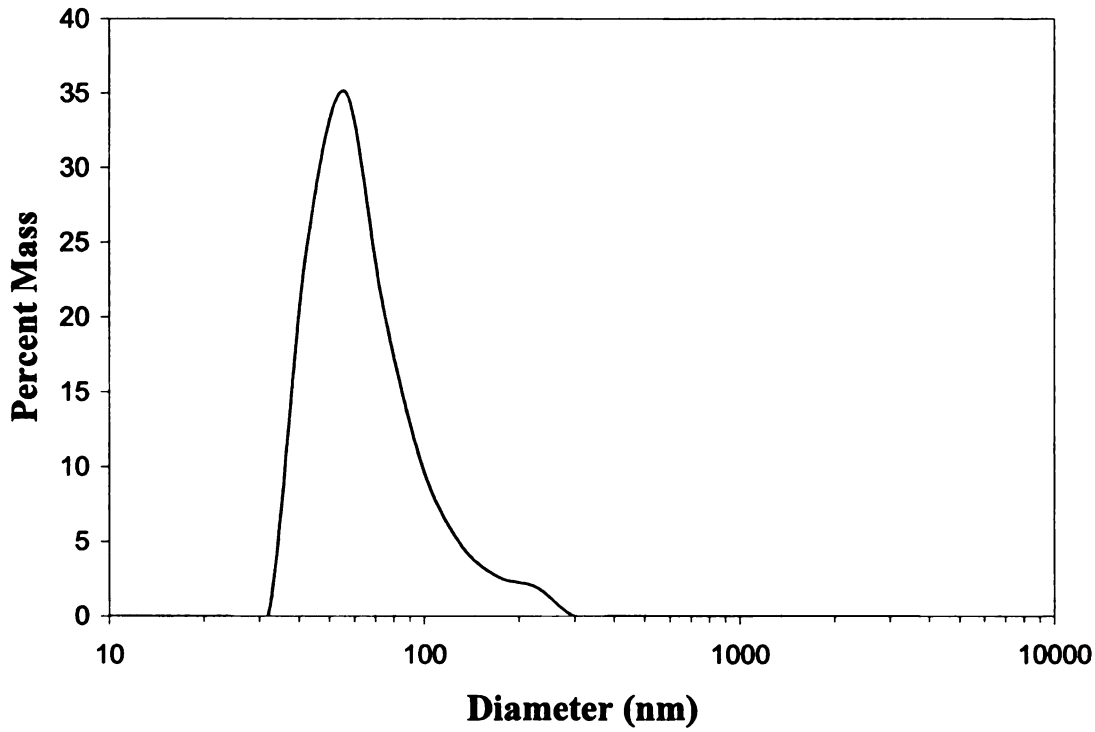

Figure 3.4. Size distribution obtained from DLS, showing percent mass as a function of diameter for extruded liposomes comprising 98 mol% DOPC and 2 mol% NBD-PC.

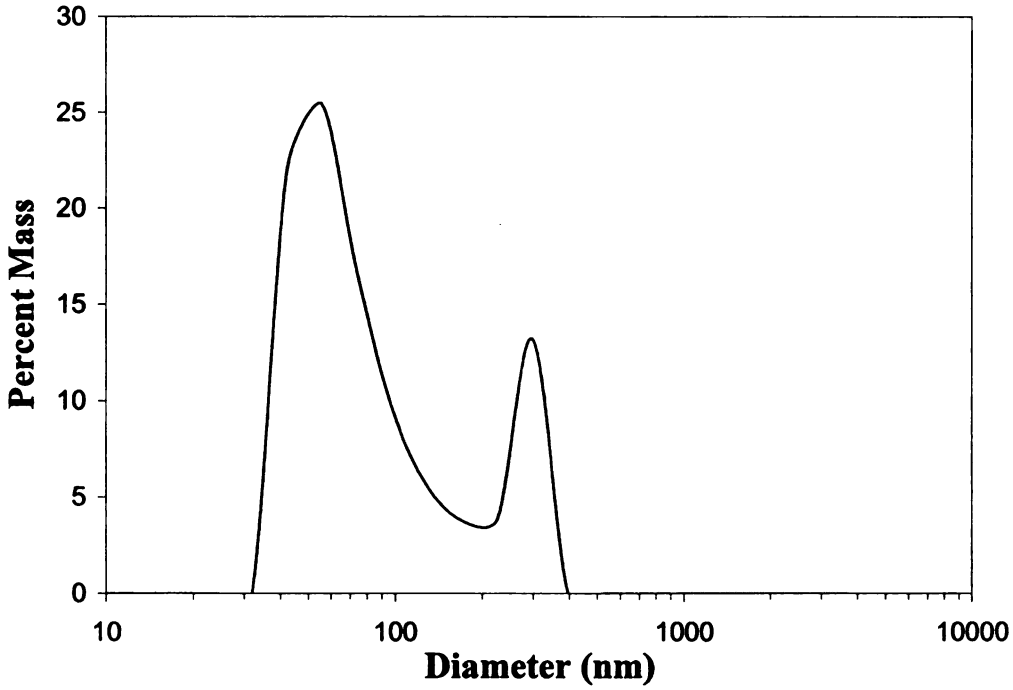

Figure 3.5. Size distribution obtained from DLS, showing percent mass as a function of diameter for extruded liposomes comprising 68 mol% DOPC, 30 mol% cholesterol, and 2 mol% NBD-PC.

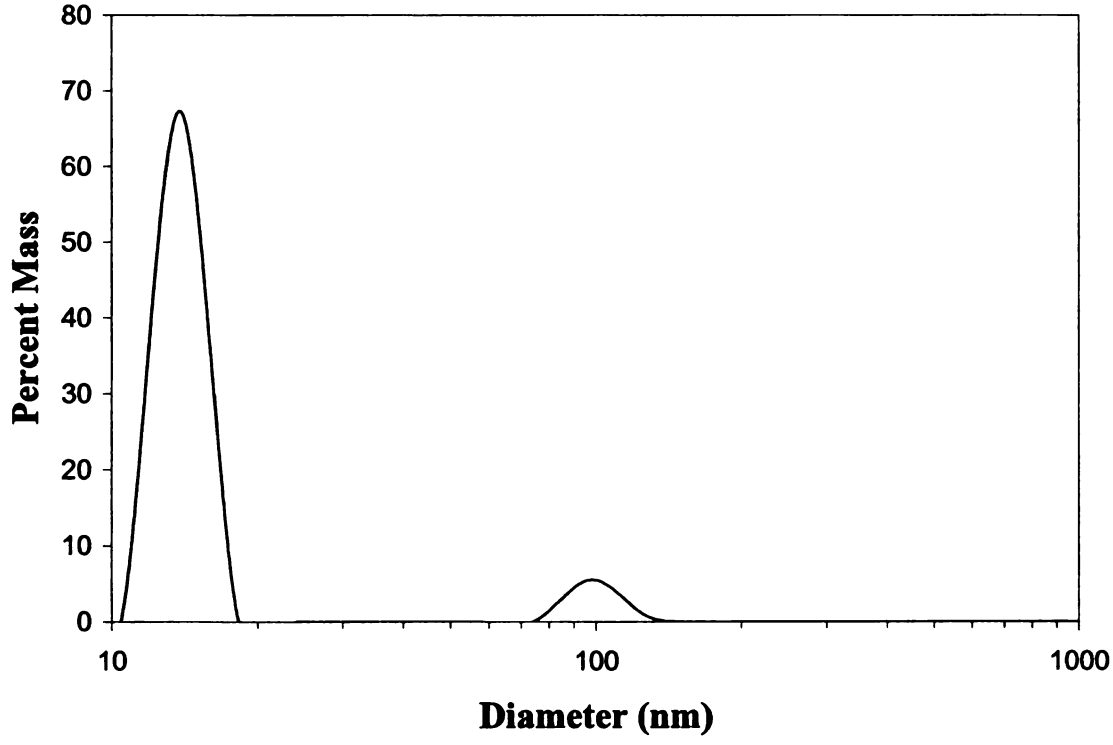

Figure 3.6. Size distribution obtained from DLS, showing percent mass as a function of diameter for sonicated liposomes comprising 98 mol% DOPC and 2 mol% NBD-PC.

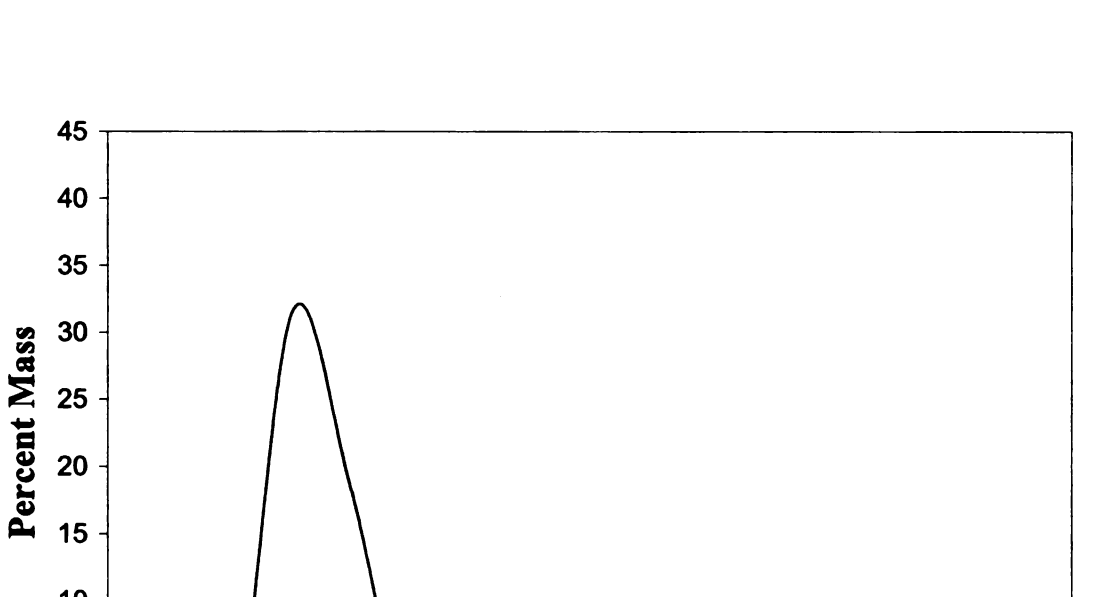

Figure 3.7. Size distribution obtained from DLS, showing percent mass as a function of diameter for sonicated liposomes comprising 68 mol% DOPC, 30 mol% cholesterol, and 2 mol% NBD-PC.

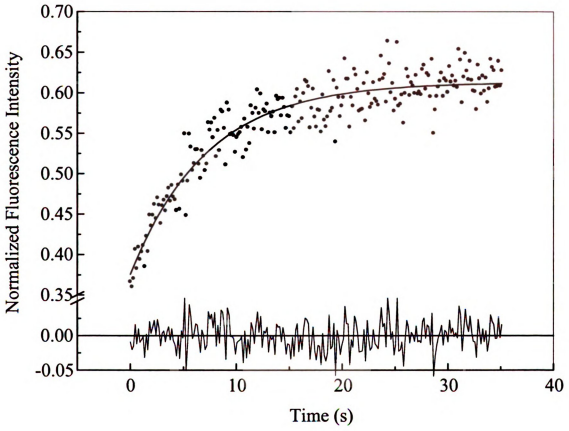

Figure 3.8. Representative FRAPP recovery curve and residual plot (below) for sBLMs comprising 98 mol% DOPC and 2 mol% NBD-PC. sBLMs were prepared with extruded liposomes. Similar recovery curves were obtained for sBLMs prepared with sonicated liposomes. Photobleaching time was 300 ms.

Table 3.1. DLS results for extruded and sonicated liposomes of two systems: (1) 98 mol% DOPC and 2 mol% NBD-PC and (2) 68 mol % DOPC, 30 mol% cholesterol, and 2 mol% NBD-PC. Data are means ± SD of three samples.

System	Mean Diameter, Extruded Vesicles (nm)	Mean Diameter, Sonicated Vesicles (nm)
1	112 ± 6	28 ± 2 and 196 ± 10
2	112 ± 6 and 600 ± 30	64 ± 3 and 259 ± 13

Table 3.2. Pre-exponential factor (A_i) ratios and fluorescence lifetimes (τ_i) of NBD-PC fluorophores in sonicated and extruded liposomes comprising (1) 98 mol% DOPC and 2 mol% NBD-PC and (2) 68 mol % DOPC, 30 mol% cholesterol, and 2 mol% NBD-PC[a].

System[b]	$A_1/(A_1+A_2)$	τ_1 (ns)	$A_2/(A_1+A_2)$	τ_2 (ns)
1 (sonicated)	0.06 ± 0.01^{A}	1.93 ± 0.26^{E}	0.94 ± 0.01^{G}	6.10 ± 0.07^{J}
1 (extruded)	0.44 ± 0.02^{B}	1.85 ± 0.10^{E}	0.56 ± 0.02^{H}	6.01 ± 0.06^{JK}
2 (sonicated)	0.31 ± 0.03^{C}	2.30 ± 0.18^{F}	0.69 ± 0.03^{I}	5.91 ± 0.10^{K}
2 (extruded)	0.27 ± 0.01^{D}	1.67 ± 0.09^{E}	0.73 ± 0.01^{I}	6.04 ± 0.08^{JK}

[a]Data represent means ± SD of three liposome solutions.

[b]Systems with statistically identical pre-exponential factor ratios and fluorescence lifetimes are labeled by common capital letters (ANOVA, Tukey post-hoc test, $p < 0.05$).

Table 3.3. Reorientation times (τ_{OR}), confined cone semi-angles (θ_0), and wobbling diffusion coefficients (D_w) of NBD-PC in sonicated and extruded liposomes comprising (1) 98 mol% DOPC and 2 mol% NBD-PC and (2) 68 mol % DOPC, 30 mol% cholesterol, and 2 mol% NBD-PC[a].

System[b]	τ_{OR} (ns)	θ_0 (°)	D_w (MHz)
1 (sonicated)	3.03 ± 0.22^{A}	62 ± 5^{C}	113 ± 27^{E}
1 (extruded)	2.94 ± 0.09^{A}	57 ± 5^{C}	98 ± 21^{E}
2 (sonicated)	3.59 ± 0.28^{B}	42 ± 3^{D}	44 ± 10^{F}
2 (extruded)	3.00 ± 0.22^{A}	37 ± 2^{D}	41 ± 8^{F}

[a]Data represent means ± SD of three liposome solutions.

[b]Systems with statistically identical τ_{OR}, θ_0, and D_w are labeled by common capital letters (ANOVA, Tukey post-hoc test, $p < 0.05$).

Table 3.4. Translational diffusion coefficients (D_L) and mobile fractions for NBD-PC in sBLMs prepared with sonicated and extruded liposomes comprising (1) 98 mol% DOPC and 2 mol% NBD-PC and (2) 68 mol % DOPC, 30 mol% cholesterol, and 2 mol% NBD-PC[a].

System[b]	D_L ($\mu m^2/s$)	Mobile Fraction
1 (extruded)	2.24 ± 0.25^{A}	0.78 ± 0.18^{C}
1 (sonicated)	2.02 ± 0.15^{A}	0.81 ± 0.11^{C}
2 (extruded)	1.65 ± 0.22^{B}	0.73 ± 0.10^{C}
2 (sonicated)	1.72 ± 0.04^{B}	0.69 ± 0.06^{C}

[a]Data represent means ± SD of three liposome solutions.

[b]Systems with statistically identical D_L and mobile fractions are labeled by common capital letters (ANOVA, Tukey post-hoc test, $p < 0.05$)

4. EFFECT OF HYDROGEN BONDING ON THE ROTATIONAL AND TRANSLATIONAL DYNAMICS OF A HEAD GROUP-BOUND FLUOROPHORE IN BILAYER MEMBRANES

4.1. Abstract

We have studied diffusion transport properties of the fluorescently tagged phospholipid 1,2-dioleoyl-*sn* glycero-3-phosphoethanolamine-N-7-nitro-2-1,3-benzoxadiazol-4-yl (18:1 NBD-PE) embedded in the head group region of bilayer lipid membranes comprising DOPC and 1,2-dioleoyl-*sn*-glycero-3-[Phospho-*rac*-(1-glycerol)] (DOPG). The dynamics of the fluorophore were examined using TCSPC to measure rotational diffusion in lipid vesicles, and FRAPP to determine translational diffusion coefficients and mobile fractions in sBLMs. TCSPC data revealed that fluorophore rotational diffusion coefficients in DOPG vesicles were not statistically different from those in DOPC and mixed DOPC/DOPG vesicles, suggesting that the NBD-PE fluorophore does not interact strongly with the head group region of these bilayers. However, FRAPP experiments showed that lateral diffusion is statistically lower in mixed DOPC/DOPG supported bilayers than in DOPC supported bilayers. These results suggest that bilayers containing DOPG likely undergo inter-lipid head group hydrogen bonding interactions that suppress translational diffusion.

4.2. Introduction

Model BLMs in the form of liposomes in solution,[89] sBLMs on underlying substrates,[22] and tBLMs on polymer cushions or monolayers[8,90] can be used to mimic the

properties and dynamics of cell membranes.[24,35] Membrane fluidity is an important property of the bilayer that influences cellular functions such as signaling,[91] protein activity,[92] and response to stimuli.[2] For example, transbilayer diffusion of nitric oxide, an important signaling molecule that transmits information between mammalian cells, has been shown to decrease with decreasing membrane fluidity.[93] An increase in the fluidity of mammalian endoplasmic reticulum (ER) membranes resulted in the activation of certain membrane-bound transcription factors, while activation of transcription factors in ER yeast membranes was triggered by a decrease in fluidity.[94]

One of several ways that cells may control membrane fluidity is by adjusting the concentration of the membrane constituents. For example, incorporation of lysophosphatidylcholine lipids into egg-phosphatidylcholine (egg-PC) sBLMs has been shown to increase the translational diffusion coefficient due to fewer van der Waals interactions between hydrophobic tailgroups. On the other hand, addition of egg-phosphatidylethanolamine into egg-PC sBLMs resulted in pronounced head group hydrogen bonding, thus enhancing van der Waals interactions due to tighter packing and lowering of the translational diffusion coefficient.[22] Bacterial cells have been shown to isomerize unsaturated membrane fatty acids from *cis* to *trans* conformations in the presence of solvents or toxins in order to decrease membrane fluidity and prevent entry into the cell.[95] The addition of cholesterol to membranes has been well-documented to decrease fluidity.[35,96]

In the present study, we investigated the effect of phospholipid head group hydrogen bonding on the translational and rotational dynamics of the chromophore 18:1 NBD-PE embedded in BLMs comprising DOPC and DOPG. The molecular structures of

these lipids are shown in Figure 4.1. DOPC and DOPG were chosen as the primary lipids in this study for two reasons. First, these lipids have low transition temperatures of -20°C for (DOPC)[97] and -18°C for (DOPG),[23] which ensures that bilayers reconstituted from these species would exist in a disordered fluid phase at room temperature (23 ± 2°C). Second, the two lipids have identical acyl chain lengths but different head group functionalities, so differences in fluorophore dynamics can be attributed primarily to head group interactions.

The DOPG glycerol head group contains two hydroxyl moieties that can function as either hydrogen bond donors or acceptors. Hydrogen bonds are comparatively strong intermolecular interactions (10 to ca. 30 kJ/mol[21]). However, the DOPC head group does not contain any functionalities for hydrogen bonding and, as such, should not participate in head group-head group interactions in a manner analogous to DOPG.

Although zwitterionic PC lipids such as DOPC comprise the majority of lipids found in biological membranes, anionic lipids such as DOPG also play significant roles in regulating membrane function.[98] PG lipids are believed to be responsible for maintaining membrane lipid surface charge density, a property that not only affects membrane permeability to ions and charged metabolites, but also the activity of certain membrane proteins.[99] MD simulations of PC lipid bilayers have generated radial distribution functions showing hydrogen bonding interactions between the oxygen atoms of adjacent phosphate molecules through water bridges, as well as screened electrostatic interactions between the negatively charged phosphate oxygen and the positively charged choline nitrogen.[100-103] PG lipids, in contrast, are rich in head group functionalities that can form hydrogen bonds with other membrane constituents.[104,105] Hydrogen-bonded

water bridges have also been predicted in MD simulations of PG bilayers,[10,11,106] and there is the additional capability of forming hydrogen bonds between the glycerol moiety and phosphate oxygen of neighboring PG lipids.[23,107] Hydrogen bonds within BLMs may be measured directly using infrared spectroscopy[108] or indirectly by using fluorescence spectroscopy to monitor the dynamics of fluorophore-tagged lipids in the BLM. In this study, we investigated interactions between 18:1 NBD-PE, which will be referred to as NBD-PE throughout the remainder of this chapter, and head group regions of neighboring lipids in liposomes and sBLMs. We measured translational diffusion coefficients and mobile fractions with FRAPP, and fluorescence lifetimes and rotational diffusion coefficients with TCSPC.

We reasoned that a lipid with a head group-bound fluorophore was a better choice for this study than a fluorescent lipid which has the fluorophore located at the terminus of a lipid acyl chain. The fluorescently-tagged lipid used in this study (NBD-PE) has the NBD fluorophore attached to its polar head group, allowing the influence of head group interactions to be investigated. In addition, the two bulk lipids used to form the BLM, DOPC and DOPG, have identical hydrophobic tailgroup structures, but differ in head group functionalities. Thus, using NBD-PE as the probe allowed us to examine molecular issues related primarily to the lipid head group interactions while maintaining comparatively constant acyl chain interactions. We note that we can make intact liposomes composed of 98 mol% DOPG, an anionic lipid. However, no direct comparison of fluorophore dynamics between purely anionic liposomes and purely anionic sBLMs can be made because, for sBLM structures on surfaces, only limited concentrations (up to 39 mol%) of anionic lipids such as DOPG can produce fluid bilayer

structures.[109] Regardless of this limitation, it is possible to compare mixed lipid systems in both liposome and sBLM structures, and FRAPP and TCSPC data provide useful insight into the dynamical properties of the NBD-PE contained within them.

4.3. Materials and Methods

4.3.1. Vesicle Preparation

Phospholipids DOPC, DOPG, and NBD-PE were purchased from Avanti Polar Lipids Inc. (Alabaster, AL) and used without further purification. 1 mM lipid solutions of DOPC/NBD-PE (98 mol%, 2 mol%), DOPG/NBD-PE (98 mol%, 2 mol%), or DOPC/DOPG/NBD-PE (59 mol%, 39 mol%, 2 mol%) were prepared by evaporating the chloroform solvent from the lipid mixture and hydrating the dry lipid film for 30 min with Tris®-HCl buffer (Sigma-Aldrich, St. Louis, MO) containing NaCl (Fisher Scientific, Fair Lawn, NJ) prior to extrusion. The buffer (10 mM Tris®, 150 mM NaCl, pH 8) was prepared using water from a Milli-Q Plus water purification system (Millipore, Bedford, MA). The mixtures were processed five times through a freeze-thaw-vortex cycle to ensure complete mixing of the sample constituents. Each cycle consisted of immersion in liquid nitrogen for 5 min, followed by immersion in a 60°C water bath for 5 min, and then vortexing the thawed sample for 2 min. The hydrated mixtures were extruded 11 times through a polycarbonate membrane with nominal pore diameters of 100 nm and 2000 nm (Avanti Polar Lipids Inc., Alabaster, AL). All extrusions were performed at room temperature (23 ± 2°C).

4.3.2. Time-Correlated Single Photon Counting

Time-resolved fluorescence anisotropy and lifetime data were measured using TCSPC. The details of this technique can be found in Section 2.3 of this dissertation. For each lipid system considered in this work, three separate liposome solutions were interrogated with TCSPC.

4.3.3. Deposition of Supported Lipid Bilayers

Fused silica microscope slides (75 mm x 25 mm x 1 mm) were purchased from Technical Glass Products, Inc. (Painesville, OH). The slides were cleaned by bath sonication (Branson 1510, Branson Ultrasonic Corporation, Danbury, CT) in detergent solution for 20 min, rinsed with DI water, baked at 160°C for 4 h, and plasma treated (Harrick Plasma, Ithaca, NY) with oxygen under vacuum (150 mTorr) for 10 min immediately before bilayer deposition. sBLMs were deposited by liposome fusion in a custom-made flow cell described elsewhere.[68] The flow cell was initially washed with buffer, followed by a 3-h incubation with liposome solution and a final buffer wash to remove unadsorbed liposomes. All experiments were performed at room temperature (23 ± 2°C).

4.3.4. Fluorescence Recovery After Pattern Photobleaching

FRAPP was used to measure the translational diffusion and mobile fractions of fluorophores embedded in sBLMs formed on fused silica microscope slides. The details of this technique are in Section 2.2 of this dissertation. For each lipid system considered

in this work, three separate sBLM interfaces were formed on silica slides and each interface was interrogated with FRAPP at five different locations of the bilayer.

4.3.5. Statistical Analysis

Data fitting was accomplished using OriginPro 7.5 (OriginLab Corporation, Northampton MA), which uses the Levenberg-Marquardt algorithm for non-linear least squares fitting. An F-test comparison was conducted to determine whether an exponential model using n parameters provided a statistically significant improvement in the goodness of the fit of fluorescence lifetime and fluorescence anisotropy data than an exponential model using n-1 parameters. Rotational diffusion coefficients (D_x, D_y , D_z) and translational diffusion coefficients (D_L) are reported as means ± SD. Multiple comparison ANOVA with a post-hoc Tukey test ($p < 0.05$) was used to determine if differences among the means were statistically significant.

4.4. Results and Discussion

The goal of this work was to investigate the intermolecular lipid-lipid interactions between head groups in bilayer structures by examining the rotational and translational diffusion behavior of a fluorophore embedded in liposomes and sBLMs. We consider the rotational diffusion and fluorescence lifetime data first.

4.4.1. Fluorescence Lifetime and Anisotropy Data

Fluorescence lifetime and anisotropy decay data provided information on the molecular environment(s) of the NBD fluorophore in vesicles of the following compositions: 1) 98 mol% DOPC and 2 mol% NBD-PE, 2) 98 mol% DOPG and 2 mol% NBD-PE, and 3) 59 mol% DOPC, 39 mol% DOPG, and 2 mol% NBD-PE. We also examined vesicles 100 nm and 2000 nm in diameter to assess the influence of membrane curvature on rotational dynamics. For all measurements, there were no statistical differences in either the lifetime or the anisotropy data (not shown) for the two vesicle sizes, suggesting that size is not an important issue.

The F-statistic analysis showed that a two-component exponential decay was the best fit for the fluorescence lifetime data for NBD-PE in each vesicle system (Figure 4.2, Table 4.1). There are two possible explanations for this finding. Either the fluorophore exists in two different environments, with populations that do not exchange significantly on the timescale of the excited state relaxation, or the fluorophore exists in a dielectric gradient where slight changes in the location and/or orientation of the fluorophore with respect to the gradient give rise to a distribution of fluorescence lifetimes (Figure 4.3). This latter condition has been previously reported for the NBD fluorophore.[65,73] While it may be tempting to ascribe the different lifetime components to specific chemical environments, the dependence of fluorescence lifetime on intramolecular and intermolecular properties is sufficiently complex that it is not possible to make such assignments in the absence of additional information. Fluorescence anisotropy decay data (Figure 4.4, Table 4.1), in contrast, can be interpreted within the context of well established theoretical models.[47,48,82,110] The anisotropy decay function, $r(t)$, is formulated

as the normalized transient difference in emission intensity parallel, $I_{\parallel}(t)$, and perpendicular, $I_{\perp}(t)$, to the polarization of the incident excitation pulse as depicted in Equation (3.1).

The functional form of $r(t)$ contains chemically relevant information. In particular, there are two possible choices for the interpretation of our fluorescence anisotropy data because the fluorophore is attached to the head group of the phospholipid. The functional form of the anisotropy decay allows us to determine whether this vesicle-incorporated fluorophore behaves as a free or hindered rotor.

A free rotor, such as a fluorophore in solution, is characterized by a zero infinite-time anisotropy because the fluorophore can assume all orientations with equal probability. It is important to note that if the fluorophore is free to reorient within a hemisphere, it will behave as a free rotor because of the inherent polarization symmetry of the incident electric field. By contrast, for a fluorophore tethered to a lipid (as NBD is in NBD-PE), under the condition that the probe is not free to access all possible orientations, a non-zero infinite-time anisotropy, $r(\infty)$, results.[47,82] Based on an F-statistic analysis, we determined that our experimental data were characterized by a two-component exponential anisotropy decay for each of the three lipid systems used in this study and, for each, the infinite-time anisotropy, $r(\infty)$, was zero within the experimental uncertainty. The absence of an infinite-time anisotropy component in the data suggests that the fluorophore is able to reorient within a hemispherical volume and, as such, it can be treated as a free rotor.

The simplest way to model a fluorophore is to assume that it sweeps out a spherical volume as it rotates. For this case, we can directly relate the reorientation time to the average diffusion rate, D, through the Debye-Stokes-Einstein equation[111]:

$$\tau_{OR} = \frac{\eta V}{k_B T} = \frac{1}{6D} \tag{4.1}$$

Here, η is the solvent viscosity, V is the spherical volume, k_B is the Boltzmann constant, and T is the absolute temperature.

Most fluorophores are not circular in shape, but rather elliptical. Therefore, the volumes they sweep out as they rotate are more ellipsoidal than spherical. A model developed by Chuang and Eisenthal[48] for fluorophores with full motional freedom in solution treats fluorophores as either Type I (prolate) or Type II (oblate) ellipsoidal rotors (Figure 4.5) and relates the anisotropy function, $r(t)$, to diffusion coefficients about each of the Cartesian axes. We interpret our anisotropy decay data in the context of this Chuang and Eisenthal model.[48] The same essential physics underlying the Chuang and Eisenthal model must also apply to the dynamics of a tethered fluorophore, especially when the fluorophore is free to relax in a hemispherical volume (*i.e.* no confining cone). In this model, the Cartesian axes are typically assigned so that the z-axis is perpendicular to the π-system plane and the absorbing and emitting transition dipole moments lie along either the x-axis (long axis) or y-axis (short axis) of the molecular plane.[112] The two limiting cases of this model treat the fluorophore as either a Type I or a Type II rotor, thereby significantly simplifying the mathematics. The excited and emitting transition

dipoles lie coincident with and perpendicular to the unique rotational axis for Type I ($D_x \neq D_y = D_z$) and Type II ($D_x = D_y \neq D_z$) rotors, respectively. The reorientation decay time constants are related to the Cartesian components of the rotational diffusion coefficients through the anisotropy decay function as given in Equation (4.2) to Equation (4.5) below:[113]

For a transition dipole oriented along the long x-axis:

$$\text{Type I:} \quad r(t) = \left(\frac{4}{10}\right)\exp\left(-6D_z t\right) \tag{4.2}$$

$$\text{Type II:} \quad r(t) = \left(\frac{1}{10}\right)\exp\left(-\left(2D_x + 4D_z\right)t\right) + \left(\frac{3}{10}\right)\exp\left(-6D_x t\right) \tag{4.3}$$

For a transition dipole oriented along the short y-axis:

$$\text{Type I:} \quad r(t) = \left(\frac{1}{10}\right)\exp\left(-\left(2D_z + 4D_x\right)t\right) + \left(\frac{3}{10}\right)\exp\left(-6D_z t\right) \tag{4.4}$$

$$\text{Type II:} \quad r(t) = \left(\frac{4}{10}\right)\exp\left(-\left(2D_z + 4D_x\right)t\right) \tag{4.5}$$

In this model, the resolution of two reorientation time constants indicates that the NBD fluorophore behaves as either an x-axis polarized Type II rotor or a y-axis polarized Type I rotor, according to Equation (4.3) and Equation (4.4). Previous studies of the solution phase NBD fluorophore using one and two-photon excitation methods suggest

that the $S_1 \leftarrow S_0$ transition of this fluorophore is short-axis polarized, and a two-component anisotropy decay would be consistent with NBD reorienting as a Type I rotor (Equation (4.4)).[77] We will use this assignment to evaluate the Cartesian components of the rotational diffusion coefficient for NBD-PE.

There are no statistically significant differences between the Cartesian components of the diffusion coefficients (Table 4.2) of tethered NBD in each of the liposome systems. The data all indicate that the tethered NBD fluorophore is a substantially anisotropic rotor, with an aspect ratio of $D_x/D_z \sim 8$. While it may be tempting to consider the subtle differences between the D_z and D_x values and the ratio of these coefficients, the uncertainty in the data is sufficiently large that it is not possible to draw any system-dependent conclusions without other information. The fact that NBD sweeps out an ellipsoidal volume that is more anisotropic than its axial ratio (see NBD-PE structure in Figure 4.1) points to the importance of the tethering bond, even in situations where motion is not constrained to a conic volume.

Rotational diffusion measurements can provide information on the molecular-scale environment of the reorienting fluorophore, and the information we obtain for NBD-PE on the molecular length scale suggests that the dynamics of the lipid head group are determined to a significant extent by the layer of fluid in immediate contact with the lipid bilayer. This finding is consistent with our observation of a two-component fluorescence lifetime, which can be accounted for in the context of the fluorophore residing in a dielectric gradient. The molecular-scale information does not provide a complete picture, however, of the fluid properties of the bilayer lipid membranes. We also need to consider molecular motion over longer length scales, and we accomplish this

task through the use of translational diffusion measurements of NBD-PE in sBLM systems.

4.4.2. Translational Diffusion in Supported Bilayer Lipid Membranes

Translational diffusion coefficients and mobile fractions were measured with FRAPP to provide information complementary to our TCSPC fluorescence lifetime and anisotropy decay data. Because DOPG vesicles did not adsorb on fused silica and rupture to form functional bilayers, FRAPP studies were limited to two systems: 1) 98 mol% DOPC and 2 mol% NBD-PE, and 2) 59 mol% DOPC, 39 mol% DOPG, and 2 mol% NBD-PE. We determined that 39 mol% DOPG was the maximum concentration of the anionic lipid that would lead to the reconstitution of stable fluid sBLMs. This finding is consistent with previous studies under similar buffer conditions.[22,114]

A typical FRAPP recovery curve for a DOPC/NBD-PE bilayer is shown in Figure 4.6, and calculated D_L values and mobile fractions are given in Table 4.3. Equation (3.5) was used to extract both diffusion coefficients and mobile fractions. We determined that differences between the mobile fractions were not statistically significant for bilayers formed with both lipid compositions. However, differences between D_L values were statistically significant. The diffusion coefficients were 2.91 ± 0.31 $\mu m^2/s$ for DOPC bilayers and 1.82 ± 0.24 $\mu m^2/s$ for mixed DOPC/DOPG bilayers, indicating that addition of DOPG retards the translational diffusion of NBD-PE.

4.4.3. Head group Hydrogen Bonding in Bilayer Membranes

Despite the fact that NBD and DOPG have the capacity to interact via hydrogen bonds, we observe no effect on the rotational diffusion measurements upon addition of DOPG. This suggests that the NBD-PE fluorophore does not have a measurable preference for interacting with either DOPG or DOPC lipid head groups. NBD-PE translational diffusion in DOPC/DOPG sBLMs does, however, seem to be hindered relative to that in pure DOPC sBLMs, suggesting that the intermolecular interactions in the head group region of the lipids may mediate the translational motion of the bilayer constituents. This finding is consistent with recent MD simulations involving PC and PG bilayers that suggest the intramolecular and intermolecular hydrogen bonding capability of PG in POPG bilayers reduces fluidity relative to 1-palmitoyl-2-oleoyl-*sn*-glycero-3-phosphocholine (POPC) bilayers.[9]

In addition to head group hydrogen bonding interactions, changes in translational bilayer fluidity may also be attributed to variations in bilayer thickness. MD simulations have reported the thickness of pure 1-palmitoyl-2-oleoyl-sn-glycero-3-phospho-(1'-sn-glycerol) (POPG) bilayers as ~ 43 Å and that of pure POPC bilayers as ~ 37 Å, suggesting that POPG lipids are organized more rigidly and therefore diffuse more slowly. Therefore, the lower D_L for the DOPC/DOPG system could also be attributed, in part, to a thicker bilayer membrane.

We now turn to a consideration of how these two bodies of data can be reconciled. The rotational diffusion data indicate that, at the molecular level, the rotational motion of fluorophores localized in the headgroup region of the bilayer is not mediated significantly by the headgroup structure or organization of the lipids. This

situation is primarily because of the presence of bulk solvent in close contact with this region of the lipid bilayer structure. The fact that the translational diffusion of these fluorophores in the bilayers does depend on lipid headgroup identity could be because the measurement involves the translational motion of the entire lipid molecule, and the fact that translational motion can depend significantly on any structural heterogeneity that is present in the bilayer. In our translational diffusion data, there appear to be regions of the supported bilayer structure that are comparatively less mobile than others. The notion of immobile regions is not surprising for the DOPC/DOPG mixed systems in light of the large amount of literature extant relating to the formation of phase-separated structures. The basis for such phase segregation is understood from a thermodynamic point of view for multicomponent systems,[115-122] but for single-component systems, it is fair to question the origin of such features. One possibility is that there exist interactions between the sBLM bottom leaflet and the supporting substrate that give rise to comparatively fewer mobile regions.

4.5. Conclusions

We have investigated the dynamics of a tethered fluorophore (NBD-PE) in unilamellar DOPC, DOPG, and mixed DOPC/DOPG vesicles, and in DOPC and mixed DOPC/DOPG supported bilayer lipid membranes. We used both PC and PG to evaluate the role of head group hydrogen bonding interactions in mediating the fluidity of lipid bilayer structures. Within the experimental uncertainty, we obtained the same rotational diffusion results for tethered NBD in each system for vesicles sizes of both 100 nm and 2000 nm diameter. Our data showed that the molecular-scale rotational motion of the

NBD fluorophore does not depend on the type of lipid in the bilayer. We also measured the translational diffusion of NBD-PE in sBLMs consisting of pure DOPC and a mixture of DOPC and DOPG. The data indicate a slower rate of translational diffusion in sBLMs containing DOPG. We believe this is due to hydrogen bonding interactions in the headgroup region of the constituent lipids, even though the effect on rotational diffusion appears to be much less pronounced.

4.6. Recommendations for Future Work

A lipid such as DOPG, with a head group functionality capable of hydrogen bonding, was shown in this study to significantly influence the translational motion of NBD-PE in sBLMs, but not the rotational motion of NBD-PE in a liposomes. Performing the same FRAPP and TCSPC experiments with an NBD tailgroup-bound fluorophore such as NBD-PC (instead of head group-bound fluorophore like NBD-PE) in DOPC and DOPG model BLMs would complement the work done with NBD-PE. A tailgroup-bound NBD-PC fluorophore is likely more sensitive to the hydrophobic region of the bilayer and should provide a more complete picture of the dynamics of lipid mixtures such as PC and PG. An additional suggestion is to use other lipids that are prone to hydrogen bonding interactions, such as phosphatidylserine, in BLMs and compare those dynamics results with those measured for PG systems.

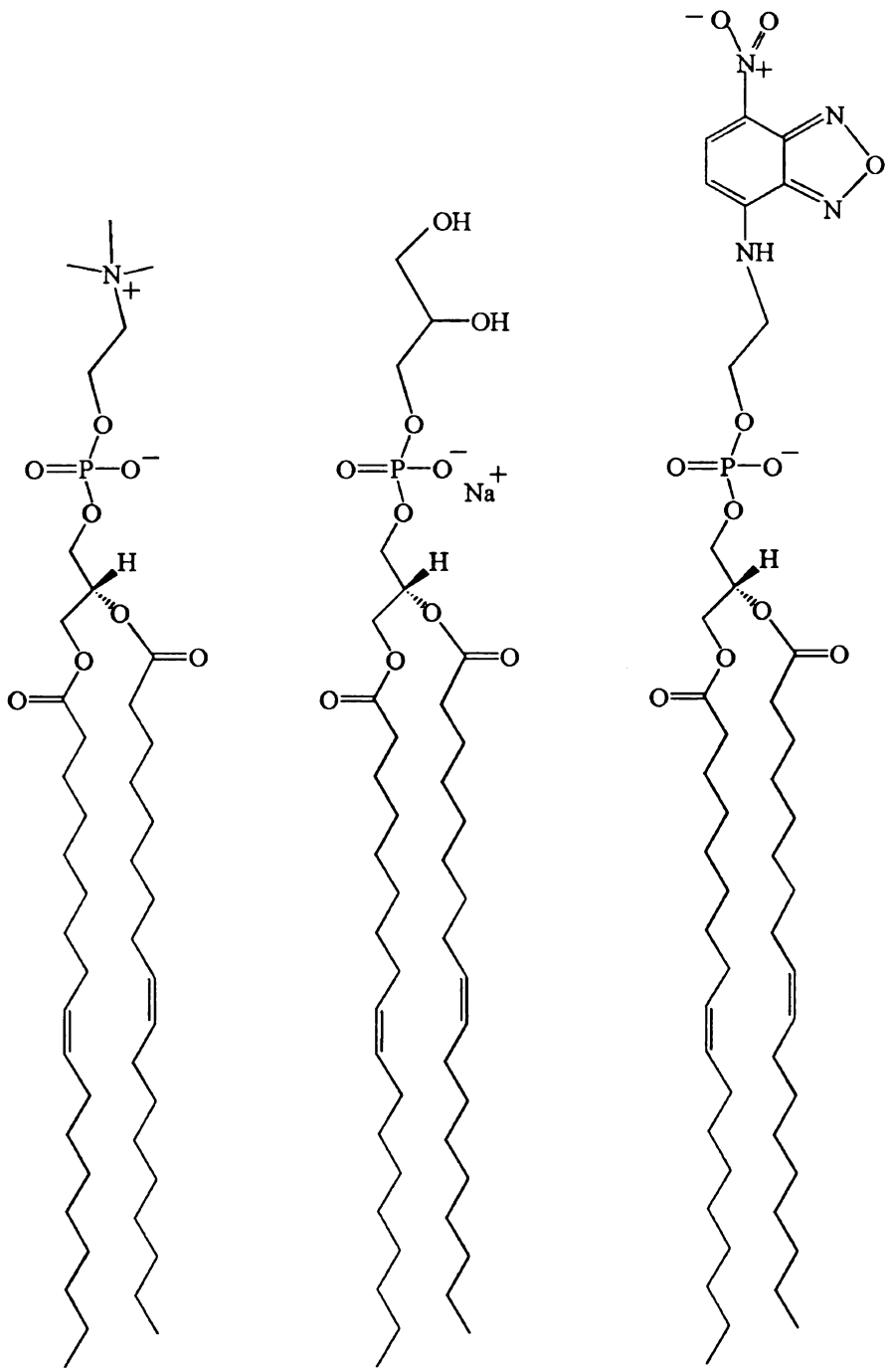

(a) (b) (c)

Figure 4.1. Molecular structures of lipids used in this study: (a) 1,2-dioleoyl-*sn*-glycero-3-phosphocholine (DOPC), (b) 1,2-dioleoyl-*sn*-glycero-3-[Phospho-*rac*-(1-glycerol)] (DOPG), (c) 1,2-dioleoyl-*sn* glycero-3-phosphoethanolamine-N-7-nitro-2-1,3-benzoxadiazol-4-yl (18:1 NBD-PE).

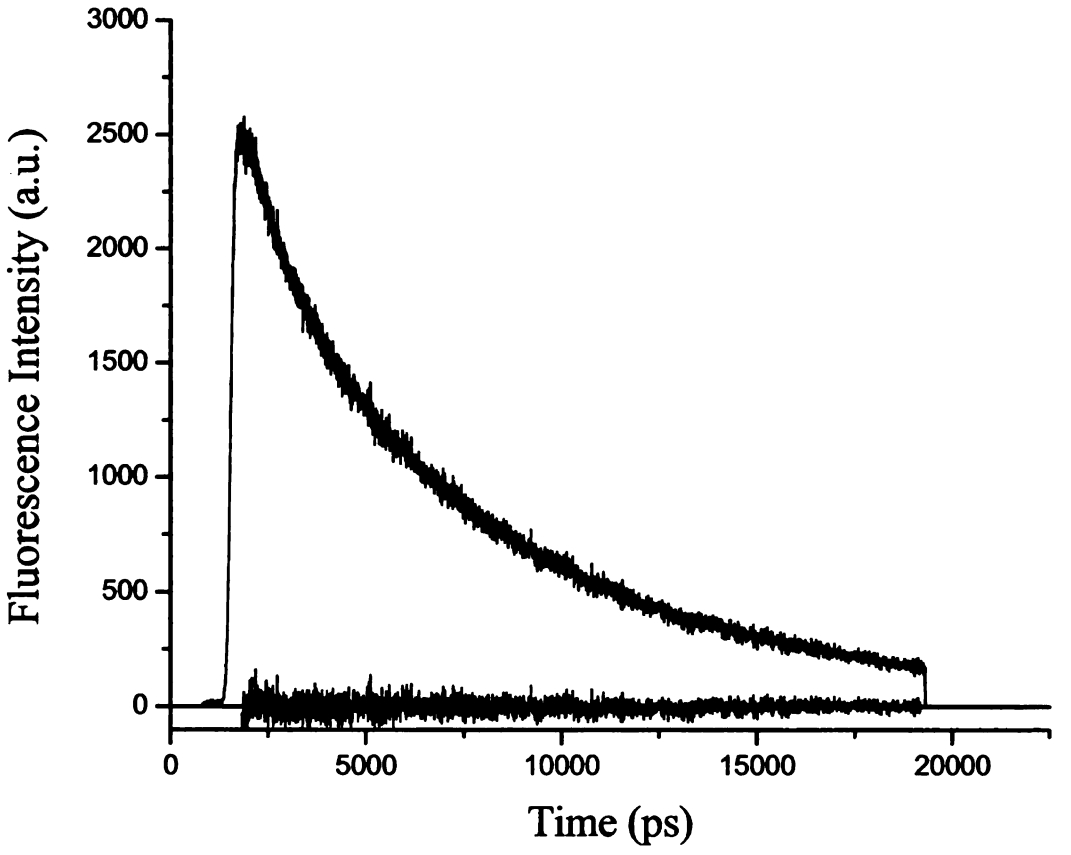

Figure 4.2. Representative fluorescence lifetime data and residual plot (below) for NBD-PE in DOPG/DOPC lipid vesicles. A two-parameter exponential decay, corresponding to two fluorescence lifetimes (τ_1 and τ_2), gave the best fit of the data. F-test statistics were used to determine the statistical difference in goodness of fit for higher parameter exponentials.

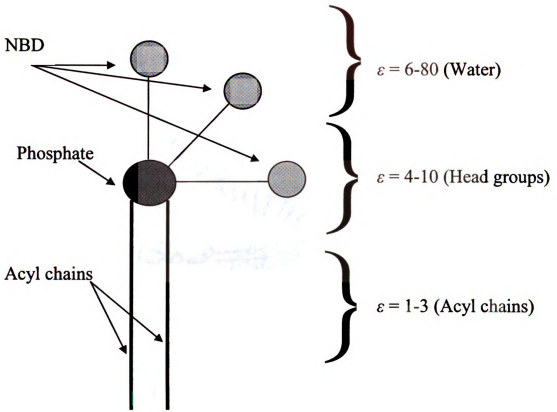

Figure 4.3. Schematic diagram of the NBD-PE molecule. The NBD fluorophore exists in a range of locations in a dielectric gradient, where ε denotes the dielectric constant in different regions of the lipid. We interpreted our results in the context that multiple fluorescence lifetimes arise from NBD diffusing in a dielectric gradient.

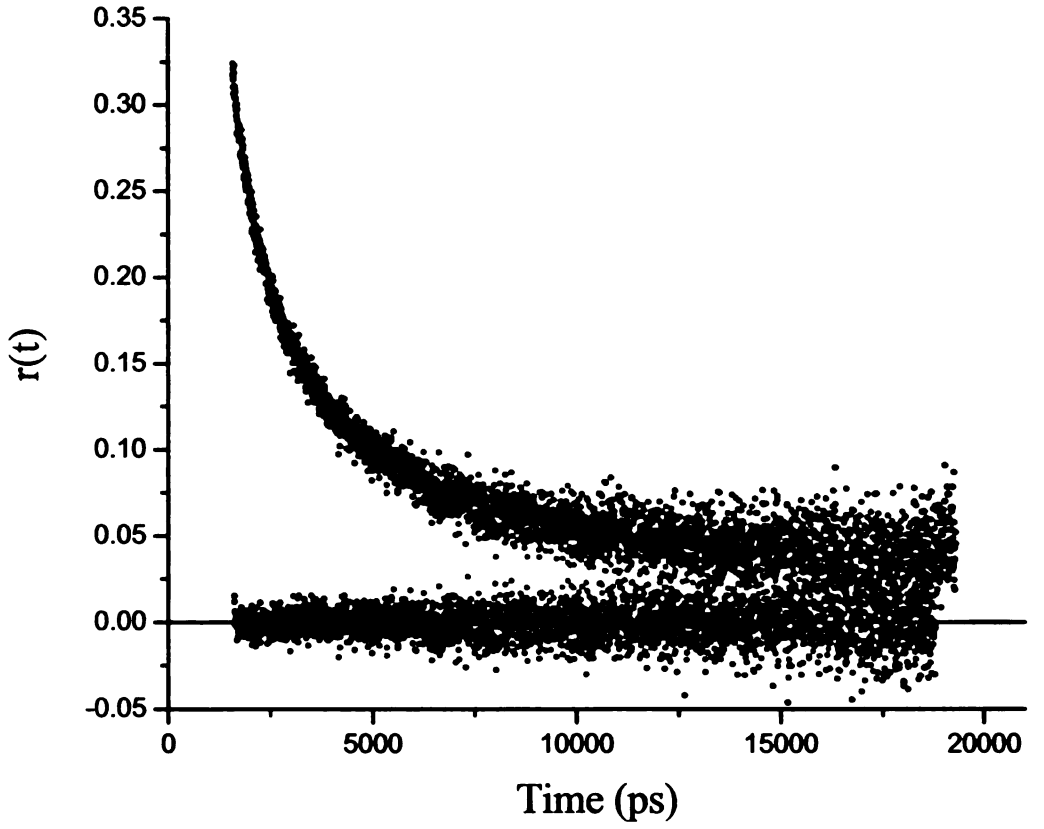

Figure 4.4. Representative induced orientational anisotropy data and residual plot (below) for NBD-PE in DOPG/DOPC lipid vesicles. A two-parameter exponential decay, corresponding to two reorientation times (τ_{OR1} and τ_{OR2}), provided the best fit of the data. F-test statistics were used to determine the statistical difference in goodness of fit for higher parameter exponentials.

(a)

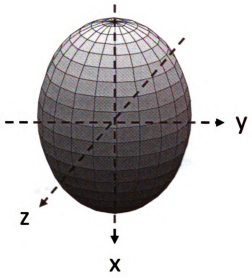

(b)

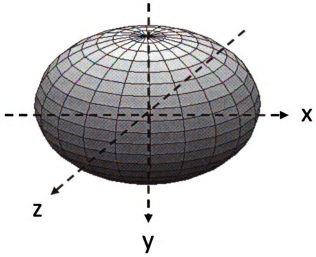

Figure 4.5. Illustrations of (a) Type I (prolate) rotor, and (b) Type II (oblate) rotor.

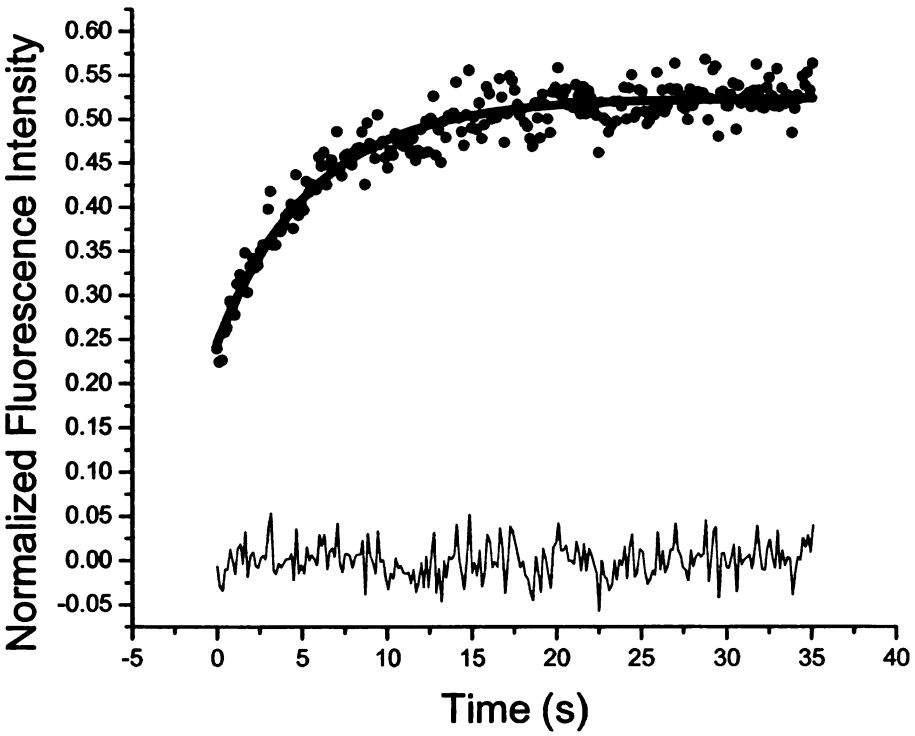

Figure 4.6. Representative FRAPP recovery curve for a DOPC/NBD-PE supported bilayer membrane (sBLM) with residuals (below). The total photobleaching time was 300 ms.

Table 4.1. Fluorescence lifetimes (τ_1 and τ_2) and reorientation times (τ_{OR1} and τ_{OR2}) of NBD-PE in DOPC, DOPG, and mixed DOPC/DOPG liposomes[a].

System[b]	τ_1 (ns)	τ_2 (ns)	τ_{OR1} (ns)	τ_{OR2} (ns)
DOPC	1.92 ± 0.12^{A}	7.83 ± 0.21^{B}	0.65 ± 0.05^{C}	3.67 ± 0.10^{D}
DOPG	2.13 ± 0.07^{A}	7.70 ± 0.11^{B}	0.49 ± 0.20^{C}	3.20 ± 0.52^{D}
DOPC/DOPG	1.89 ± 0.19^{A}	7.48 ± 0.14^{B}	0.77 ± 0.52^{C}	3.93 ± 0.05^{E}

[a]Data represent means ± SD of three liposome solutions.

[b]Systems with statistically identical fluorescence lifetimes and reorientation times are labeled by common capital letters (ANOVA, Tukey post-hoc test, $p < 0.05$).

Table 4.2. Cartesian components of the rotational diffusion coefficients (D_x and D_z) and the diffusion aspect ratio (D_x/D_z) of NBD-PE in DOPC, DOPG, and mixed DOPC/DOPG liposomes[a]. $D_y = D_z$ for Type I (prolate) rotors.

System[b]	D_x (MHz)	D_z (MHz)	D_x/D_z
DOPC	362 ± 27^{A}	45 ± 2^{B}	7.97 ± 0.82^{D}
DOPG	484 ± 148^{A}	52 ± 7^{B}	9.30 ± 4.22^{D}
DOPC/DOPG	303 ± 131^{A}	42 ± 1^{B}	7.16 ± 3.18^{D}

[a]Data represent means ± SD of three liposome solutions.

[b]Systems with statistically identical rotational diffusion coefficients and diffusion aspect ratios are labeled by common capital letters (ANOVA, Tukey post-hoc test, $p < 0.05$).

Table 4.3. Translational diffusion coefficients (D_L) and mobile fractions of NBD-PE in DOPC and mixed DOPC/DOPG sBLMs on fused silica[a].

System[b]	D_L ($\mu m^2/s$)	Mobile Fraction
DOPC	2.91 ± 0.31^{A}	0.79 ± 0.11^{C}
DOPC/DOPG	1.82 ± 0.24^{B}	0.61 ± 0.08^{C}

[a]Data represent means ± SD of three liposome solutions.

[b]Systems with statistically identical D_L and mobile fractions are labeled by common capital letters (ANOVA, Tukey post-hoc test, $p < 0.05$).

5. INFLUENCE OF LYSOPHOSPHOLIPID HYDROLYSIS BY THE CATALYTIC DOMAIN OF NEUROPATHY TARGET ESTERASE ON BILAYER LIPID MEMBRANE FLUIDITY

5.1. Abstract

NTE is an integral membrane protein localized in the endoplasmic reticulum in neurons and in organelles of other cell types. Irreversible inhibition of NTE by certain organophosphorus compounds produces a type of paralysis known as organophosphorus compound-induced delayed neuropathy. NTE mutations are also associated with motor neuron disease. NTE has been identified as a phospholipase/lysophospholipase that hydrolyzes single-chain lysophospholipids in preference to dual-chain phospholipids. The physiological role of NTE is poorly understood, although recent studies suggest that it may control the cytotoxic accumulation of lysophospholipids in membranes. The NTE catalytic domain (NEST) was used in this work to hydrolyze palmitoyl-2-hydroxy-*sn*-glycero-3-phosphocholine (p-lysoPC) to palmitic acid in bilayer membranes composed of DOPC and the lipid fluorophore NBD-PC. Translational diffusion coefficients and mobile fractions were measured in sBLMs by FRAPP. The average D_L (mean ± SD, $\mu m^2 s^{-1}$) for membranes that did not contain NEST was 2.44 ± 0.09; the average D_L for membranes containing NEST as well as its inhibitor by diisopropylphosphorofluoridate was nearly identical at 2.45 ± 0.08. By contrast, membranes containing NEST and p-lysoPC gave an average D_L of 2.28 ± 0.07. This value is significantly different from the system with no p-lysoPC, and is due to NEST hydrolysis. By comparison, the system without NEST which contained the amount of palmitic acid that would have been

produced by NEST-catalyzed hydrolysis of p-lysoPC gave a statistically identical average D_L of 2.26 ± 0.06. These results indicate that NEST hydrolysis induces a statistically significant decrease in the fluidity of sBLMs and that fluidity may be used as a measure of NTE hydrolysis of lysophospholipids in mammalian cells.

5.2. Introduction

NTE is a 147 kDa serine esterase located in endoplasmic reticulum membranes of neurons as well as other cell types such as lymphocytes.[37,123-126] NTE activity has traditionally been measured *in vitro* via hydrolysis of its non-physiological substrate, phenyl valerate.[127] More recently, NTE activity has been measured by hydrolysis of its more physiologically relevant lysophospholipid substrates, which are distinguished from other phospholipids by their single hydrophobic acyl chain.[39,128-130] Aging of NTE activity by irreversible binding of certain organophosphorus (OP) compounds to the serine in the active site results in a type of paralysis known as OP compound-induced delayed neuropathy (OPIDN), for which there is no effective treatment.[131-133] Only those OP compounds that are involved in the aging reaction in which a negative charge is created on the phosphyl group of NTE[134,135] have been associated with OPIDN. Mutations in the gene encoding NTE have also been linked to motor neuron disease.[38] Although NTE plays essential roles in embryonic development[136,137] and the protection of axons from degeneration,[138,139] its physiological function in mammalian cells is poorly understood.

Lysophospholipids in healthy mammalian cell membranes constitute between 0.5 and 6% of the total lipid weight. However, at elevated concentrations, these lipids have

been linked to a number of disease states including atherosclerosis, inflammation, and hyperlipidemia.[85,140] In addition, these lipids form micelles that generally have a high positive average intrinsic curvature because their projected head group area is much larger than that of their tail group.[141]

Lysophospholipids act as neurotoxic agents *in vitro* when added to cell types such as cerebellar granular neurons and rat spinal cord motor neurons at micromolar concentrations.[142,143] Microscopy images have shown the formation of bulges and bead-like structures in the aforementioned cells as a result of an imbalance between exocytosis and endocytosis.[142] Lysophospholipids aid in the pore-forming exocytosis event that releases neurotransmitters from presynaptic vesicles, but inhibit the subsequent endocytosis and vesicle fission events.[143] Channel-independent influx of calcium ions into cells from the extracellular environment, a supplementary effect of lysophospholipid addition, has been shown to aid in presynaptic vesicle exocytosis.[144] A possible mechanism of this influx is the spontaneous formation of pore structures in the lipid membrane.[144]

Lysophospholipases help control lysophospholipid levels in biological membranes.[140, 145] A recent study demonstrated that the IC_{50} for lysophosphatidylcholine exposed to Neuro-2a cells increased nearly three-fold upon the addition of recombinant NTE, suggesting that NTE may control the cytotoxic lysophospholipid concentration.[129] Other studies also indicate that NTE enzymatic activity helps control lysophospholipid concentrations.[128,146]

Because of inherent difficulties in expressing the full length NTE,[147] we used the catalytically active domain of NTE called NEST in this work. NEST is a 55 kDa

membrane-associated protein containing amino acids 727-1216 of the full length 1327-amino-acid NTE protein.[39] NEST is used as a surrogate for NTE because it reacts with ester substrates and inhibitors in the same manner as NTE and is readily produced heterologously.[39,148] In the present work, we assessed the influence of NEST hydrolysis of lysophospholipids on the fluidity of bilayer lipid membranes. Membrane fluidity was assessed by measuring the translational diffusion coefficients and mobile fractions of fluorescently-tagged lipids in several systems using FRAPP.

5.3. Materials and Methods

5.3.1. Chemicals and Reagents

Phospholipids DOPC, p-lysoPC, and NBD-PC were purchased from Avanti Polar Lipids Inc. (Alabaster, AL) and used without further purification. The structures of the phospholipids used in this work are shown in Figure 5.1. The NBD fluorescent moiety of the NBD-PC is located in the tail region of the lipid. A reasonable assumption of the result of NEST hydrolysis of a p-lysoPC molecule is that the hydrophilic head group of the lipid will diffuse into the aqueous mass outside the bilayer while the hydrophobic tail will remain inside the bilayer. Thus, we expect that much of the change in lipid dynamics due to NEST hydrolysis will be manifested in the hydrophobic region of the membrane.

CHAPS detergent (purity $\geq$ 99% by high performance liquid chromatography) was purchased from Anatrace (Maumee, OH). Palmitic acid, imidazole, phenylmethylsulfonylfluoride (PMSF, purity $\geq$ 98.5% by gas chromatography (GC)), and

diisopropylphosphorofluoridate (DFP, 98% pure by GC) were purchased from Sigma Aldrich (St. Louis, MO).

5.3.2. NEST Expression and Purification

A gene that encodes human brain NEST was cloned into a pET-21b vector containing a C-terminal His_6-tag and an N-terminal T7 sequence. The expression vector was subsequently transformed into *E. coli* BL21(DE3). A 50 mL culture of transformed *E. coli* was used to inoculate a 5 L solution of terrific broth (TB) media containing ampicillin (0.1 mg/mL) in a fermentation vessel. Cells were grown for 12 h, with intermittent additions of glucose and ammonium phosphate, until the optical density of the culture reached ~1.0. The culture was then induced with isopropyl β-D-1-thiogalactopyranoside (1 mM) and allowed to grow for an additional 4 h before harvesting. Five g of harvested cell pellet were then suspended in 50 mL PEN buffer (50 mM sodium phosphate, 300 mM NaCl, 0.5 mM EDTA, pH 7.4) containing 3% (w/v) CHAPS detergent. This solution was tip sonicated five times on ice (15 s per time) at a power of approximately 80 W and centrifuged at 14,900g for 30 min at 4°C. The supernatant was incubated with 6 mL of nickel-nitrilotriacetic acid (Ni-NTA) resin (Qiagen, Valencia, CA) for 1 h at 4°C. Two minicolumns (3 mL per column) were prepared by centrifugation of the protein-bound Ni-NTA resin and the minicolumns were washed six times with PEN buffer containing 0.3% (w/v) CHAPS. NEST was collected in elution fractions using PEN buffer containing 0.3% (w/v) CHAPS and 300 mM imidazole. SDS-PAGE (sodium dodecyl sulfate polyacrylamide gel electrophoresis) was used to confirm protein expression (Figure 5.2). Protein concentration was estimated by

measuring the absorbance at 280 nm in a spectrophotometer. NEST protein was then incorporated into liposomes to form proteoliposomes as described below.

5.3.3. NEST Proteoliposome Formation

2 mM solutions of DOPC/NBD-PC (98:2, mol/mol) and DOPC/p-lysoPC/NBD-PC (69:29:2 mol/mol/mol), referred to as 98:2 and 69:29:2, respectively, throughout the remainder of this chapter, were prepared by evaporating chloroform solvent from the lipid mixture with nitrogen gas, lyophilizing the lipid film under vacuum for 1 h, and hydrating the dry lipid film with PEN buffer containing 10% (w/v) CHAPS. An upper limit p-lysoPC concentration of 29 mol% was chosen because it is not possible to form bilayer structures at lysophospholipid concentrations approaching 40 mol%.[149] The NEST protein solution (0.1 mg/mL) was added to lipid/CHAPS solutions in a 880:1 lipid:protein (w/w) ratio to a final volume of 5 mL. The CHAPS/lipid/NEST solutions were then dialyzed against three 1 L exchanges of PEN buffer for a total of 48 h at 4°C using snake skin dialysis tubing with a 10,000 MWCO (Thermo Fisher Scientific, Rockford, IL). Dialysis was performed at 4°C to minimize NEST denaturation. After 48 h, DFP was added at 50 μM to stop the NEST-induced hydrolysis reaction.

5.3.4. Inhibition Studies

Stock solutions of 10 mM DFP in acetone and 200 mM PMSF in 2-propanol were prepared and stored at 4°C. DFP at 50 μM or PMSF at 1 mM was preincubated with 0.1 mg/mL NEST in PEN buffer at room temperature (23 ± 2°C) for 20 min before addition

to lipid solutions containing 10% (w/v) CHAPS. To ensure a high level of enzyme inactivation, inhibitor concentrations used in our experiments were relatively large compared to reported 20 min IC_{50} values for DFP (~ 0.96 μM) and PMSF (~ 0.15 mM) against NEST activity at 37°C.[148] Subsequent steps were repeated as listed above. NEST/DFP or NEST/PMSF solutions (0.1 mg protein/mL) were added to lipid/CHAPS solutions in an 880:1 lipid:protein (w/w) ratio to a final volume of 5 mL. The CHAPS/lipid/NEST solutions were then dialyzed against three 1 L exchanges of PEN buffer for a total of 48 h at 4°C.

5.3.5. Determination of Free Fatty Acid Concentration

An FFA assay kit from Roche Diagnostics (Penzberg, Germany) was used to measure the concentration of fatty acids incorporated into liposomes and proteoliposomes. The assay is based on a reaction scheme developed by Shimizu.[150] Briefly, FFA reacts with coenzyme A (CoA) and adenosine 5′-triphosphate in the presence of acyl-CoA synthetase to form acyl-CoA, adenosine 5′-monophosphate, and pyrophosphate. Acyl-CoA then forms 2,3-enoyl CoA and hydrogen peroxide in the presence of acyl-CoA oxidase. Upon reaction with 2,4,6-tribromo-3-hydroxy-benzoic acid and 4-aminoantipyrine in the presence of peroxidase, hydrogen peroxide forms a red dye, the absorbance of which is measured with a spectrophotometer.

To ensure that the assay was suitable for this study, chloroform-solubilized palmitic acid was added to chloroform-solubilized lipids and a lipid/palmitic acid film was formed by drying with nitrogen gas prior to lyophilization and hydration with PEN buffer containing 10% (w/v) CHAPS. After liposome formation by dialysis, an additional

10% (w/v) CHAPS was added to the sample and the concentration of FFA in the resulting mixed micelle structures (size measured with DLS) was verified using the kit.

Following dialysis, the concentration of FFA in liposomes and in NEST proteoliposomes was measured after the addition of 10% (w/v) CHAPS to 1 mL samples to form mixed micelle structures. A steady-state condition was verified by measuring the FFA concentration 3 h after the DFP addition. The partition coefficient of palmitic acid into 1,2-dipalmitoyl-sn-glycero-3-phosphocholine (DPPC) unilamellar liposomes at 23°C is approximately 5.23×10^6.[151] Although we provide no direct evidence that palmitic acid is present within the membrane phase of unilamellar liposomes, this large partition coefficient for palmitic acid into DPPC suggests that most of the palmitic acid would be associated with the hydrophobic region of lipid bilayer rather than the aqueous phase.

5.3.6. Dynamic Light Scattering

The mean particle sizes and size distributions of liposomes and NEST proteoliposomes in solution were measured with a Brookhaven Instruments 90 Plus/BI-MAS/ZetaPlus machine (Holtsville, NY).

5.3.7. Transmission Electron Microscopy

A 10 μL aliquot of 69:29:2 liposomes, with and without NEST, was diluted 100-fold with PEN buffer and fixed on a copper-coated grid using a 2% uranyl acetate stain. Images were obtained with a JEOL 100CX TEM using an accelerating voltage of 100 kV.

5.3.8. Deposition of Supported Lipid Bilayers

Fused silica microscope slides (75 mm × 25 mm × 1 mm) were purchased from Technical Glass Products, Inc. (Painesville, OH). The slides were cleaned by bath sonication (Branson 1510, Branson Ultrasonic Corporation, Danbury, CT) in detergent solution for 20 min, rinsed with deionized water, baked at 160°C for 4 h, and plasma treated (Harrick Plasma, Ithaca, NY) with oxygen under vacuum (150 mTorr) for 10 min immediately before bilayer deposition. sBLMs were deposited by liposome or proteoliposome fusion in a custom-made flow cell described elsewhere.[68] The flow cell was initially washed with buffer, followed by a 1-h incubation with liposome or NEST proteoliposome solution and a final buffer wash to remove unadsorbed particles. All experiments were performed at room temperature (23 ± 2°C).

5.3.9. Fluorescence Recovery After Pattern Photobleaching

FRAPP was used to measure the translational diffusion coefficients and mobile fractions of fluorophores in sBLMs formed on fused silica microscope slides. The details of this technique are discussed in Section 2.2 of this dissertation. For each lipid system considered in this work, three separate sBLM interfaces were formed on silica slides and each interface was interrogated with FRAPP at five different locations of the bilayer.

5.3.10. Statistical Analysis

Data were fit using OriginPro 7.5 (OriginLab Corporation, Northampton MA) which uses the Levenberg-Marquardt algorithm for non-linear least squares fitting.

Mobile fractions, translational diffusion coefficients, and particle diameters are reported as means ± SD. Multiple comparison ANOVA with a post-hoc Tukey test ($p < 0.05$) was used to determine if differences among the means were statistically significant.

5.4. Results and Discussion

We interrogated seven systems of reconstituted BLMs. To aid in interpretation of the data, the seven systems were divided among three groups (A,B,C) based on the identity of the lipids and molecules present:

- Group A (Systems 1 and 2 - BLMs containing DOPC and NBD-PC): System 1 and system 2 consisted of 98 mol% DOPC and 2 mol% NBD-PC reconstituted without NEST and with NEST, respectively. System 1 is the basic BLM formulation used in our lab and serves as an important control to assess the effect of incorporating NEST into the membrane.
- Group B (Systems 3, 4, and 5 - BLMs containing DOPC, p-lysoPC, and NBD-PC): BLMs in this group consisted of 69 mol% DOPC, 29 mol% p-lysoPC, and 2 mol% NBD-PC, with the following variations: no additional constituents (system 3), with the NEST inhibitor DFP incorporated (system 4), and with both DFP and NEST incorporated (system 5).
- Group C (Systems 6 and 7 - BLMs containing DOPC, p-lysoPC, palmitic acid, and NBD-PC): System 6 had a composition of 69 mol% DOPC, 29 mol% p-lysoPC, and 2 mol% NBD-PC, with NEST incorporated to measure the effect of lysophospholipid hydrolysis. System 7 was 69 mol% DOPC, 20 mol% p-lysoPC, 9 mol% palmitic acid, and 2 mol% NBD-PC. The fraction of palmitic acid in system

7 is equivalent to the amount of FFA that would be expected from NEST hydrolysis in system 6, and was used to provide comparative data.

System compositions are summarized in Table 5.1. We used FRAPP to assess the translational diffusion coefficient and mobile fraction of fluorophores embedded in the hydrophobic region of each of the seven systems above.

5.4.1. Transmission Electron Microscopy Images

TEM images (Figure 5.3) showed that the 69:29:2 liposomes and 69:29:2/NEST proteoliposomes formed after dialysis were unilamellar, ensuring that sBLMs formed from them would also be unilamellar.[141,152] Because liposomes and NEST proteoliposomes were subjected to high vacuum conditions and to a high-energy electron beam, it is difficult to use TEM images to evaluate the size distribution of liposomes and proteoliposomes. Thus, size distribution data were obtained by DLS.

5.4.2. Dynamic Light Scattering Data

We used DLS to assess the transition from mixed CHAPS/69:29:2 micelles to liposomes and mixed CHAPS/69:29:2/NEST micelles to proteoliposomes during dialysis. This was done by measuring the mean particle diameter as a function of time (Figure 5.4). The DLS results show that the mean diameter of NEST-containing micelles before dialysis was 2.3 ± 0.2 nm and that the steady state mean diameter of proteoliposomes

after a 30-h dialysis was 40.8 ± 3.1 nm. The sigmoidal natur of our data has been reported by others for the transition from micelles to liposomes via detergent dialysis.[153,154]

The mean diameter of 69:29:2 liposomes, without NEST, after dialysis was not significantly different from proteoliposomes containing NEST, suggesting that, at the significantly large lipid to protein ratio (880:1 w/w) used in this study, the incorporation of NEST has no effect on particle size.

5.4.3. Measurement of Free Fatty Acid Concentration

Negligible conversion of DOPC or NBD-PC to FFA was measured in 98:2 liposomes (system 1) and in 98:2 proteoliposomes with NEST (system 2), in agreement with previously published results showing that dual acyl chain lipids are not easily hydrolyzed by NEST [39,129]. There was also negligible conversion of DOPC, p-lysoPC, or NBD-PC to FFA in 69:29:2 liposomes, without DFP (system 3) and with DFP (system 4), indicating that p-lysoPC did not significantly auto-hydrolyze and that DFP did not hydrolyze the lipids to form FFA. Results obtained using PMSF in place of DFP in systems 3 and 4 were not statistically different. When NEST was mixed with DFP (system 5) prior to dialysis, negligible conversion of DOPC, p-lysoPC, or NBD-PC to FFA was observed in 69:29:2 proteoliposomes. Significant conversion of the DOPC, p-lysoPC, and NBD-PC mixture to FFA was measured in 69:29:2 liposomes containing NEST (system 6) after 48 h of dialysis (Table 5.1 and Figure 5.5). Control experiments showed negligible conversion of DOPC and NBD-PC to FFA in system 2 as well as negligible conversion of DOPC, p-lysoPC, and NBD-PC in system 3. Thus, the significant levels of FFA observed in system 6 were attributed entirely to the hydrolysis

of p-lysoPC to palmitic acid. To aid in comparing data on other systems, the mean conversion of p-lysoPC to palmitic acid in the 69:29:2 liposomes containing uninhibited NEST after 48 h of dialysis was assigned a value of 100%, and formed the base value for all comparisons. We note that when NEST was mixed with PMSF prior to dialysis, conversion of p-lysoPC to palmitic acid decreased from 100% to 17%. FFA conversion values (Table 5.1) for p-lysoPC-containing NEST proteoliposomes were calculated as a ratio of the total moles of palmitic acid measured to the total moles of p-lysoPC present before the addition of NEST. Specific activities (Table 5.1) were calculated as μmol FFA produced per mg NEST per hour, after a reaction time of 48 h.

5.4.4. Translational Diffusion in Supported Bilayer Lipid Membranes

Mobile fractions and D_L of NBD fluorophores in sBLMs on fused silica slides were measured with FRAPP. There was no statistical difference between the D_L values for group A (systems 1 and 2) of sBLMs, as shown in Figure 5.6. Hence, incorporating NEST in the sBLM at a sufficiently large lipid to protein ratio (880:1 w/w) does not significantly affect the translational diffusion of lipids in the absence of enzymatic activity. In a previous study, proteoliposomes with relatively small lipid to membrane protein ratios had identical diffusion characteristics as pure lipid membranes, suggesting that the protein has little effect on membrane dynamics.[155] Also, the differences in the mobile fractions of NBD in group A (systems 1 and 2) were not statistically significant (Figure 5.7), indicating that the protein did not impede proteoliposome rupture and subsequent sBLM formation at the low protein concentration used. On the other hand, no fluorescence recovery was measured when proteoliposomes with lipid to protein ratios

less than 80:1 (w/w) were adsorbed on silica slides, indicating negligible mobile fractions. This result is consistent with proteoliposome adsorption without subsequent rupture and sBLM formation.

The D_L for 69:29:2 sBLMs (system 3) was higher than for 98:2 sBLMs (systems 1 and 2). This should be expected based on simple geometric considerations. P-lysoPC has a head group area that is essentially the same as the dual acyl chain lipids. Therefore, when the lipid is incorporated into a sBLM, it provides essentially equivalent packing levels in the head group region of the bilayer. However, its single acyl chain results in lower packing densities in the hydrophobic regions of the bilayer, thus leading to a more fluid system. The increase in membrane fluidity upon addition of p-lysoPC to model membranes has been observed previously, although our data show a more modest increase in the D_L than was reported by Leu et al.[22], who attributed the increase in fluidity upon addition of p-lysoPC to DOPC bilayers to a decrease in tail group van der Waals interactions between adjacent lipids. The other two systems in group B (69:29:2 sBLMs containing DFP (system 4) and 69:29:2 sBLMs containing both NEST and its inhibitor DFP (system 5)) had statistically similar D_L values as those of system 3. Thus, the incorporation of either DFP or NEST inhibited by DFP did not significantly affect the fluidity of the membrane. The two inhibitors, DFP and PMSF, are similar in that they both irreversibly inhibit esterase activity. However, the former does not undergo the aging reaction the latter does. As has already been discussed, the inhibition of NEST activity by DFP and PMSF reduced the conversion of p-lysoPC to palmitic acid in solution by ~83 and ~100%, respectively (Table 5.1).

5.4.5. NEST-induced Hydrolysis of P-lysoPC to Palmitic Acid Decreases Membrane Fluidity

Incorporation of NEST into a 69:29:2 sBLMs led to a statistically lower D_L value, indicating a less fluid membrane. This result, which is attributed to conversion of p-lysoPC to palmitic acid by NEST hydrolysis, can be explained on purely geometric considerations. As already noted, upon hydrolysis of p-lysoPC, the head group of the lipid is assumed to migrate into the aqueous phase while the hydrocarbon tail remains in the hydrophobic region of the membrane. The net result is that the head group area per lipid will contract somewhat because of the missing head groups, which would lead to a denser hydrophobic region in which the diffusion of constituent species will be retarded. We have demonstrated that hydrolysis of p-lysoPC by NEST decreases D_L in model bilayer membranes (system 6) and that inhibition of NEST activity by DFP (system 5) or PMSF negates this effect. Since palmitic acid is formed by NEST-induced hydrolysis of p-lysoPC, we can determine if the decrease in membrane fluidity is solely the result of uninhibited NEST. To asses this, we adjusted the lipid composition *a priori* to correspond to the 100% p-lysoPC conversion to palmitic acid measured with the FFA assay. The resulting system contained 69 mol% DOPC, 20 mol% p-lysoPC, 9 mol% palmitic acid, and 2 mol% NBD-PC as the fluorophore (system 7). The D_L measured in sBLMs reconstituted with this composition was not statistically different than that measured in 69:29:2 sBLMs containing NEST, which is consistent with the reduction in fluidity being solely due to NEST hydrolysis. In summary, systems in group C (systems 6 and 7) were less fluid than those in group B (systems 3, 4, and 5), but more fluid than those in group A (systems 1 and 2).

The ability of saturated fatty acids to decrease BLM fluidity has been well documented.[156-160] For example, addition of palmitic acid to DOPC bilayers has been shown by digital scanning calorimetry to increase the gel-to-liquid-crystalline phase transition temperature, which is an indication of a less fluid bilayer.[161] A two-dimensional Voronoi tessellation analysis of 1-palmitoyl-2-oleoyl-sn-glycero-3-phosphocholine (POPC) / 1-palmitoyl-2-oleoyl-sn-glycero-3-phosphoethanolamine (POPE) bilayers showed that, upon addition of palmitic acid, the area per constituent lipid decreased while the area per palmitic acid molecule remained constant.[161] This suggests that palmitic acid is incompressible within the bilayer and acts to decrease the void space between lipids, leading to a decrease in the area per lipid and a decrease in membrane fluidity. Electron paramagnetic resonance (EPR) measurements also demonstrated that membrane fluidity decreased in HepG2 cells exposed to palmitic acid. An MD simulation of palmitic acid in 1,2-dimyristoyl-*sn*-glycero-3-phosphocholine (DMPC) bilayers also predicted that the carboxyl carbon atom of the protonated, neutral form of the acid embeds itself deeply into the membrane, adjacent to the ester group of the DMPC lipids.[162] Palmitic acid molecules at this position in the bilayer induce tighter lateral packing, stretching of hydrophobic lipid chains, and increased lipid order. Another study involving the addition of stearic acid to Langmuir monolayers comprising 1,2-dipalmitoyl-*sn*-glycero-3-phosphocholine (DPPC) and cholesterol showed an increase in monolayer rigidity with increasing stearic acid concentration.[163]

The present study may provide some insight into the possible physiological role of NTE. Cells are known to adjust membrane fluidity by producing phospholipids that either increase or decrease fluidity based on lipid-lipid intermolecular interactions. These

lipids are generally synthesized in the cytosol, mitochondria, and endoplasmic reticulum.[21] The results of the present work involving NEST and model membranes are consistent with a hypothesis that mammalian neurons and other cell types may use NTE-induced lysophospholipid hydrolysis as a way of adjusting membrane fluidity. Alternatively, cells may use NTE-induced lysophospholipid hydrolysis to control toxic lysophospholipid accumulation in cells. In the latter case, the results of the present study may provide insight into the important effects of the regulation of lysophospholipid concentration in cells by NTE.

5.5. Conclusions

We have demonstrated that at sufficiently large lipid to protein ratios, NEST proteoliposomes adsorbed onto silica substrates rupture to form fluid sBLMs. We have used FRAPP to study seven different bilayer lipid membrane compositions to assess the effect of p-lysoPC hydrolysis by the catalytic domain of NTE (NEST) on the fluidity of the systems. There are two important conclusions based on the results of this study. First, NEST hydrolysis induces a statistically significant decrease in the fluidity of sBLMs reconstituted on silica. Second, it has been proposed that one physiological role of NTE is to maintain lysophospholipid homeostasis in mammalian cells. The results of this study suggest that BLM fluidity may provide a convenient physical measurement that could be used to assess this function.

5.6. Recommendations for Future Work

We used p-lysoPC in this work for primarily two reasons. First, NEST hydrolyzes p-lysoPC to a greater extent than 1-oleoyl-2-hydroxy-sn-glycero-3-phosphocholine (o-lysoPC), an unsaturated fatty acid. This increases the probability that a sufficient amount of p-lysoPC would be hydrolyzed to enable us to observe a measurable difference in bilayer fluidity. Second, the product of p-lysoPC hydrolysis, palmitic acid, has been shown to significantly decrease bilayer fluidity. In future studies, it would be interesting to replace p-lysoPC with o-lysoPC and measure the fluidity in the presence of an unsaturated fatty acid, which has been reported in some cases to increase bilayer fluidity.

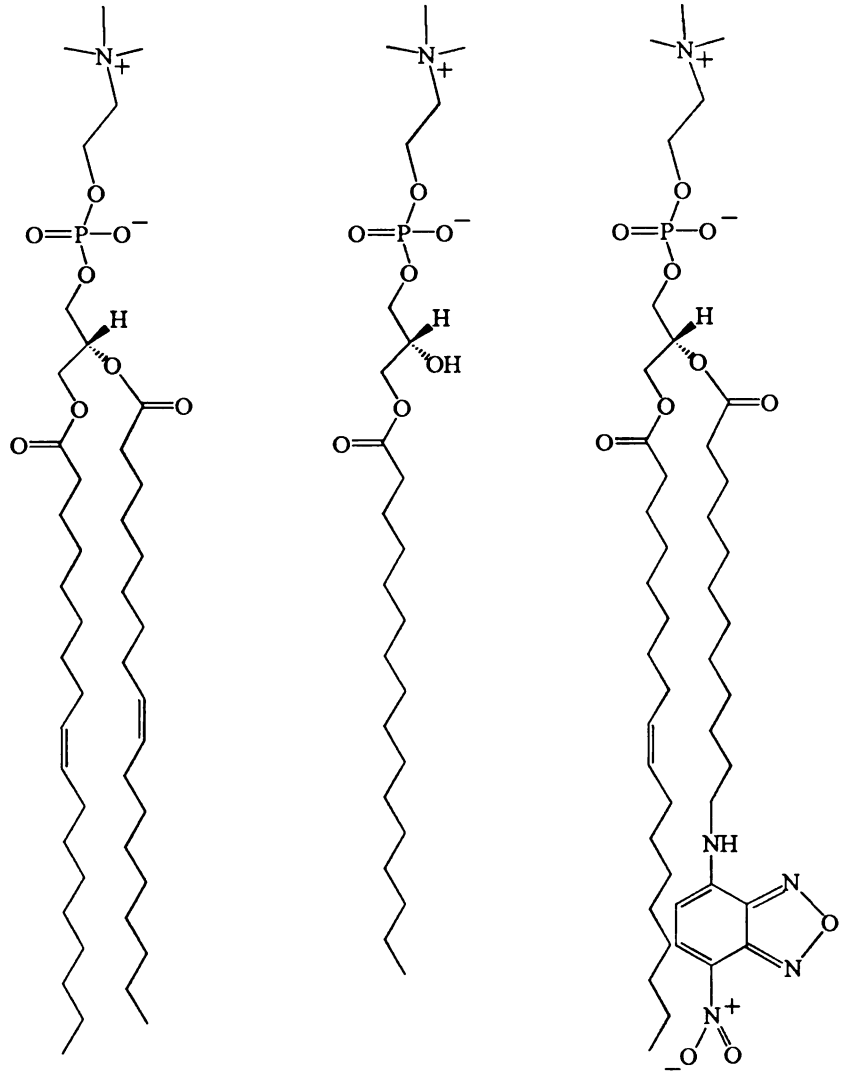

(a) (b) (c)

Figure 5.1. Molecular structures of the lipids used in this study: (a) 1,2-dioleoyl-*sn*-glycero-3-phosphocholine (DOPC), (b) 1-palmitoyl-2-hydroxy-*sn*-glycero-3-phosphocholine (p-lysoPC), and (c) the fluorophore 1-oleoyl-2-[12-[(7-nitro-2-1,3-benzoxadiazol-4-yl)amino]dodecanoyl]-*sn*-glycero-3-phosphocholine (NBD-PC).

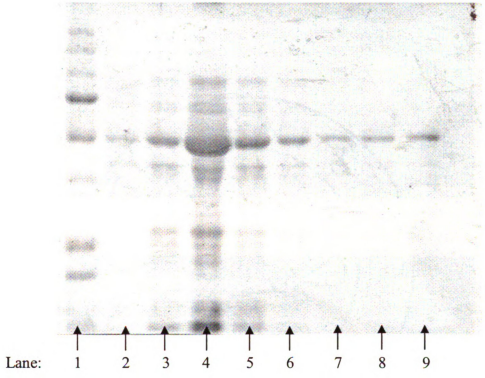

Figure 5.2. Representative SDS-PAGE (sodium dodecyl sulfate polyacrylamide gel electrophoresis) processed during NEST purification. Lane assignments are as follows: Lane 1: marker, lane 2: 3rd column wash, lanes 3 through 8: 1st through 6th column elutions, lane 9: sample after 48-hour dialysis using 4th elution.

(a)

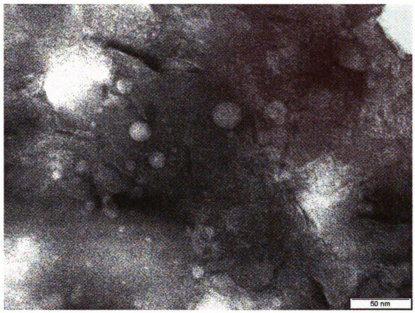

(b)

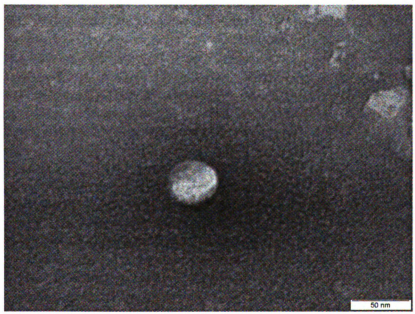

Figure 5.3. (a) TEM image showing representative 69:29:2 liposomes after dialysis. (b) TEM image showing a representative 69:29:2/NEST proteoliposome after dialysis. Such unilamellar liposomes and proteoliposomes were used to form sBLM structures on silica.

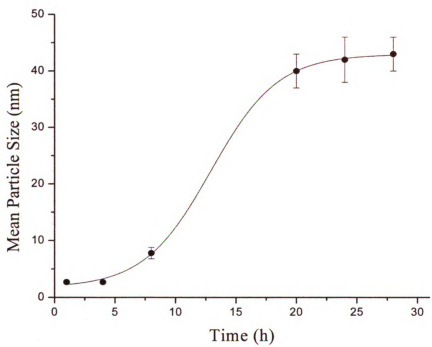

Figure 5.4. DLS results showing the CHAPS/69:29:2/NEST micelle to proteoliposome transition during dialysis. Data represent means ± SD of three separate dialysis runs. A Boltzmann sigmoid function, $d = d_2+((d_1-d_2)/(1+\exp((t-t_0)/dt)))$, was fitted to the data. In this function, d is the time-dependent mean particle diameter, t is time, d_1 is the initial particle diameter, d_2 is the final particle diameter, t_0 is the center time value, and dt is the time constant. The fitted sigmoid had a correlation coefficient of 0.999. Fitted parameters were as follows: $d_1 = 1.7 \pm 0.6$ nm, $d_2 = 43.0 \pm 0.5$ nm, $t_0 = 12.9 \pm 0.4$ h, and $dt = 2.7 \pm 0.2$ h.

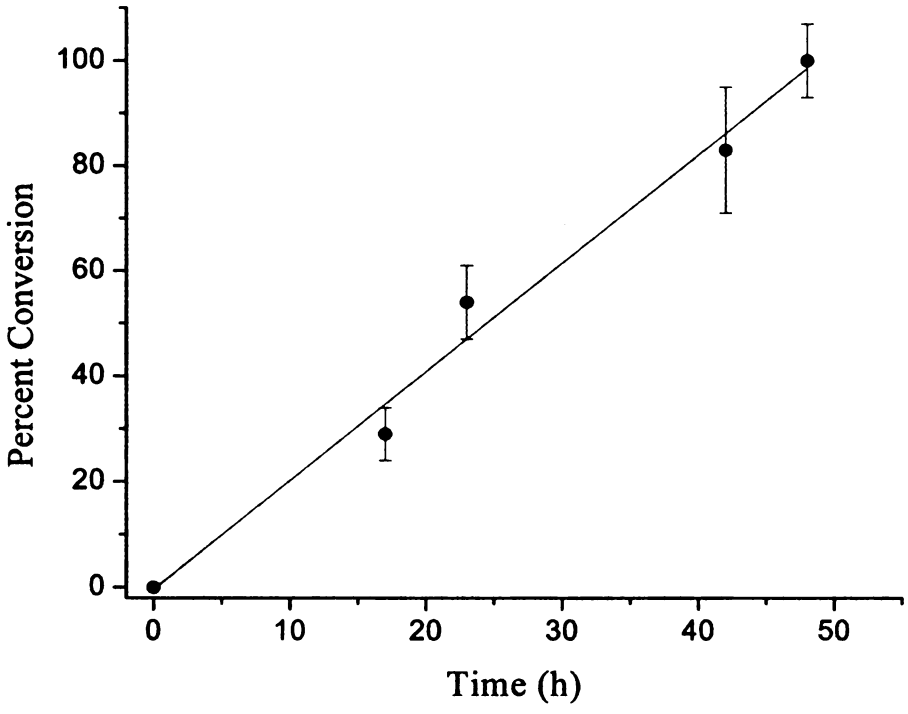

Figure 5.5. Time-course of conversion of p-lysoPC to palmitic acid during dialysis. A 100% conversion of p-lysoPC to palmitic acid was assigned to 69:29:2 liposomes containing uninhibited NEST after 48-h dialysis. Data are means ± SD of two separate assays. A line was fitted to the data using linear regression analysis. The fitted line had a correlation coefficient of 0.990.

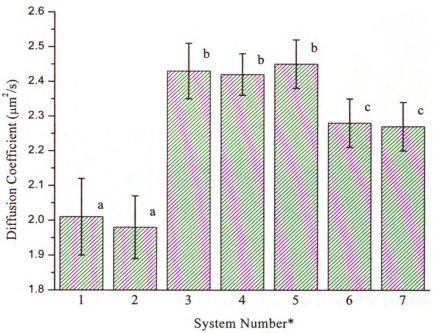

Figure 5.6. D_L of NBD-PC in sBLMs for several systems identified by the following system numbers*: (1) 98:2 (98 mol% DOPC, 2 mol% NBD-PC), (2) 98:2 (w/NEST), (3) 69:29:2 (69 mol% DOPC, 29 mol% p-lysoPC, and 2 mol% NBD-PC), (4) 69:29:2 (w/DFP), (5) 69:29:2 (w/NEST+DFP), (6) 69:29:2 (w/NEST), (7) 69:20:9:2 (69 mol% DOPC, 20 mol% p-lysoPC, 9 mol% palmitic acid, and 2 mol% NBD-PC. Data are means ± SD from three different bilayers. Systems with statistically identical D_L are labeled by a common letter (ANOVA, Tukey post-hoc test, $p < 0.05$). D_L for 69:29:2 bilayers treated with PMSF and 69:29:2 bilayers with PMSF-inhibited NEST (data not shown) were statistically identical to 69:29:2 lipid systems with DFP in place of PMSF.

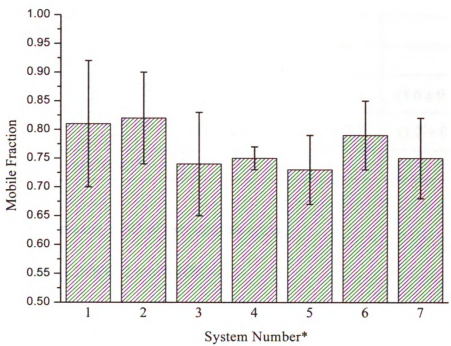

Figure 5.7. Mobile fractions of NBD-PC for several systems identified by the following system numbers*: (1) 98:2 (98 mol% DOPC, 2 mol% NBD-PC), (2) 98:2 (w/NEST), (3) 69:29:2 (69 mol% DOPC, 29 mol% p-lysoPC, and 2 mol% NBD-PC), (4) 69:29:2 (w/DFP), (5) 69:29:2 (w/NEST+DFP), (6) 69:29:2 (w/NEST), (7) 69:20:9:2 (69 mol% DOPC, 20 mol% p-lysoPC, 9 mol% palmitic acid, and 2 mol% NBD-PC. Data are means ± SD from three different bilayers. The mobile fractions of all systems are statistically identical (ANOVA, Tukey post-hoc test, $p < 0.05$), indicating that neither lipid composition nor the presence of protein and/or inhibitors influenced liposome rupture.

Table 5.1. Percent conversion and specific activity of p-lysoPC to palmitic acid for several systems[a]

System Number	Composition	Percent Conversion[e]	Percent Inhibition[f]	Enzyme Activity[g] (μmol FFA produced/hr)
1	98:2[b]	-	-	-
2	98:2 (with NEST)	-	-	-
3	69:29:2[c]	0.3 ± 0.1	-	-
4	69:29:2 (with DFP)	0.3 ± 0.1	-	-
5	69:29:2 (with NEST)	100 ± 7	-	$(3.6 \pm 0.24) \times 10^{-2}$
6	69:29:2 (with NEST and DFP)	0.3 ± 0.1	99.7 ± 7.0	$(1.2 \pm 0.24) \times 10^{-4}$
7	69:20:9:2[d]	-	-	-

[a]Data represent means ± SD of two separate assays.

[b]98:2 is 98 mol% DOPC, 2 mol% NBD-PC.

[c]69:29:2 is 69 mol% DOPC, 29 mol% p-lysoPC, and 2 mol% NBD-PC.

[d]69:20:9:2 is 69 mol% DOPC, 20 mol% p-lysoPC, 9 mol% palmitic acid, 2 mol% NBD-PC

[e]100% conversion of p-lysoPC to palmitic acid was assigned to the mean conversion value in 69:29:2 liposomes containing uninhibited NEST after 48-h dialysis.

[f]Percent reduction in conversion for systems with NEST and either DFP or PMSF, relative to the mean conversion value in 69:29:2 liposomes containing uninhibited NEST after 48-h dialysis.

[g]Specific activities are reported in terms of FFA produced per mg NEST and after a time period of 48 h.

6. EFFECT OF MEMBRANE PROTEIN CONCENTRATION ON THE TRANSLATIONAL DYNAMICS OF AN EMBEDDED FLUOROPHORE IN SUPPORTED BILAYER MEMBRANES CONSTITUTED FROM PROTEOLIPOSOMES

6.1. Abstract

sBLMs are model membranes commonly formed via self-assembly of liposomes adsorbed to silica, quartz, or mica surfaces. When membrane proteins are incorporated into liposomes, they form proteoliposomes, which have also been shown to form sBLMs via self-assembly on similar surfaces. Although many studies have demonstrated that sBLMs can serve as an important tool in the study of membrane protein activity and functionality, the relationship between protein concentration in proteoliposomes and their ability to form sBLMs via self-assembly is poorly understood. The objective of this work was to use FRAPP to assess how the concentration of a membrane-associated protein affects the translational dynamics and mobile fractions of an imbedded chromophore in a sBLM reconstituted from proteoliposomes. We used NEST as a model membrane-associated protein in DOPC/NEST/NBD-PC proteoliposomes self-assembled into sBLMs on fused silica. At a lipid to protein ratio of 80:1 (w/w), we observed no measurable fluorescence recovery of NBD-PC in sBLMs, suggesting that the fluorophores resided in unruptured liposomes on the substrate. The minimum lipid to protein ratio at which we observed fluid sBLM formation upon proteoliposome deposition on silica was 880:1 (w/w). We also qualitatively assessed the effect of membrane protein concentration on the dynamics of NBD-PC in bilayer interfaces formed from microsome membrane fractions of *Saccharomyces pombe* yeast cells.

6.2. Introduction

tBLMs are commonly used to characterize protein-protein interactions,[33] ion-channel activity,[32] and membrane protein activity.[34] sBLM interfaces are, in contrast to tBLMs, only separated from the substrate by a 1 Å-thick layer of water. sBLMs formed from liposome self-assembly have been widely used to study liposome rupture and fusion processes[4,42,164,165], lipid-lipid interactions,[22] and lipid migration in applied electric fields.[166] One of the major drawbacks of using sBLM interfaces to study membrane proteins is that the proteins often come into contact and interact with the substrate and become denatured and/or immobile. In spite of this, many studies have shown that sBLMs do in fact provide useful tools for characterizing the interactions of trans-membrane proteins in membranes,[167,168] as well as determining membrane protein activity and function.[14] For example, a peripheral membrane protein acetylcholinesterase and integral membrane proteins bacteriorhodopsin and cytochrome oxidase have been shown to retain their biological activities when placed in PC BLMs reconstituted on silicon wafers and platinum-coated silica.[169,170] Trans-membrane photosynthetic reaction centers (RCs) that were incorporated into fluid sBLMs on glass retained their charge separation and cytochrome *c* binding properties even though the RCs themselves were immobile.[15] Chan et al. demonstrated that not only did glycosyl-phosphatidylinositol (GPI)-anchored membrane receptors remain fluid in sBLMs on glass substrates, but that the fluid nature of the protein enhanced cell adhesion to the membrane.[171] We also showed in Chapter 5 that sBLMs formed from proteoliposomes containing the membrane-associated protein NEST and p-lysoPC exhibited a decrease in membrane fluidity as a result of the enzymatic activity of the protein.

In each of these cases, the lipid to protein ratio was selected to ensure that proteoliposomes adsorbed and ruptured to form fluid sBLMs when exposed to either glass substrates[171] or lipid SAMs formed by the Langmuir-Blodgett technique.[170] In the present work, we estimated a range of lipid to protein ratios that produce fluid sBLMs on fused silica using proteoliposome self-assembly. We used DOPC as the primary lipid, NBD-PC as the lipid fluorophore, and NEST as a model membrane-associated protein. Diffusion coefficients and mobile fractions of fluorophores in the sBLMs were obtained from FRAPP data. We also qualitatively evaluated the effect of membrane proteins on the fluidity of interfaces formed from microsome membrane fractions of *Saccharomyces pombe* yeast cells.

6.3. Materials and Methods

6.3.1. Chemicals and Reagents

Phospholipids DOPC, POPC, and NBD-PC were purchased from Avanti Polar Lipids Inc. (Alabaster, AL) and used without further purification. The molecular structures of these lipids are shown in Figure 6.1. CHAPS detergent (purity $\geq$ 99% by high performance liquid chromatography) was purchased from Anatrace (Maumee, OH). Imidazole was purchased from Sigma Aldrich (St. Louis, MO).

6.3.2. NEST Expression and Purification

NEST was expressed and purified according to the protocol in Section 5.3.2 of this dissertation.

6.3.3. NEST Proteoliposome Formation

NEST proteoliposomes were formed by the dialysis method described in Section 5.3.3. NEST protein solution (0.1 mg/mL) was added to 98 mol% DOPC, 2 mol% NBD-PC, 10 wt% CHAPS solutions in 1600:1 (w/w) (118,000:1 mol/mol), 880:1 (w/w) (65,000:1 mol/mol), 270:1 (w/w) (20,000:1 mol/mol), and 80:1 (w/w) (6,000:1 mol/mol) lipid to protein ratios. In terms of notation, an interface formed from proteoliposomes with, for example, an 80:1 (w/w) lipid to protein ratio will be referred to as an 80:1 (w/w) interface throughout this chapter. The presence of liposomes was confirmed by monitoring the micelle to liposome transition with TEM and DLS (Figures 5.3 and 5.4).

6.3.4. Preparation of Yeast Membrane Fractions

This procedure is described in detail elsewhere.[90] Briefly, *Saccharomyces pombe* cells were grown in yeast peptone dextrose (YPD) medium (20 g/L yeast peptone, 10 g/L yeast extract and 2% w/v glucose). Cells were harvested by centrifugation and suspended in lysis buffer (25 mM Tris buffer, pH 8.0, containing 250 mM sucrose). The cells were then passed three times through an Emulsiflex-C3 homogenizer and the debris was centrifuged at 14,900g for 30 min at 4°C. The supernatant was centrifuged and the membrane pellet was frozen at −80°C. To prepare membrane fractions, a portion of the membrane pellet was suspended in 20 mM Tris-HCl buffer, pH 8.0, containing 200 mM NaCl and 10% glycerol. The suspension containing the membrane fraction was sonicated for 5 min, then passed through a 200 nm filter. To incorporate the lipid fluorophore into membrane fractions, a chloroform solution of NBD-PC was dried under nitrogen and

placed under vacuum at -45°C for 3 h. After the lipid film was hydrated with the membrane fraction suspension, the mixture was sonicated for 20 min.

6.3.5. Extraction of Lipids From Yeast Cells

A mixture of 10 mL methanol, 20 mL chloroform, and 1.5 mL aqueous membrane fraction suspension were stirred continuously for 1 h at room temperature. After separation of the organic and aqueous phases, 0.034% $MgCl_2$ was added to the organic phase and the solution was stirred for 10 min. The organic phase was then centrifuged at 3,000 rpm for 5 min after which the upper aqueous phase was aspirated. The organic phase was then washed with a 10 mL solution of 4:1 (v/v) KCl/methanol, the mixture was centrifuged, and the upper phase aspirated. The organic phase was then washed with a 10 mL solution of 3:48:47 (v/v/v) chloroform/methanol/water. The mixture was then centrifuged, washed again with the chloroform/methanol/water solution, and the upper phase was aspirated. The organic phase was placed in a rotary evaporator at 55°C and 200 mbar until a dry lipid film was formed. The lipid film was dissolved in a 2:1 (v/v) chloroform:methanol solution and stored at -20°C. Liposomes formed from microsome lipid fractions were created by adding 2 mol% NBD-PC to the lipid/chloroform/methanol solution, drying the solution with nitrogen to create a lipid film, placing the film under vacuum at -45°C for 3 h, and hydrating the film with Tris buffer at pH 8.0.

6.3.6. POPC Liposome Preparation

Solutions containing 1 mM POPC/NBD-PC (98:2, mol/mol) in chloroform were dried under nitrogen and placed under vacuum at -45°C for 3 h. The dried lipid mixtures were then hydrated in Tris buffer at pH 8.0, and sonicated for 20 min.

6.3.7. Deposition of Interfaces

Fused silica microscope slides (75 mm x 25 mm x 1 mm) were purchased from Technical Glass Products, Inc. (Painesville, OH). The slides were cleaned by bath sonication (Branson 1510, Branson Ultrasonic Corporation, Danbury, CT) in detergent solution for 20 min, rinsed with DI water, baked at 160°C for 4 h, and plasma treated (Harrick Plasma, Ithaca, NY) with oxygen under vacuum (150 mTorr) for 10 min immediately before bilayer deposition. Interfaces were deposited by either liposome, proteoliposome, or membrane fraction adsorption in a custom-made flow cell described elsewhere.[68] The flow cell was initially washed with buffer, followed by a 1 h incubation with either solutions of POPC synthetic liposomes, NEST proteoliposomes at various lipid to protein ratios, or yeast membrane fractions. The flow cell was then rinsed with buffer to remove unadsorbed species. All experiments were performed at room temperature (23 ± 2°C).

6.3.8. Fluorescence Recovery After Pattern Photobleaching

FRAPP was used to measure D_L and mobile fractions of fluorophores in the interfaces formed on fused silica microscope slides. The details of this technique are

given in Section 2.2 of this dissertation. For each lipid system used in this work, three separate interfaces were formed on silica slides and each interface was interrogated by FRAPP at five different locations.

6.3.9. Statistical Analysis

Data fitting was accomplished using OriginPro 7.5 (OriginLab Corporation, Northampton MA) which uses the Levenberg-Marquardt algorithm for non-linear least squares fitting. Diffusion coefficients and mobile fractions are reported as means ± SD. Multiple comparison ANOVA with a post-hoc Tukey test ($p < 0.05$) was used to determine if differences among the means were statistically significant.

6.4. Results and Discussion

6.4.1. Interfaces Formed with NEST Proteoliposomes

Equation 3.5, which assumes one mobile and one immobile species,[44] was fit to the FRAPP data to extract D_L values and mobile fractions of the embedded lipid fluorophores. When proteoliposomes with DOPC lipid to NEST ratios of less than 80:1 (w/w) were deposited on silica slides, no fluorescence recovery was observed, indicating that the NBD fluorophores were not mobile (Figure 6.2). We interpret the mobile species as fluorophores in fluid sBLMs and the immobile species as fluorophores in adsorbed but unruptured liposomes. Therefore, when there is no measurable fluorescence recovery, it suggests that proteoliposomes adsorbed onto the silica but did not rupture to form

sBLMs. At this protein concentration, the transition from adsorbed proteoliposomes to a fluid sBLM via proteoliposome fusion and rupture is completely inhibited.

Mobile fractions and D_L for all DOPC/NEST/NBD-PC interfaces are summarized in Table 6.1. There was a measurable recovery for the case of proteoliposomes with a 270:1 (w/w) lipid to protein ratio. The D_L and mobile fraction of these interfaces were 1.72 ± 0.25 $\mu m^2/s$ and 0.75 ± 0.13, respectively. Interfaces formed from proteoliposomes with an 880:1 (w/w) lipid to protein ratio had a D_L of 1.98 ± 0.09 $\mu m^2/s$ and a mobile fraction of 0.79 ± 0.06. ANOVA analysis shows that the D_L and mobile fraction for these interfaces were not statistically different. However, the standard deviations in D_L (~5%) and mobile fraction (~8%) for the 880:1 (w/w) interfaces were less than those for the 270:1 (w/w) interfaces (~15% in D_L and ~17% in the mobile fraction). We believe the large standard deviations in the D_L and mobile fraction for the 270:1 (w/w) interfaces relative to the 880:1 (w/w) interfaces are the result of a heterogeneous interface in which some fluorophores diffuse freely in patches of fluid sBLMs, while others remain immobile in adsorbed but unruptured liposomes. The D_L and mobile fraction (2.01 ± 0.13 $\mu m^2/s$ and 0.81 ± 0.05, respectively) for 1600:1 (w/w) interfaces were not statistically different to those for 880:1 (w/w) interfaces. In addition, the standard deviations in D_L and mobile fractions were comparable for both interfaces. At an 880:1 (w/w) lipid to protein ratio, it appears the formation of fluid sBLMs constituted from proteoliposomes is unimpeded. Therefore, the minimum DOPC lipid to NEST protein ratio at which we observed fluid sBLM formation upon proteoliposome deposition on silica was 880:1 (w/w). It is conceivable that a fluid interface could be obtained at some other ratio between 270:1 and 880:1. However, we did not investigate this possibility.

6.4.2. Interfaces Formed with Yeast Membrane Fractions

Membrane fractions of *Saccharomyces pombe* yeast cells with NBD-PC fluorophores yielded a mobile fraction of 0.24 ± 0.06 and a D_L of 1.71 ± 0.44 $\mu m^2/s$ after deposition on silica (Figure 6.3). The low average mobile fraction shows that the majority of fluorophores were in adsorbed membrane fractions consisting of lipid and protein that did not spontaneously form fluid sBLMs. We also speculate that the large standard deviation in D_L values is likely due to mobile fluorophores that experienced hindered diffusion from proteins and other cell debris in the microsomes. After separation of membrane proteins from the lipids, the lipid fraction of the yeast membranes produced sBLMs with a mobile fraction of 0.67 ± 0.03 and D_L of 1.90 ± 0.14 $\mu m^2/s$ (Figure 6.4). We measured comparable D_L and mobile fractions in sBLMs reconstituted from POPC and NBD-PC with no proteins (Figure 6.5). The D_L and mobile fractions for interfaces formed from mixtures of NBD-PC with POPC and with microsome membrane fractions are summarized in Table 6.2.

The removal of proteins from the yeast membrane fractions led to a near 3-fold increase in the mobile fraction. The 21% reduction in the standard deviation of D_L also suggests a more uniform bilayer. Although we did not quantify the concentration of protein or lipid present in the yeast membrane fractions, these results give a qualitative sense of how membrane protein concentration can significantly influence fluorophore dynamics in sBLMs.

6.4.3. Significance of Lipid to Protein Ratios in the Formation of sBLM Interfaces

The minimum ratio of DOPC lipid to NEST protein at which we observed a fluid sBLMs upon proteoliposome reconstitution on silica was 880:1 (w/w) (65,000 mol/mol). In studies using a 47 kDa trans-membrane glycoprotein called tissue factor (TF), Contino et al. used a 100,000:1 mol/mol lipid to protein ratio to form sBLMs on the inner surface of glass microcapillary tubes.[172] The TF protein, which forms complexes that initiate blood coagulation after tissue damage, has an extracellular domain (residues 1-219), a transmembrane domain (residues 220-242), and a cytoplasmic domain (residues 243-263).[172] Salafsky et al. incorporated 100 kDa trans-membrane RC's in proteoliposomes at a 350:1 mol/mol lipid to protein ratio to form fluid sBLMs on glass surfaces.[15] There is no evidence that the protein concentrations used in the Contino and Salafsky experiments corresponded to the minimum lipid to protein ratio for fluid sBLM formation. It is possible that these concentrations were arbitrarily chosen.

6.5. Conclusions

We used four different DOPC lipid to NEST protein ratios to assess the effect of protein concentration on the dynamics of NBD-PC in interfaces formed by proteoliposome self-assembly on silica. At a ratio of 80:1 (w/w), proteoliposomes adsorbed to the silica surface but did not rupture to form a bilayer. At a ratio of 270:1 (w/w), we observed only patches of fluid bilayers, with interspersed regions of unruptured liposomes. Although the minimum lipid to protein ratio at which we observed fluid sBLM formation was 880:1 (w/w), previous work suggests that sBLM formation

from proteoliposomes may be a function of several variables besides than protein concentration. We also observed that interfaces formed from membrane fractions of *Saccharomyces pombe* cells were relatively immobile compared to interfaces formed from the extracted lipids of these cells.

6.6. Recommendations for Future Work

Based on the above discussion, we could suggest a systematic study with proteins of different molecular weights and electrostatic charge (adjusted by pH) to understand how these variables influence sBLM formation. Also, it would be meaningful to assess if the activity of supported bilayer membrane-bound proteins is preserved. These studies may be useful in the design of supported BLM-based sensors that incorporate membrane proteins.

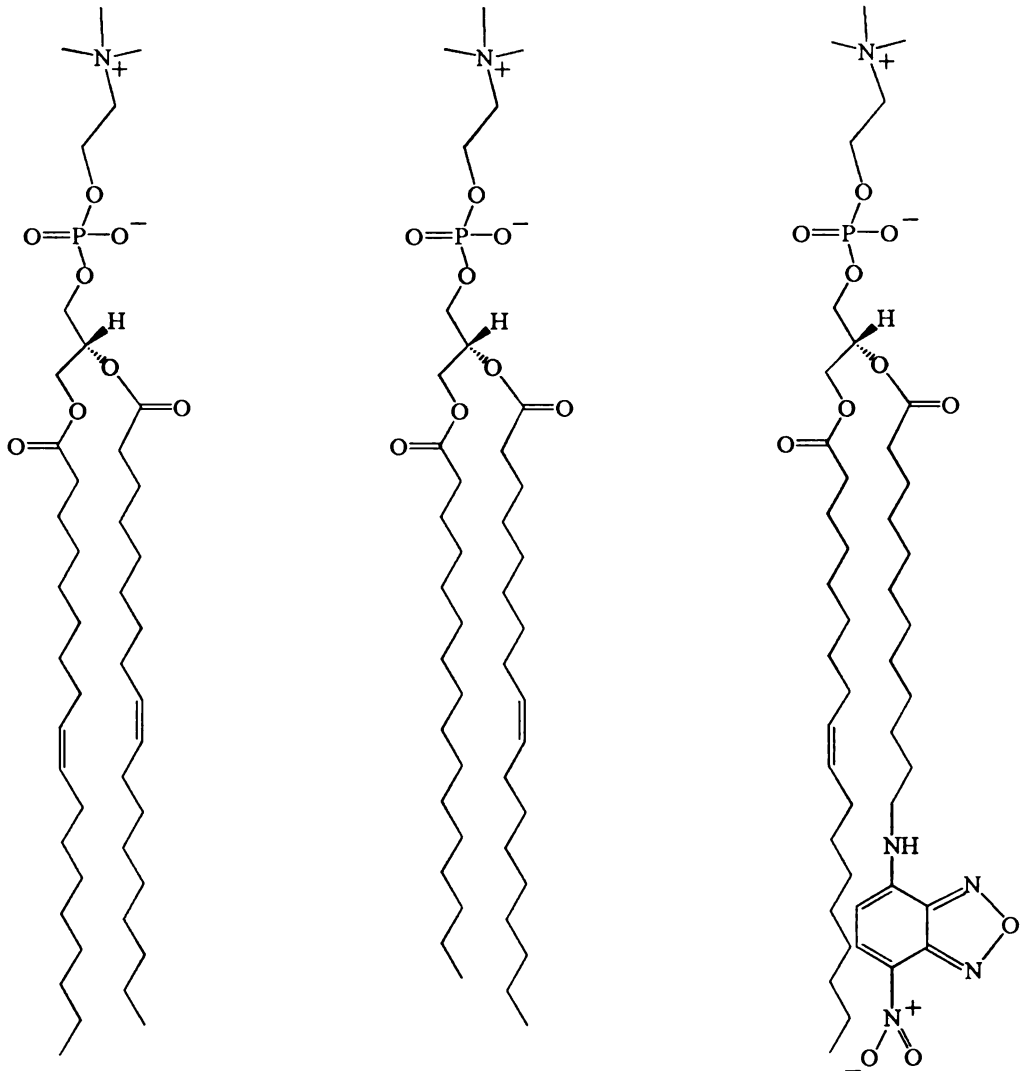

(a) (b) (c)

Figure 6.1. Molecular structures of the synthetic lipids used in this study: dioleoylphosphatidylcholine (DOPC), palmitoyl-oleoyl phosphatidylcholine (POPC), and the fluorophore NBD-phosphatidylcholine (NBD-PC).

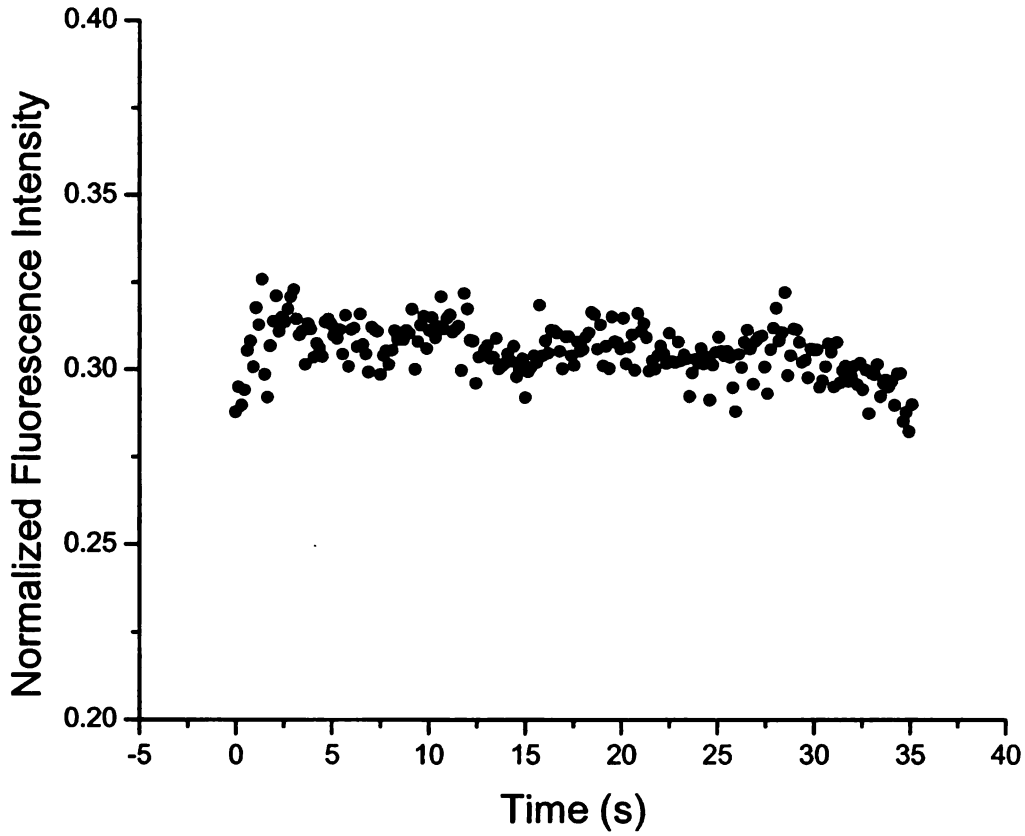

Figure 6.2. Representative FRAPP recovery curve for an interface formed from proteoliposomes at an 80:1 (w/w) lipid to protein ratio.

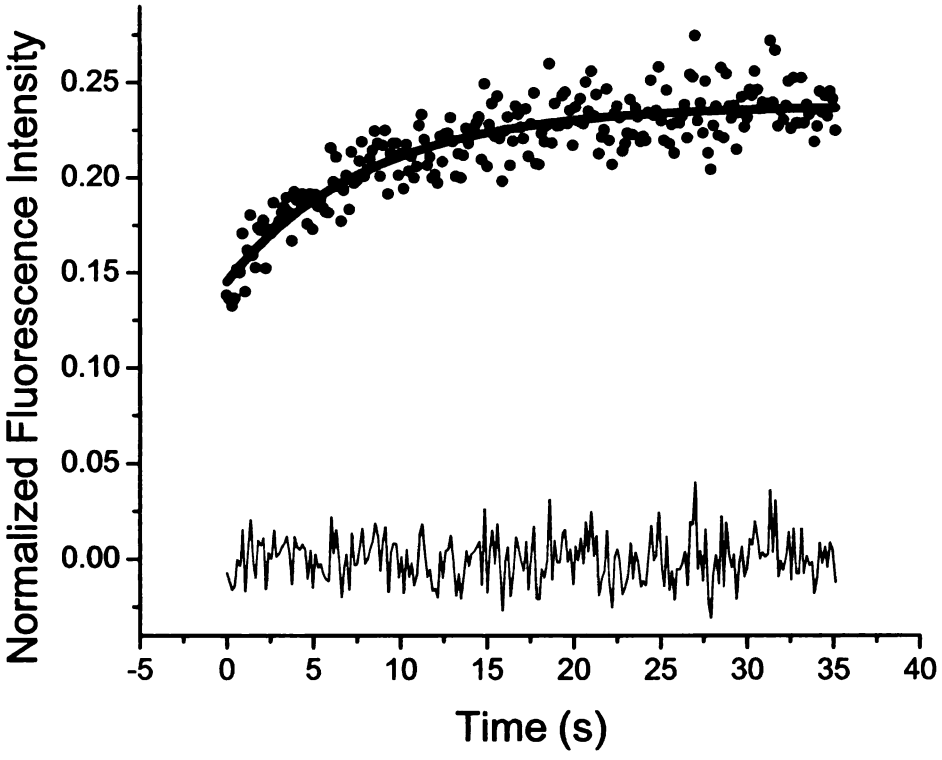

Figure 6.3. Representative FRAPP recovery curve with residuals (below) for an interface formed from membrane fractions of *Saccharomyces pombe* cells.

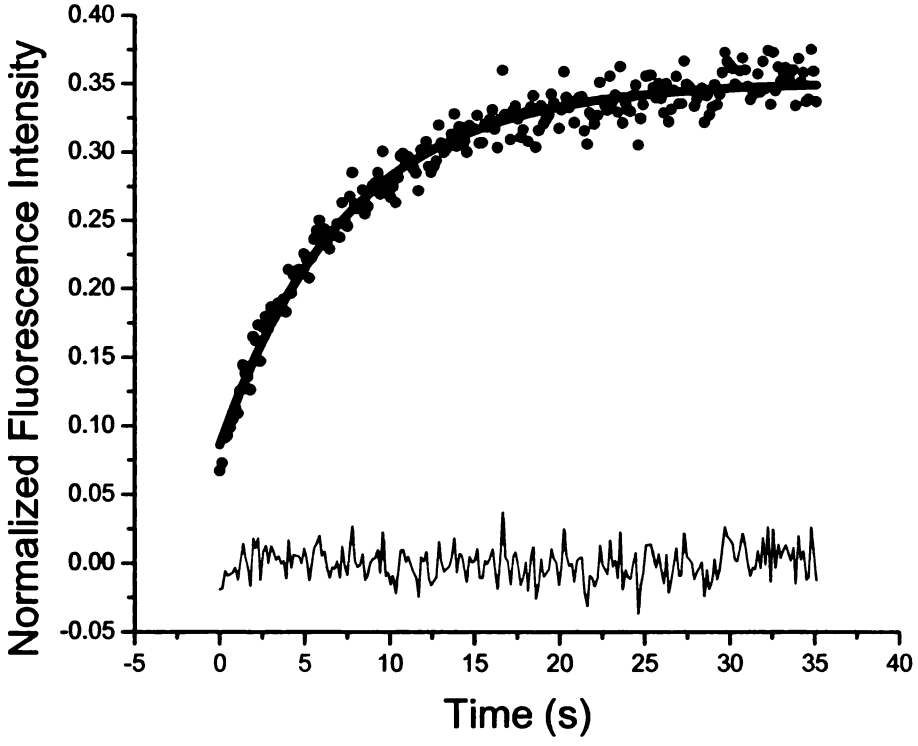

Figure 6.4. Representative FRAPP recovery curve with residuals (below) for an interface formed from the lipid fraction of *Saccharomyces pombe* cell membrane.

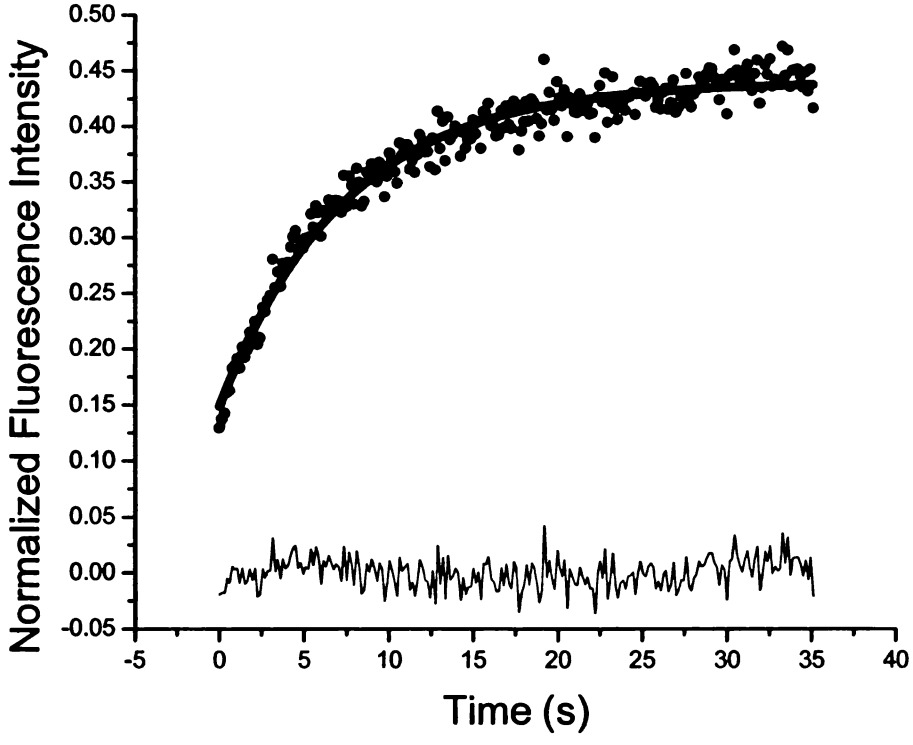

Figure 6.5. Representative FRAPP recovery curve with residuals (below) for a POPC sBLM.

Table 6.1. Translational diffusion coefficients (D_L) and mobile fractions for interfaces formed from systems containing DOPC, NEST, and NBD-PC[a].

System[b,c]	D_L (μm²/s)	Mobile Fraction
1600:1	2.01 ± 0.13^{A}	0.81 ± 0.05^{B}
880:1	1.98 ± 0.09^{A}	0.79 ± 0.06^{B}
270:1	1.72 ± 0.25^{A}	0.75 ± 0.13^{B}
80:1	-	-

[a]Data represent means ± SD of three liposome solutions.

[b]DOPC lipid to NEST protein ratio (w/w).

[c]Systems with statistically identical D_L values and mobile fractions are labeled by common capital letters (ANOVA, Tukey post-hoc test, $p < 0.05$).

Table 6.2. Translational diffusion coefficients (D_L) and mobile fractions for interfaces formed from systems containing 2 mol% NBD-PC[a].

System[b]	D_L (μm²/s)	Mobile Fraction
Yeast microsomes	1.71 ± 0.44^{A}	0.24 ± 0.06^{B}
Yeast microsome lipids	1.90 ± 0.14^{A}	0.67 ± 0.03^{C}
POPC	2.06 ± 0.20^{A}	0.76 ± 0.02^{D}

[a]Data represent means ± SD of three liposome solutions.

[b]Systems with statistically identical D_L and mobile fractions are labeled by common capital letters (ANOVA, Tukey post-hoc test, $p < 0.05$).

7. CONCLUSIONS

The overall goals of the four studies outlined in this dissertation were to 1) measure the effect of selected molecules and macromolecules on model BLM fluidity, and 2) understand on a fundamental level how these molecules and macromolecules influence membrane fluidity. We accomplished these goals by assessing lipid fluorophore dynamics in several model BLM systems. Chapter 3 describes the effect of two liposome preparation methods, sonication and extrusion, on the mean diameter, size distribution, and rotational and translational dynamics of a fluorophore embedded in DOPC and DOPC/cholesterol systems. We observed that while the mean diameter and size distribution of the liposomes depended on the preparation method, the rotational and translational dynamics of NBD-PC fluorophores embedded in liposomes prepared by either of the two techniques were not statistically different. The dynamics in DOPC/cholesterol systems were slower than in DOPC systems due to enhanced van der Waals interactions in the hydrophobic region of the BLM.

We demonstrated in Chapter 4 that the addition of DOPG to DOPC liposomes had no statistically significant effect on the rotational dynamics of NBD-PE fluorophores, but did influence the translational dynamics in sBLMs. Based on this result, we concluded that the NBD moiety likely rotates as a free rotor and does not interact strongly with surrounding lipids. However, inter lipid-head group hydrogen bonding involving the glycerol moiety of DOPG likely retards translational diffusion.

Chapter 5 covers a study on NEST, the catalytic fragment of NTE. We observed that DOPC bilayer fluidity increased upon addition of p-lysoPC lipids due to fewer van der Waals interactions in the hydrophobic region of the BLM, but decreased after NEST

hydrolyzed a fraction of the p-lysoPC to form palmitic acid. This latter effect can be explained on the basis of geometric considerations. The projected area of the head group of p-lysoPC would decrease as it is hydrolyzed to palmitic acid, resulting in a denser hydrophobic region. This is an important finding in that it suggests a physical parameter that may be used in characterizing lysophospholipid control by NTE in mammalian neuron and other cell types.

In Chapter 6 we studied the effect of a model membrane-associated protein (NEST) on sBLM formation on silica using proteoliposomes of various lipid to protein ratios. The minimum lipid to protein ratio at which we observed fluid sBLMs reconstituted from proteoliposomes was 880:1 (w/w). We also qualitatively assessed the effect of membrane protein on bilayer formation using natural yeast membrane fragments.

We believe the results of the four studies may be useful in understanding the molecules and macromolecules that mediate membrane fluidity in cell membranes. Also, these results may suggest molecules and macromolecules that can be used to manipulate membrane fluidity for the development of BLM-based protein biosensors and related devices.

8. APPENDICES

8.1. Analysis of Variance (ANOVA) Methodology in Data Analysis

Multi-comparison ANOVA with a post-hoc Tukey test ($p < 0.05$) was used throughout this dissertation to determine if there are statistical differences between the means of multiple data sets. We used the total number of data sets being compared (k) and the number of data points (y) in each data set to calculate the studentized degrees of freedom (ν) with Equation (A.1):

$$\nu = k(y-1) \tag{A.1}$$

An α value of 0.95, corresponding to a 95% confidence limit, was chosen and a q parameter was determined from a table of critical values for F distributions. The q parameter is a function of k, ν, and α. We calculated the mean square for error (MSE) from Equation (A.2):

$$MSE = \frac{\sum_{i=1}^{k} S_i^2}{k} \tag{A.2}$$

Here, S_i refers to the standard deviation of the ith data set. The Tukey parameter (Tu) was calculated with Equation (A.3):

$$Tu = q\sqrt{\frac{MSE}{y}} \tag{A.3}$$

Any means that differed by more than Tu were considered significantly different.

8.2. Non-linear Curve Fitting Analysis

Throughout this dissertation, we used mathematical models to interpret fluorescence lifetime, fluorescence anisotropy, and FRAPP data. In general, a model with *n* parameters will fit data at least as well as a model with *n*-1 parameters. An F-test comparison was conducted to determine whether a model with *n* parameters provided a statistically significant improvement in the goodness of fit over a model with *n*-1 parameters. The F-statistic was defined as:

$$F = \frac{(\chi_1^2 - \chi_2^2)(N-5)}{2\chi_2^2} \tag{A.4}$$

where N is the number of data points and χ_1^2 and χ_2^2 are the chi-squared goodness-of-fit statistics for models with *n*-1 and *n* parameters, respectively. If this F statistic exceeded 3.0, the fit using the model with *n* parameters is considered a significant improvement.[160, 173]

9. REFERENCES

1. Garcia, J. J.; Martinez-Ballarin, E.; Millan-Plano, S.; Allue, J. L.; Albendea, C.; Fuentes, L.; Escanero, J. F., Effects of trace elements on membrane fluidity. *Journal of Trace Elements in Medicine and Biology* **2005,** 19, (1), 19-22.

2. Beney, L.; Gervais, P., Influence of the fluidity of the membrane on the response of microorganisms to environmental stresses. *Applied Microbiology and Biotechnology* **2001,** 57, (1-2), 34-42.

3. Epand, R. M., Studies of membrane physical properties and their role in biological function. *Biochemical Society Transactions* **1997,** 25, (3), 1073-1079.

4. Cremer, P. S.; Boxer, S. G., Formation and spreading of lipid bilayers on planar glass supports. *Journal of Physical Chemistry B* **1999,** 103, (13), 2554-2559.

5. Carmichael, M.; Vidu, R.; Maksumov, A.; Palazoglu, A.; Stroeve, P., Using wavelets to analyze AFM images of thin films: Surface micelles and supported lipid bilayers. *Langmuir* **2004,** 20, (26), 11557-11568.

6. Dorvel, B. R.; Keizer, H. M.; Fine, D.; Vuorinen, J.; Dodabalapur, A.; Duran, R. S., Formation of tethered bilayer lipid membranes on gold surfaces: QCM-Z and AFM study. *Langmuir* **2007,** 23, (13), 7344-7355.

7. Jadhav, S. R.; Zheng, Y.; Garavito, R. M.; Worden, R. M., Functional characterization of PorB class II porin from Neisseria meningitidis using a tethered bilayer lipid membrane. *Biosensors & Bioelectronics* **2008,** 24, (4), 831-835.

8. Raguse, B.; Braach-Maksvytis, V.; Cornell, B. A.; King, L. G.; Osman, P. D. J.; Pace, R. J.; Wieczorek, L., Tethered lipid bilayer membranes: Formation and ionic reservoir characterization. *Langmuir* **1998,** 14, (3), 648-659.

9. Dickey, A.; Faller, R., Examining the contributions of lipid shape and headgroup charge on bilayer behavior. *Biophysical Journal* **2008,** 95, (6), 2636-2646.

10. Elmore, D. E., Molecular dynamics simulation of a phosphatidylglycerol membrane. *Febs Letters* **2006,** 580, (1), 144-148.

11. Kaznessis, Y. N.; Kim, S. T.; Larson, R. G., Simulations of zwitterionic and anionic phospholipid monolayers. *Biophysical Journal* **2002,** 82, (4), 1731-1742.

12. Heinrich, F.; Ng, T.; Vanderah, D. J.; Shekhar, P.; Mihailescu, M.; Nanda, H.; Losche, M., A New Lipid Anchor for Sparsely Tethered Bilayer Lipid Membranes. *Langmuir* **2009,** 25, (7), 4219-4229.

13. Knoll, W.; Koper, I.; Naumann, R.; Sinner, E. K., Tethered bimolecular lipid membranes - A novel model membrane platform. *Electrochimica Acta* **2008,** 53, (23), 6680-6689.

14. Brian, A. A.; McConnell, H. M., Allogeneic Stimulation of Cyto-Toxic T-Cells by Supported Planar Membranes. *Proceedings of the National Academy of Sciences of the United States of America-Biological Sciences* **1984,** 81, (19), 6159-6163.

15. Salafsky, J.; Groves, J. T.; Boxer, S. G., Architecture and function of membrane proteins in planar supported bilayers: A study with photosynthetic reaction centers. *Biochemistry* **1996,** 35, (47), 14773-14781.

16. Ge, G. X.; Wu, J.; Lin, Q. S., Effect of membrane fluidity on tyrosine kinase activity of reconstituted epidermal growth factor receptor. *Biochemical and Biophysical Research Communications* **2001,** 282, (2), 511-514.

17. Cai, C. X.; Zhu, H.; Chen, J. W., Overexpression of caveolin-1 increases plasma membrane fluidity and reduces P-glycoprotein function in Hs578T/Dox. *Biochemical and Biophysical Research Communications* **2004,** 320, (3), 868-874.

18. Kadoya, A.; Miyake, H.; Ohyashiki, T., Contribution of lipid dynamics on the inhibition of bovine brain synaptosomal Na+-K+-ATPase activity induced by 4-hydroxy-2-nonenal. *Biological & Pharmaceutical Bulletin* **2003,** 26, (6), 787-793.

19. McGarry, J. D.; Brown, N. F., Reconstitution of purified, active and malonyl-CoA-sensitive rat liver carnitine palmitoyltransferase I: relationship between membrane environment and malonyl-CoA sensitivity. *Biochemical Journal* **2000,** 349, 179-187.

20. Velitchkova, M.; Popova, A.; Markova, T., Effect of membrane fluidity on photoinhibition of isolated thylakoids membranes at room and low temperature. *Zeitschrift Fur Naturforschung C-a Journal of Biosciences* **2001,** 56, (5-6), 369-374.

21. Garret, R. H., Grisham, C.M., *Biochemistry.* 3rd ed.; Thompson Brooks/Cole: Belmont, CA, 2007; p 13-21.

22. Seu, K. J.; Cambrea, L. R.; Everly, R. M.; Hovis, J. S., Influence of lipid chemistry on membrane fluidity: Tail and headgroup interactions. *Biophysical Journal* **2006,** 91, (10), 3727-3735.

23. Zhang, Y. P.; Lewis, R.; McElhaney, R. N., Calorimetric and spectroscopic studies of the thermotropic phase behavior of the n-saturated 1,2-diacylphosphatidylglycerols. *Biophysical Journal* **1997,** 72, (2), 779-793.

24. Chan, Y. H. M.; Boxer, S. G., Model membrane systems and their applications. *Current Opinion in Chemical Biology* **2007,** 11, (6), 581-587.

25. Smith, L. M.; Weis, R. M.; McConnell, H. M., Measurement of Rotational Motion in Membranes Using Fluorescence Recovery after Photobleaching. *Biophysical Journal* **1981,** 36, (1), 73-91.

26. Keller, C. A.; Glasmastar, K.; Zhdanov, V. P.; Kasemo, B., Formation of supported membranes from vesicles. *Physical Review Letters* **2000,** 84, (23), 5443-5446.

27. Keller, C. A.; Kasemo, B., Surface specific kinetics of lipid vesicle adsorption measured with a quartz crystal microbalance. *Biophysical Journal* **1998,** 75, (3), 1397-1402.

28. Kalb, E.; Frey, S.; Tamm, L. K., Formation of Supported Planar Bilayers by Fusion of Vesicles to Supported Phospholipid Monolayers. *Biochimica Et Biophysica Acta* **1992,** 1103, (2), 307-316.

29. Smith, E. A.; Coym, J. W.; Cowell, S. M.; Tokimoto, T.; Hruby, V. J.; Yamamura, H. I.; Wirth, M. J., Lipid bilayers on polyacrylamide brushes for inclusion of membrane proteins. *Langmuir* **2005,** 21, (21), 9644-9650.

30. Keizer, H. M.; Dorvel, B. R.; Andersson, M.; Fine, D.; Price, R. B.; Long, J. R.; Dodabalapur, A.; Koper, I.; Knoll, W.; Anderson, P. A. V.; Duran, R. S., Functional ion channels in tethered bilayer membranes - Implications for biosensors. *Chembiochem* **2007,** 8, (11), 1246-1250.

31. Lei, S. B.; Tero, R.; Misawa, N.; Yamamura, S.; Wan, L. J.; Urisu, T., AFM characterization of gramicidin-A in tethered lipid membrane on silicon surface. *Chemical Physics Letters* **2006,** 429, (1-3), 244-249.

32. Deniaud, A.; Rossi, C.; Berquand, A.; Homand, J.; Campagna, S.; Knoll, W.; Brenner, C.; Chopineau, J., Voltage-dependent anion channel transports calcium ions through biomimetic membranes. *Langmuir* **2007,** 23, (7), 3898-3905.

33. Rossi, C.; Chopineau, J., Biomimetic tethered lipid membranes designed for membrane-protein interaction studies. *European Biophysics Journal with Biophysics Letters* **2007,** 36, (8), 955-965.

34. Weiss, S. A.; Bushby, R. J.; Evans, S. D.; Henderson, P. J. F.; Jeuken, L. J. C., Characterization of cytochrome bo(3) activity in a native-like surface-tethered membrane. *Biochemical Journal* **2009,** 417, 555-560.

35. Lapinski, M. M.; Castro-Forero, A.; Greiner, A. J.; Ofoli, R. Y.; Blanchard, G. J., Comparison of liposomes formed by sonication and extrusion: Rotational and translational diffusion of an embedded chromophore. *Langmuir* **2007,** 23, 11677-11683.

36. Greiner, A. J.; Pillman, H. A.; Worden, R. M.; Blanchard, G. J.; Ofoli, R. Y., Effect of hydrogen bonding on the rotational and translational dynamics of a headgroup-

bound chromophore in bilayer lipid membranes. *J Phys Chem B* **2009,** 113, (40), 13263-8.

37. Glynn, P., Neuropathy target esterase. *Biochemical Journal* **1999,** 344, 625-631.

38. Rainier, S.; Bui, M.; Mark, E.; Thomas, D.; Tokarz, D.; Ming, L.; Delaney, C.; Richardson, R. J.; Albers, J. W.; Matsunami, N.; Stevens, J.; Coon, H.; Leppert, M.; Fink, J. K., Neuropathy target esterase gene mutations cause motor neuron disease. *American Journal of Human Genetics* **2008,** 82, (3), 780-785.

39. van Tienhoven, M.; Atkins, J.; Li, Y.; Glynn, P., Human neuropathy target esterase catalyzes hydrolysis of membrane lipids. *Journal of Biological Chemistry* **2002,** 277, (23), 20942-20948.

40. Langner, M.; Isac, T.; Hui, S. W., Interaction of Free Fatty-Acids with Phospholipid-Bilayers. *Biochimica Et Biophysica Acta-Biomembranes* **1995,** 1236, (1), 73-80.

41. Pjura, W. J.; Kleinfeld, A. M.; Karnovsky, M. J., Partition of Fatty-Acids and Fluorescent Fatty-Acids into Membranes. *Biochemistry* **1984,** 23, (9), 2039-2043.

42. Nollert, P.; Kiefer, H.; Jahnig, F., Lipid Vesicle Adsorption Versus Formation of Planar Bilayers on Solid-Surfaces. *Biophysical Journal* **1995,** 69, (4), 1447-1455.

43. Zhdanov, V. P.; Kasemo, B., Comments on rupture of absorbed vesicles. *Langmuir* **2001,** 17, (12), 3518-3521.

44. Starr, T. E.; Thompson, N. L., Fluorescence pattern photobleaching recovery for samples with multi-component diffusion. *Biophysical Chemistry* **2002,** 97, (1), 29-44.

45. Corporation, B. E., What is Time Correlated Single Photon Counting? In *http://www.boselec.com/products/documents/WhatisTimeCorrelatedSinglePhotonCounting01-10-00.pdf*.

46. Kinosita, K.; Kawato, S.; Ikegami, A., Theory of Fluorescence Polarization Decay in Membranes. *Biophysical Journal* **1977,** 20, (3), 289-305.

47. Lipari, G.; Szabo, A., Effect of Librational Motion on Fluorescence Depolarization and Nuclear Magnetic-Resonance Relaxation in Macromolecules and Membranes. *Biophysical Journal* **1980,** 30, (3), 489-506.

48. Chuang, T. J.; Eisentha.Kb, Theory of Fluorescence Depolarization by Anisotropic Rotational Diffusion. *Journal of Chemical Physics* **1972,** 57, (12), 5094-5098.

49. DelaCruz, J. L.; Blanchard, G. J., Understanding the Balance between Ionic and Dispersion Interactions in Aqueous Micellar Media. *Journal of Physical Chemistry B* **2003,** 107, (29), 7102-7108.

50. Dewitt, L.; Blanchard, G. J.; Legoff, E.; Benz, M. E.; Liao, J. H.; Kanatzidis, M. G., Determination of Ground-State and Excited-State Isomerization Barriers for the Oligothiophene 3',4'-Dibutyl-2,2'-5',2"-Terthiophene. *Journal of the American Chemical Society* **1993,** 115, (25), 12158-12164.

51. Manconi, M.; Isola, R.; Falchi, A. M.; Sinico, C.; Fadda, A. M., Intracellular distribution of fluorescent probes delivered by vesicles of different lipidic composition. *Colloids and Surfaces, B: Biointerfaces* **2007,** 57, (2), 143-151.

52. Wang, S.; Huang, J.; Song, Q.; Fu, H., Characterizing assembly morphology changes during solubilization process of dimyristoyl phosphocholine vesicles by n-dodecyl triethylammonium bromide. *Journal of Colloid and Interface Science* **2007,** 311, (1), 296-302.

53. Kim, S. H.; Haimovich-Caspi, L.; Omer, L.; Talmon, Y.; Franses, E. I., Effect of sonication and freezing-thawing on the aggregate size and dynamic surface tension of aqueous DPPC dispersions. *Journal of Colloid and Interface Science* **2007,** 311, (1), 217-227.

54. Chen, K.; Luo, W.; Rahman, Z. U.; Guo, Y.; Schulte, A., DOPE/DDAB magneto-vesicles: synthesis and characterization. *Journal of Dispersion Science and Technology* **2007,** 28, (3), 471-476.

55. Driessen, A. J. M.; Vandenhooven, H. W.; Kuiper, W.; Vandekamp, M.; Sahl, H. G.; Konings, R. N. H.; Konings, W. N., Mechanistic Studies of Lantibiotic-Induced Permeabilization of Phospholipid-Vesicles. *Biochemistry* **1995,** 34, (5), 1606-1614.

56. Hunter, D. G.; Frisken, B. J., Effect of extrusion pressure and lipid properties on the size and polydispersity of lipid vesicles. *Biophysical Journal* **1998,** 74, (6), 2996-3002.

57. Womack, M. D.; Kendall, D. A.; Macdonald, R. C., Detergent Effects on Enzyme-Activity and Solubilization of Lipid Bilayer-Membranes. *Biochimica Et Biophysica Acta* **1983,** 733, (2), 210-215.

58. Mayer, L. D.; Hope, M. J.; Cullis, P. R., Vesicles of variable sizes produced by a rapid extrusion procedure. *Biochimica et Biophysica Acta* **1986,** 858, (1), 161-168.

59. Subbarao, N. K.; MacDonald, R. I.; Takeshita, K.; MacDonald, R. C., Characteristics of spectrin-induced leakage of extruded, phosphatidylserine vesicles. *Biochimica et Biophysica Acta* **1991,** 1063, (1), 147-154.

60. Unger, E. C.; MacDougall, P.; Cullis, P.; Tilcock, C., Liposomal Gd-DTPA: effect of encapsulation on enhancement of hepatoma model by MRI. *Magnetic Resonance Imaging* **1989,** 7, (4), 417-423.

61. Maulucci, G.; De Spirito, M.; Arcovito, G.; Boffi, F.; Castellano, A. C.; Briganti, G., Particle size distribution in DMPC vesicles solutions undergoing different sonication times. *Biophysical Journal* **2005,** 88, (5), 3545-3550.

62. Feitosa, E.; Barreleiro, P. C. A.; Olofsson, G., Phase transition in dioctadecyldimethylammonium bromide and chloride vesicles prepared by different methods. *Chemistry and Physics of Lipids* **2000,** 105, (2), 201-213.

63. Cornell, B. A.; Fletcher, G. C.; Middlehurst, J.; Separovic, F., The lower limit to the size of small sonicated phospholipid vesicles. *Biochimica et Biophysica Acta, Biomembranes* **1982,** 690, (1), 15-19.

64. Schroeder, R.; London, E.; Brown, D., Interactions between saturated acyl chains confer detergent resistance on lipids and glycosylphosphatidylinositol (GPI)-anchored proteins: GPI-anchored proteins in liposomes and cells show similar behavior. *Proceedings of the National Academy of Sciences of the United States of America* **1994,** 91, (25), 12130-4.

65. Chattopadhyay, A.; London, E., Spectroscopic and ionization properties of N-(7-nitrobenz-2-oxa-1,3,-diazol-4-yl)-labeled lipids in model membranes. *Biochimica et Biophysica Acta: Biomembranes* **1988,** 938, 24-34.

66. Fery-Forgues, S.; Fayet, J.-P.; Lopez, A., Drastic changes in the fluorescence properties of 7-nitrobenz-2-1,3-diazol-4-yl derivative (NBD) probes with the polarity of the medium: Involvement of a TICT state? *Journal of Photochemistry and Photobiology A: Chemistry* **1993,** 70, 229-243.

67. Mazeres, S.; Schram, V.; Tocane, J.-F.; Lopez, A., 7-Nitrobenz-2-oxa-1,3-diazol-4-yl-labeled phospholipids in lipid membranes: Differences in fluorescence behavior. *Biophysical Journal* **1996,** 91, 327-335.

68. Gajraj, A.; Ofoli, R. Y., Quantitative technique for investigating macromolecular adsorption and interactions at the liquid-liquid interface. *Langmuir* **2000,** 16, (9), 4279-4285.

69. Berne, B. J., Pecora, R., *Dynamic Light Scatterings with Application to Chemistry, Biology, and Physics*. Wiley: New York, 1976.

70. Aragon, S. R.; Pecora, R., Theory of dynamic light scattering from polydisperse systems. *Journal of Chemical Physics* **1976,** 64, (6), 2395-404.

71. Hallett, F. R.; Craig, T.; Marsh, J.; Nickel, B., Particle size analysis: number distributions by dynamic light scattering. *Canadian Journal of Spectroscopy* **1989,** 34, (3), 63-70.

72. Hupfeld, S.; Holsaeter, A. M.; Skar, M.; Frantzen, C. B.; Brandl, M., Liposome size analysis by dynamic/static light scattering upon size exclusion-/field flow-fractionation. *Journal of Nanoscience and Nanotechnology* **2006,** 6, (9/10), 3025-3031.

73. Raghuraman, H.; Shrivastava, S.; Chattopadhyay, A., Monitoring the looping up of acyl chain labeled NBD lipids in membranes as a function of membrane phase state. *Biochimica Et Biophysica Acta-Biomembranes* **2007,** 1768, (5), 1258-1267.

74. Huster, D.; Muller, P.; Arnold, K.; Herrmann, A., Dynamics of membrane penetration of the fluorescent 7-nitrobenz-2-oxa-1,3-diazol-4-yl (NBD) group attached to an acyl chain of phosphatidylcholine. *Biophysical Journal* **2001,** 80, (2), 822-831.

75. Huster, D.; Muller, P.; Arnold, K.; Herrmann, A., Dynamics of lipid chain attached fluorophore 7-nitrobenz-2-oxa-1,3-diazol-4-yI (NBD) in negatively charged membranes determined by NMR spectroscopy. *European Biophysics Journal with Biophysics Letters* **2003,** 32, (1), 47-54.

76. Mukherjee, S.; Raghuraman, H.; Dasgupta, S.; Chattopadhyay, A., Organization and dynamics of N-(7-nitrobenz-2-oxa-1,3-diazol-4-yl)-labeled lipids: a fluorescence approach. *Chemistry and Physics of Lipids* **2004,** 127, (1), 91-101.

77. Greenough, K. P.; Blanchard, G. J., Evaluating the role of chromophore side group identity in mediating solution-phase rotational motion. *Journal of Physical Chemistry A* **2007,** 111, (4), 558-566.

78. Feng, Z. V.; Spurlin, T. A.; Gewirth, A. A., Direct visualization of asymmetric behavior in supported lipid bilayers at the gel-fluid phase transition. *Biophysical Journal* **2005,** 88, (3), 2154-2164.

79. Drexhage, K. H., Influence of a dielectric interface on fluorescence decay time. *Proc. Int. Conf. Lumin.* **1970,** 693-701.

80. Karpovich, D. S.; Blanchard, G. J., Dynamics of a Tethered Chromophore Imbedded in a Self-Assembled Monolayer. *Langmuir* **1996,** 12, (23), 5522-5524.

81. Kinosita, K., Jr.; Ikegami, A.; Kawato, S., On the wobbling-in-cone analysis of fluorescence anisotropy decay. *Biophysical Journal* **1982,** 37, (2), 461-4.

82. Szabo, A., Theory of fluorescence depolarization in macromolecules and membranes. *Journal of Chemical Physics* **1984,** 81, (1), 150-67.

83. Filippov, A.; Oradd, G.; Lindblom, G., Influence of cholesterol and water content on phospholipid lateral diffusion in bilayers. *Langmuir* **2003,** 19, (16), 6397-6400.

84. Kahya, N.; Schwille, P., How Phospholipid-Cholesterol Interactions Modulate Lipid Lateral Diffusion, as Revealed by Fluorescence Correlation Spectroscopy. *Journal of Fluorescence* **2006,** 16, (5), 671-678.

85. Liu-Wu, Y.; Hurt-Camejo, E.; Wiklund, O., Lysophosphatidylcholine induces the production of IL-1 beta by human monocytes. *Atherosclerosis* **1998,** 137, (2), 351-357.

86. Nishimura, S. Y.; Vrljic, M.; Klein, L. O.; McConnell, H. M.; Moerner, W. E., Cholesterol depletion induces solid-like regions in the plasma membrane. *Biophysical Journal* **2006,** 90, (3), 927-938.

87. Cullis, P. R., Lateral diffusion rates of phosphatidylcholine in vesicle membranes: effects of cholesterol and hydrocarbon phase transitions. *FEBS Letters* **1976,** 70, (1), 223-8.

88. Oradd, G.; Lindblom, G.; Westerman, P. W., Lateral diffusion of cholesterol and dimyristoylphosphatidylcholine in a lipid bilayer measured by pulsed field gradient NMR spectroscopy. *Biophysical Journal* **2002,** 83, (5), 2702-2704.

89. M'Baye, G.; Mely, Y.; Duportail, G.; Klymchenko, A. S., Liquid ordered and gel phases of lipid bilayers: Fluorescent probes reveal close fluidity but different hydration. *Biophysical Journal* **2008,** 95, (3), 1217-1225.

90. Jadhav, S. R.; Sui, D. X.; Garavito, R. M.; Worden, R. M., Fabrication of highly insulating tethered bilayer lipid membrane using yeast cell membrane fractions for measuring ion channel activity. *Journal of Colloid and Interface Science* **2008,** 322, (2), 465-472.

91. Cook, S. L.; Bouma, S. R.; Huestis, W. H., Cell to Vesicle Transfer of Intrinsic Membrane-Proteins - Effect of Membrane Fluidity. *Biochemistry* **1980,** 19, (20), 4601-4607.

92. Fong, T. M.; McNamee, M. G., Correlation between Acetylcholine-Receptor Function and Structural-Properties of Membranes. *Biochemistry* **1986,** 25, (4), 830-840.

93. Miersch, S.; Espey, M. G.; Chaube, R.; Akarca, A.; Tweten, R.; Ananvoranich, S.; Mutus, B., Plasma membrane cholesterol content affects nitric oxide diffusion dynamics and signaling. *Journal of Biological Chemistry* **2008,** 283, (27), 18513-18521.

94. Schroder, M., Endoplasmic reticulum stress responses. *Cellular and Molecular Life Sciences* **2008,** 65, (6), 862-894.

95. Loffeld, B.; Keweloh, H., cis/trans Isomerization of unsaturated fatty acids as possible control mechanism of membrane fluidity in Pseudomonas putida P8. *Lipids* **1996,** 31, (8), 811-815.

96. Hui, S. W.; He, N. B., Molecular organization in cholesterol-lecithin bilayers by x-ray and electron diffraction measurements. *Biochemistry* **1983,** 22, (5), 1159-64.

97. Schroeder, R.; London, E.; Brown, D., Interactions between Saturated Acyl Chains Confer Detergent Resistance on Lipids and Glycosylphosphatidylinositol (Gpi)-Anchored Proteins - Gpi-Anchored Proteins in Liposomes and Cells Show Similar Behavior. *Proceedings of the National Academy of Sciences of the United States of America* **1994,** 91, (25), 12130-12134.

98. Sakurai, I.; Mizusawa, N.; Ohashi, S.; Kobayashi, M.; Wada, H., Effects of the lack of phosphatidylglycerol on the donor side of photosystem II. *Plant Physiology* **2007,** 144, (3), 1336-1346.

99. Wada, H.; Murata, N., The essential role of phosphatidylglycerol in photosynthesis. *Photosynthesis Research* **2007,** 92, (2), 205-215.

100. Pandit, S. A.; Bostick, D.; Berkowitz, M. L., Molecular dynamics simulation of a dipalmitoylphosphatidylcholine bilayer with NaCl. *Biophysical Journal* **2003,** 84, (6), 3743-3750.

101. PasenkiewiczGierula, M.; Takaoka, Y.; Miyagawa, H.; Kitamura, K.; Kusumi, A., Hydrogen bonding of water to phosphatidylcholine in the membrane as studied by a molecular dynamics simulation: Location, geometry, and lipid-lipid bridging via hydrogen-bonded water. *Journal of Physical Chemistry A* **1997,** 101, (20), 3677-3691.

102. Bockmann, R. A.; Hac, A.; Heimburg, T.; Grubmuller, H., Effect of sodium chloride on a lipid bilayer. *Biophysical Journal* **2003,** 85, (3), 1647-1655.

103. Pasenkiewicz-Gierula, M.; Takaoka, Y.; Miyagawa, H.; Kitamura, K.; Kusumi, A., Charge pairing of headgroups in phosphatidylcholine membranes: A molecular dynamics simulation study. *Biophysical Journal* **1999,** 76, (3), 1228-1240.

104. Greenough, K. P.; Blanchard, G. J., Lipid headgroups mediate organization and dynamics in bilayers. *Spectrochimica Acta Part a-Molecular and Biomolecular Spectroscopy* **2009,** 71, (5), 2050-2056.

105. Uragami, M.; Miyake, Y.; Tokutake, N.; Zhang, L. H.; Regen, S. L., Design and synthesis of phosphatidylcholine mimics and their mixing behavior with phosphatidylglycerol mimics in the fluid bilayer state. *Langmuir* **2000,** 16, (21), 8010-8015.

106. Zhao, W.; Rog, T.; Gurtovenko, A. A.; Vattulainen, I.; Karttunen, M., Role of phosphatidylglycerols in the stability of bacterial membranes. *Biochimie* **2008,** 90, (6), 930-938.

107. Dicko, A.; Bourque, H.; Pezolet, M., Study by infrared spectroscopy of the conformation of dipalmitoylphosphatidylglycerol monolayers at the air-water interface and transferred on solid substrates. *Chemistry and Physics of Lipids* **1998,** 96, (1-2), 125-139.

108. Hull, M. C.; Cambrea, L. R.; Hovis, J. S., Infrared spectroscopy of fluid lipid bilayers. *Analytical Chemistry* **2005,** 77, (18), 6096-6099.

109. Richter, R. P.; Brisson, A. R., Following the formation of supported lipid bilayers on mica: A study combining AFM, QCM-D, and ellipsometry. *Biophysical Journal* **2005,** 88, 3422-3433.

110. Debye, P., Polar Molecules. In *Chemical Catalog Co.*, New York, 1929.

111. Edward, J. T., Molecular volumes and the Stokes-Einstein equation. *Journal of Chemical Education* **1970,** 47, (4), 261-70.

112. Lapinski, M. M.; Blanchard, G. J., Interrogating the role of liposome size in mediating the dynamics of a chromophore in the acyl chain region of a phospholipid bilayer. *Chemistry and Physics of Lipids* **2008,** 153, (2), 130-137.

113. Blanchard, G. J., Picosecond Spectroscopic Measurement of a Solvent Dependent Change of Rotational Diffusion Rotor Shape. *Journal of Chemical Physics* **1987,** 87, (12), 6802-6808.

114. Shoemaker, S. D.; Vanderlick, T. K., Intramembrane electrostatic interactions destabilize lipid vesicles. *Biophysical Journal* **2002,** 83, (4), 2007-2014.

115. Anderson, T. G.; McConnell, H. M., A thermodynamic model for extended complexes of cholesterol and phospholipid. *Biophysical Journal* **2002,** 83, (4), 2039-2052.

116. Radhakrishnan, A.; McConnell, H. M., Thermal dissociation of condensed complexes of cholesterol and phospholipid. *Journal of Physical Chemistry B* **2002,** 106, (18), 4755-4762.

117. Anderson, T. G.; McConnell, H. M., Condensed complexes and the calorimetry of cholesterol-phospholipid bilayers. *Biophysical Journal* **2001,** 81, (5), 2774-2785.

118. Keller, S. L.; Radhakrishnan, A.; McConnell, H. M., Saturated phospholipids with high melting temperatures form complexes with cholesterol in monolayers. *Journal of Physical Chemistry B* **2000,** 104, (31), 7522-7527.

119. Radhakrishnan, A.; McConnell, H. M., Cholesterol-phospholipid complexes in membranes. *Journal of the American Chemical Society* **1999,** 121, (2), 486-487.

120. Keller, S. L.; McConnell, H. M., Stripe phases in lipid monolayers near a miscibility critical point. *Physical Review Letters* **1999,** 82, (7), 1602-1605.

121. Keller, S. L.; Pitcher, W. H.; Huestis, W. H.; McConnell, H. M., Red blood cell lipids form immiscible liquids. *Physical Review Letters* **1998,** 81, (22), 5019-5022.

122. Subramaniam, S.; McConnell, H. M., Critical Mixing in Monolayer Mixtures of Phospholipid and Cholesterol. *Journal of Physical Chemistry* **1987,** 91, (7), 1715-1718.

123. Maroni, M.; Bleecker, M. L., Neuropathy Target Esterase in Human-Lymphocytes and Platelets. *Journal of Applied Toxicology* **1986,** 6, (1), 1-7.

124. Glynn, P.; Holton, J. L.; Nolan, C. C.; Read, D. J.; Brown, L.; Hubbard, A.; Cavanagh, J. B., Neuropathy target esterase: Immunolocalization to neuronal cell bodies and axons. *Neuroscience* **1998,** 83, (1), 295-302.

125. Muehlig-Versen, M.; da Cruz, A. B.; Tschape, J.-A.; Moser, M.; Buettner, R.; Athenstaedt, K.; Glynn, P.; Kretzschmar, D., Loss of Swiss cheese/neuropathy target esterase activity causes disruption of phosphatidylcholine homeostasis and neuronal and glial death in adult Drosophila. *Journal of Neuroscience* **2005,** 25, (11), 2865-2873.

126. Li, Y.; Dinsdale, D.; Glynn, P., Protein domains, catalytic activity, and subcellular distribution of neuropathy target esterase in mammalian cells. *J. Biol. Chem.* **2003,** 278, (10), 8820-8825.

127. Reiner, E.; Davis, C. S.; Schwab, B. W.; Schopfer, L. M.; Richardson, R. J., Kinetics of Heat Inactivation of Phenyl Valerate Hydrolases from Hen and Rat-Brain. *Biochemical Pharmacology* **1987,** 36, (19), 3181-3185.

128. Quistad, G. B.; Barlow, C.; Winrow, C. J.; Sparks, S. E.; Casida, J. E., Evidence that mouse brain neuropathy target esterase is a lysophospholipase. *Proceedings of the National Academy of Sciences of the United States of America* **2003,** 100, (13), 7983-7987.

129. Vose, S. C.; Fujioka, K.; Gulevich, A. G.; Lin, A. Y.; Holland, N. T.; Casida, J. E., Cellular function of neuropathy target esterase in lysophosphatidylcholine action. *Toxicology and Applied Pharmacology* **2008,** 232, (3), 376-383.

130. Vose, S. C.; Holland, N. I.; Eskenazi, B.; Casida, J. E., Lysophosphatidylcholine hydrolases of human erythrocytes, lymphocytes, and brain: Sensitive targets of conserved specificity for organophosphorus delayed neurotoxicants. *Toxicol. Appl. Pharmacol.* **2007,** 224, (1), 98-104.

131. Abou-Donia, M. B., Organophosphorus ester-induced chronic neurotoxicity. *Archives of Environmental Health* **2003,** 58, (8), 484-497.

132. Jamal, G. A., Neurological syndromes of organophosphorus compounds. *Adverse Drug Reactions and Toxicological Reviews* **1997,** 16, (3), 133-170.

133. Richardson, R. J.; Worden, R. M.; Makhaeva, G. F., *Biomarkers and Biosensors of Delayed Neuropathic Agents*. Academic Press/Elsevier: Amsterdam, 2009; p pp. 859-876.

134. Kropp, T. J.; Glynn, P.; Richardson, R. J., The mipafox-inhibited catalytic domain of human neuropathy target esterase ages by reversible proton loss. *Biochemistry* **2004,** 43, (12), 3716-3722.

135. Wijeyesakere, S. J.; Richardson, R. J., *Neuropathy Target Esterase*. 3rd ed.; Elsevier: Oxford, UK, 2010 (in press); p 64.

136. Farageelawar, M., Development of Esterase-Activities in the Chicken before and after Hatching. *Neurotoxicology and Teratology* **1991,** 13, (2), 147-152.

137. Hoffman, D. J.; Sileo, L., Neurotoxic and Teratogenic Effects of an Organo-Phosphorus Insecticide (Phenyl Phosphonothioic Acid-O-Ethyl-O-[4-Nitrophenyl] Ester) on Mallard Development. *Toxicology and Applied Pharmacology* **1984,** 73, (2), 284-294.

138. Carrera, V.; Barril, J.; Mauricio, M.; Pellin, M.; Vilanova, E., Local Application of Neuropathic Organophosphorus Compounds to Hen Sciatic-Nerve - Inhibition of Neuropathy Target Esterase and Peripheral Neurological Impairments. *Toxicology and Applied Pharmacology* **1992,** 117, (2), 218-225.

139. Glynn, P., Neural development and neurodegeneration: two faces of Neuropathy Target Esterase. *Prog. Neurobiol.* **2000,** 61, (1), 61-74.

140. Wang, A. J.; Dennis, E. A., Mammalian lysophospholipases. *Biochimica Et Biophysica Acta-Molecular and Cell Biology of Lipids* **1999,** 1439, (1), 1-16.

141. Hamai, C.; Yang, T. L.; Kataoka, S.; Cremer, P. S.; Musser, S. M., Effect of average phospholipid curvature on supported bilayer formation on glass by vesicle fusion. *Biophysical Journal* **2006,** 90, (4), 1241-1248.

142. Caccin, P.; Rossetto, O.; Montecucco, C., Neurotoxicity of inverted-cone shaped lipids. *Neurotoxicology* **2009,** 30, (2), 174-181.

143. Rigoni, M.; Caccin, P.; Gschmeissner, S.; Koster, G.; Postle, A. D.; Rossetto, O.; Schiavo, G.; Montecucco, C., Equivalent effects of snake PLA2 neurotoxins and lysophospholipid-fatty acid mixtures. *Science* **2005,** 310, (5754), 1678-1680.

144. Rigoni, M.; Pizzo, P.; Schiavo, G.; Weston, A. E.; Zatti, G.; Caccin, P.; Rossetto, O.; Pozzan, T.; Montecucco, C., Calcium influx and mitochondrial alterations at synapses exposed to snake neurotoxins or their phospholipid hydrolysis products. *Journal of Biological Chemistry* **2007,** 282, (15), 11238-11245.

145. Selle, H.; Chapman, B. E.; Kuchel, P. W., Glycerophosphocholine Release in Human Erythrocytes - H-1 Spin-Echo and P-31-Nmr Evidence for Lysophospholipase. *European Journal of Biochemistry* **1993,** 212, (2), 411-416.

146. Quistad, G. B.; Casida, J. E., Lysophospholipase inhibition by organophosphorus toxicants. *Toxicology and Applied Pharmacology* **2004,** 196, (3), 319-326.

147. Kohli, N.; Srivastava, D.; Sun, J.; Richardson, R. J.; Lee, I. S.; Worden, R. M., Nanostructured biosensor for measuring neuropathy target esterase activity. *Analytical Chemistry* **2007,** 79, (14), 5196-5203.

148. Atkins, J.; Glynn, P., Membrane association of and critical residues in the catalytic domain of human neuropathy target esterase. *Journal of Biological Chemistry* **2000,** 275, (32), 24477-24483.

149. Hull, M. C.; Sauer, D. B.; Hovis, J. S., Influence of lipid chemistry on the osmotic response of cell membranes: Effect of non-bilayer forming lipids. *Journal of Physical Chemistry B* **2004,** 108, (40), 15890-15895.

150. Shimizu, S.; Tani, Y.; Yamada, H.; Tabata, M.; Murachi, T., Enzymatic Determination of Serum-Free Fatty-Acids - a Colorimetric Method. *Analytical Biochemistry* **1980,** 107, (1), 193-198.

151. Hoyrup, P.; Davidsen, J.; Jorgensen, K., Lipid membrane partitioning of lysolipids and fatty acids: Effects of membrane phase structure and detergent chain length. *Journal of Physical Chemistry B* **2001,** 105, (13), 2649-2657.

152. Gutberlet, T.; Steitz, R.; Fragneto, G.; Klosgen, B., Phospholipid bilayer formation at a bare Si surface: a time-resolved neutron reflectivity study. *Journal of Physics-Condensed Matter* **2004,** 16, (26), S2469-S2476.

153. Schurholz, T.; Kehne, J.; Gieselmann, A.; Neumann, E., Functional Reconstitution of the Nicotinic Acetylcholine-Receptor by Chaps Dialysis Depends on the Concentrations of Salt, Lipid, and Protein. *Biochemistry* **1992,** 31, (21), 5067-5077.

154. Seddon, A. A.; Curnow, P.; Booth, P. J., Membrane proteins, lipids and detergents: not just a soap opera. *Biochimica Et Biophysica Acta-Biomembranes* **2004,** 1666, (1-2), 105-117.

155. Peters, R.; Cherry, R. J., Lateral and Rotational Diffusion of Bacteriorhodopsin in Lipid Bilayers - Experimental Test of the Saffman-Delbruck Equations. *Proceedings of the National Academy of Sciences of the United States of America-Biological Sciences* **1982,** 79, (14), 4317-4321.

156. Hac-Wydro, K.; Jedrzejek, K.; Dynarowicz-Latka, P., Effect of saturation degree on the interactions between fatty acids and phosphatidylcholines in binary and ternary Langmuir monolayers. *Colloids and Surfaces B-Biointerfaces* **2009,** 72, (1), 101-111.

157. Inoue, T.; Yanagihara, S.; Misono, Y.; Suzuki, M., Effect of fatty acids on phase behavior of hydrated dipalmitoylphosphatidylcholine bilayer: saturated versus unsaturated fatty acids. *Chemistry and Physics of Lipids* **2001,** 109, (2), 117-133.

158. Lapshina, E. A.; Zavodnik, I. B.; Bryszewska, M., Effect of Free Fatty-Acids on the Structure and Properties of Erythrocyte-Membrane. *Scandinavian Journal of Clinical & Laboratory Investigation* **1995,** 55, (5), 391-397.

159. Zavodnik, H. B.; Zaborowski, A.; Niekurzak, A.; Bryszewska, M., Effect of free fatty acids on erythrocyte morphology and membrane fluidity. *Biochemistry and Molecular Biology International* **1997,** 42, (1), 123-133.

160. Leekumjorn, S.; Cho, H. J.; Wu, Y. F.; Wright, N. T.; Sum, A. K.; Chan, C., The role of fatty acid unsaturation in minimizing biophysical changes on the structure and local effects of bilayer membranes. *Biochimica Et Biophysica Acta-Biomembranes* **2009,** 1788, (7), 1508-1516.

161. Leekumjorn, S.; Wu, Y. F.; Sum, A. K.; Chan, C., Experimental and computational studies investigating trehalose protection of HepG2 cells from palmitate-induced toxicity. *Biophysical Journal* **2008,** 94, (7), 2869-2883.

162. Peters, G. H.; Hansen, F. Y.; Moller, M. S.; Westh, P., Effects of Fatty Acid Inclusion in a DMPC Bilayer Membrane. *Journal of Physical Chemistry B* **2009,** 113, (1), 92-102.

163. Hac-Wydro, K.; Wydro, P., The influence of fatty acids on model cholesterol/phospholipid membranes. *Chemistry and Physics of Lipids* **2007,** 150, (1), 66-81.

164. Anderson, T. H.; Min, Y. J.; Weirich, K. L.; Zeng, H. B.; Fygenson, D.; Israelachvili, J. N., Formation of Supported Bilayers on Silica Substrates. *Langmuir* **2009,** 25, (12), 6997-7005.

165. Sackmann, E., Supported membranes: Scientific and practical applications. *Science* **1996,** 271, (5245), 43-48.

166. Groves, J. T.; Boxer, S. G., Electric field-induced concentration gradients in planar supported bilayers. *Biophysical Journal* **1995,** 69, (5), 1972-1975.

167. Merzlyakov, M.; Li, E.; Hristova, K., Surface supported bilayer platform for studies of lateral association of proteins in membranes (Mini Review). *Biointerphases* **2008,** 3, (2), FA80-FA84.

168. Kouzayha, A.; Wattraint, O.; Sarazin, C., Interactions of two transmembrane peptides in supported lipid bilayers studied by a P-31 and N-15 MAOSS NMR strategy. *Biochimie* **2009,** 91, (6), 774-778.

169. Puu, G.; Gustafson, I.; Artursson, E.; Ohlsson, P. A., Retained Activities of Some Membrane-Proteins in Stable Lipid Bilayers on a Solid Support. *Biosensors & Bioelectronics* **1995,** 10, (5), 463-476.

170. Ohlsson, P. A.; Tjarnhage, T.; Herbai, E.; Lofas, S.; Puu, G., Liposome and Proteoliposome Fusion onto Solid Substrates, Studied Using Atomic-Force Microscopy, Quartz-Crystal Microbalance and Surface-Plasmon Resonance - Biological-Activities of Incorporated Components. *Bioelectrochemistry and Bioenergetics* **1995,** 38, (1), 137-148.

171. Chan, P. Y.; Lawrence, M. B.; Dustin, M. L.; Ferguson, L. M.; Golan, D. E.; Springer, T. A., Influence of Receptor Lateral Mobility on Adhesion Strengthening between Membranes Containing Lfa-3 and Cd2. *Journal of Cell Biology* **1991,** 115, (1), 245-255.

172. Contino, P. B.; Hasselbacher, C. A.; Ross, J. B. A.; Nemerson, Y., Use of an Oriented Transmembrane Protein to Probe the Assembly of a Supported Phospholipid-Bilayer. *Biophysical Journal* **1994,** 67, (3), 1113-1116.

173. Ameloot, M.; Hendrickx, H., Criteria for Model Evaluation in the Case of Deconvolution Calculations. *Journal of Chemical Physics* **1982,** 76, (9), 4419-4432.